CDF/ANAL/EXOTIC/CDFR/7262
Version 4.0
November 27, 2011

Search for the Vh Production Using High-p_T Like-Sign Dilepton Events in Run II

Toru Okusawa, Yoshihiro Seiya, Takayuki Wakisaka, Kazuhiro Yamamoto, and Daisuke Yamato

Osaka City University, Japan

Abstract

We search for the neutral higgs production associated with the weak vector boson using high-p_T like-sign dilepton events in 7.6 fb^{-1} of data. The expected numbers of Wh and Zh events are 2.4 and 0.24, respectively, for the fermiophobic higgs of the mass 110 GeV/c^2 assuming the Standard Model production cross section. The expected numbers of events for the Standard Model higgs of the mass 160 GeV/c^2 are 0.72 and 0.084, respectively. The number of background events is estimated to be 124.4±8.4, while we observed 134 in the data. Applying the Boosted Decision Tree technique to get more sensitivity, we obtain limits on the cross section ratio to be 4.5 for the 110 GeV/c^2 fermiophobic higgs and 10 for the 160 GeV/c^2 Standard Model higgs at the 95% confidence level.

1 Introduction

Our physics objective is to search for the low-mass fermiophobic higgs and the high-mass Standard-Model (SM) higgs boson using like-sign (LS) dilepton events produced by

$$qq' \rightarrow Vh \rightarrow VW^*W^* \rightarrow \ell^\pm\ell^\pm + X, \quad V = W, Z\,. \tag{1}$$

This note corresponds to an update of the previous analysis [1] to use data corresponding to an integrated luminosity of 7.6 fb^{-1} and to employ a multivariate analysis technique (Boosted Decision Tree). Updated documents to support this analysis include the likelihood-based lepton identification[2], the baseline high-p_T dilepton selection [3], the estimation of Monte Carlo (MC) scale factors and checks of Z cross sections [4]. The method for the residual conversion background is the same as before [5], but we modify the method for the fake lepton background estimation from the previous [6], and we show the method in this document.

2 Signal Monte-Carlo Samples

We use the Wh and Zh official Monte Carlo samples enforced $h \rightarrow WW$ decay at 10 higgs mass points from 110 to 200 GeV/c^2 generated by Pythia, so-called `fhgp4*,` and `uhgp4*.` The Monte Carlo samples are filtered to get $W \rightarrow \ell\nu$ decay efficiently. The filter efficiencies are about 70% for all mass point Monte Carlo. Tables 1 and 2 show the higgs Monte Carlo samples.

3 Signal Acceptance and Expected Events

We estimate the higgs acceptance for the $Vh \rightarrow VWW \rightarrow$ LS-dilepton and expected number of events using official Monte Carlo samples. The event selections are shown in Table 3 and Table 4. Tables 5 and 6 show the signal acceptance for each higgs mass point. Tables 7-8 show the expected number of events for fermiophobic higgs, and tables 9-10 show for the Standard Model higgs.

4 Background Estimation

Although the LS requirement is quite effective to suppress QCD and known electroweak process, we expect that fake lepton background and residual photon-conversion still remain at a considerable level. They are estimated by data-driven methods. For the fake-background estimation, however, we introduce MC-based electroweak subtraction instead of W veto to avoid some bias, and five-dimensional parametrization to predict better than the previous analysis [6]. While other backgrounds containing prompt real-leptons (physics backgrounds) are estimated by MC.

4.1 Residual Photon-Coversions

This prediction method is the same as the previous analysis, and the details are found in [5]. In this note, we show the method briefly.

The amount of residual conversion backgrounds is estimated from multiplying the rate of identified photon conversions by appropriate weights that connect the yields of identified conversions and residual conversions. These weights are expressed in terms of the detection efficiency for conversions $\varepsilon_{\rm con}$ as

$$R_{\rm res} = \frac{1-\varepsilon_{\rm con}}{\varepsilon_{\rm con}} \,. \tag{2}$$

Then, we estimate the number of residual conversion events by

$$N_{\rm res} = R_{\rm res} \times N_{\rm con} \,, \tag{3}$$

where $N_{\rm con}$ is the number of conversion events.

4.2 Fake Leptons

Fake-lepton backgrounds are estimated from multiplying the number of events with one good lepton candidate passing the high-p_T cut plus isolated tracks by appropriate weights (fake rates). Here, the term "fake lepton" is a generic word including non-prompt leptons such as coming from (semi-)leptonic decays of heavy-flavor hadrons as well as literal fake leptons. As the previous [6], we adopt hadronic tracks as the denominator objects for the fake rate. It is an isolated track passing the low p_T cut, a set of track-quality cuts, and the requirements on the energy depositions in the corresponding calorimeter towers, which we refer to as hadronic tracks. The cuts on the energy deposition have no overlap with the nominal lepton selection, thus the hadronic tracks are fake-enriched objects. Then, the fake-lepton events can be estimated by

$$N_{\text{fake}} = R_{\text{fake}} \times N_{\text{track}} \tag{4}$$

where R_{fake} and N_{track} are the fake rate and the number of hadronic tracks in the event, respectively.

We newly introduce the five dimensional parametrization of the fake rate and MC-based electroweak subtraction compared to the previous analysis [1], and we show the method in the next.

4.2.1 (Monte Carlo)-based Electroweak Subtraction

For the estimation of the fake rate, we use jet samples. The jet samples, however, contain non-neglegible real leptons, mainly from W or Z. In the previous analysis [6], we apply the W and Z veto to remove those as possible. The W veto is defined as

- $E_T > 20$ GeV ($p_T > 20$ GeV/c) for electron (muon) passing lepton selections, and
- $\not\!\!E_T > 30$ GeV or (transverse mass) $> 40\text{GeV}/c^2$.

In the current analysis, we use MC-based subtraction instead of W veto because we found that the W veto causes some bias for the p_T distribution (see figure 1). p_T is used the for the fake-rate parametrization in the previous analysis, and this is also one of the most important variables in this analysis.

First, we require the hadronic track selection in the jet samples. Then, we convert the data and MC to the cross section (pb). After that, we fit the MC to data by using the function

$$p_0 \cdot (\text{MC histogram}) + \exp(p_1 x + p_2) \tag{5}$$

where the exponential component represents the fake lepton distribution, and p_0, p_1, and p_2 are the fitting parameters. p_0 determines the normalization of the MC samples. Then, we rescale MC samples in each variable by using p_0, and subtract the components from the distributions. We consider the remaining as fake leptons. The distributions of transverse mass are shown in figures 2 and 3.

4.2.2 Five-Dimensional Fake Rate Parametrization

We use five variables to parametrize the fake rates instead of only p_T, because the fake rate also depend on those variables to some extent. The variables we choose are

- p_T,
- Isolation ($\mathrm{ISO}_{0.4}^{\mathrm{cal}}$),
- pseudorapidity (η),
- impact parameter (d_0), and
- ϕ within the wedge of the calorimeter.

The p_T distributions for fake electrons and fake muons are shown in figures 4-5. Then, we parametrize the fake rates as

$$R_{\mathrm{fake}} = \frac{n}{d} \cdot r(p_T) \cdot r(\eta) \cdot f(\mathrm{ISO}_{0.4}) \cdot f(d_0) \cdot f(\phi_{\mathrm{wedge}}), \tag{6}$$

where

- n : the number of fake leptons (passing our selection cuts),
- d : the number of hadronic tracks,
- r : normalized ratio, and use the histogram for fake rate estimation,
- f : normalized ratio, and use the polynomial function for fake rate estimation.

Figures 6 and 7 show the fake rate and the normalized rate for each variable.

Finally, we estimate fake leptons by

$$N_{\mathrm{fake}} = R_{\mathrm{fake}} \times N_{\mathrm{track}} \tag{7}$$

where N_{track} is the number of hadronic tracks.

4.3 Physics Backgrounds

The physics backgrounds can be classified into reducible and irreducible backgrounds:

- Reducible backgrounds

  1. $Z/\gamma^* \rightarrow \ell^+\ell^-$,
  2. W+(heavy-flavor hadrons)$\rightarrow \ell\ell + X$,
  3. $t\bar{t} \rightarrow (W^+b)(W^-\bar{b}) \rightarrow \ell\ell + X$,
  4. $W^+W^- \rightarrow (\ell^+\nu)(\ell^-\nu)$.

- Irreducible backgrounds

    1. $WZ \rightarrow (\ell^{\pm}\nu)(\ell^{+}\ell^{-})$,
    2. $ZZ \rightarrow (\ell^{+}\ell^{-})(\ell^{+}\ell^{-})$,

The reducible backgrounds are reduced first of all by the LS requirement. When they contribute to LS dilepton events, the events are most likely due to residual conversions or fake leptons contained in these physics events, thus reduced also by the isolation cut.

The MC samples were produced by the Electroweak and the Top groups. Table 11 lists the MC samples and related information of them. The MC samples are all applied with the relevant scale factors that are discussed in [4]. A rather important point regarding our MC prediction is that residual photon-conversions and fake-leptons including non-prompt leptons from (semi-)leptonic decays of heavy-flavor hadrons found in the MC events are explicitly removed from the MC contributions by looking at the `OBSP` information since their contributions are assumed to be directly estimated from the data-driven methods.

4.4 Expected Backgrounds

We show the expected number of events passing our events selection cuts. For this purpose, we use the 2 dimensional plane ($p_{T_{12}}$ vs. p_T). The definition is

- Region 1 : Dilepton system $p_T < 15$ GeV/c and 2nd lepton $p_T \geq 20$ GeV/c
- Region 2 : Dilepton system $p_T < 15$ GeV/c and 2nd lepton $p_T < 20$ GeV/c
- Region 3 : Dilepton system $p_T \geq 15$ GeV/c and 2nd lepton $p_T < 20$ GeV/c
- Region 4 : Dilepton system $p_T \geq 15$ GeV/c and 2nd lepton $p_T \geq 20$ GeV/c.

This plane was introduced in our history [7]. While we do not use this plane as the final discriminant, we use this to look at the number of events closely. The numbers are shown in Table 13-14. From them, we see no significant discrepancies between the data and background expectations.

5 Boosted Decision Tree

We obtain 2.4(0.24) signal events for 110 GeV/c^2 Wh (Zh) Fermiophobic higgs, and 124.4$\pm$8.35 expected events of backgrounds. To get more search sensitivity, we employ a multivariate analysis technique based on Boosted Decision Tree (BDT), instead of cut-based counting analysis. We use the TMVA package integrated in ROOT framework [8].

A Decision Tree is a binary tree structured classifier. Repeated yes/no decisions are performed on a single variable at a time until some stop criterion is reached. But a single tree is sensitive to statistical fluctuations in the training data. This problem is overcome by constructing a forest of decision trees, and in this process, the events which were misclassified are given an extra weight and the tree is retrained. The boosting increases the statistical stability of the classifier and typically also improves the separation performance compared to a single decision tree. One of the most popular boosting algorithm is AdaBoost(adaptive boost). We use the algorithm in this analysis.

The Decision tree can be strongly overtrained. Therefore we need to prune the decision tree to avoid overtraining. Pruning is the process of cutting back a tree from the bottom up after it has been built to its maximum size.

5.1 BDT Training Samples

According to our background estimation, there are 2 main background events for like-sign dilepton events. One is residual-photon conversions event, which is electron originated from photon conversion with unobserved partner track. The other is the fake leptons. The components of the fake lepton are interactive $\pi^{\pm}$, overlap of π^0 and a track, punch-through hadrons, and non-prompt leptons. We, therefore, train the BDT using residual photon-conversion and fake lepton events as background which derived from data samples. The signal event are Wh higgs Monte Carlo samples shown in Table 1. We perform the training to the backgrounds and Wh signal in each mass point. These samples are passing all selection criteria.

5.2 BDT Input Variables

We need to care about the input variables for BDT. We select 9 variables based on the ranking and the shape systematic uncertainty of jet energy scale (JES) (We do not choose the input variables affected significantly by JES):

- 1st lepton $p_T(p_{T1})$
- 2nd lepton $p_T(p_{T2})$
- Dilepton system $p_T(p_{T12})$
- Missing E_T
- Dilepton mass
- MetSpec : $\not\!\!E_T$ if $\Delta\phi(\not\!\!E_T, \ell$ or jet$) > \pi/2$ or
  . : $\not\!\!E_T \sin(\Delta\phi(\not\!\!E_T, \ell$ or jet$))$ if $\Delta\phi(\not\!\!E_T, \ell$ or jet$) < \pi/2$
- H$_T$ (Sum of p_{T1}, p_{T2}, jets E_T ($E_T > 15$ GeV and $|\eta| < 2.0$), and Missing E_T)
- Number of Jets with $E_T > 15.0$ GeV
- Sphericity.

We introduce the new variable, sphericity [9], compared to the previous analysis [1] to look at the event shape. The sphericity tensor is defined as

$$S^{\alpha\beta} = \frac{\sum_i p_i^\alpha p_i^\beta}{\sum_i |\mathbf{p}_i|^2}, \tag{8}$$

where $\alpha, \beta = 1, 2, 3$ corresponds to the x, y, and z components, and p_i is the 4-momentum for the i-th particle in the event. Generally, sphericity tensor has three eigenvalues, λ_1, λ_2, and λ_3 with $\lambda_1 \geq \lambda_2 \geq \lambda_3$ and $\lambda_1 + \lambda_2 + \lambda_3 = 1$. Then, sphericity S is defined by

$$S = \frac{3}{2}(\lambda_2 + \lambda_3), \tag{9}$$

so that $0 \leq S \leq 1$.

Figures 8-14 show some kinematical variables after passing our selections, that is, our signal region. To validate our estimation, we also prepare some pilot regions: side-band region, opposite-sign region, and zero-silicon region. We call the 1st lepton passing all selection criteria and the 2nd lepton passing all selection except for the lepton identification as the side-band region. The opposite-sign region is the same as the signal region except for the charge combination of dilepton. The zero-silicon region is defined by

- 1st lepton with nominal silicon hit requirement
- 2nd lepton with zero-silicon hit requirement
- Silicon fiducial cut, that is, 2nd lepton passing through SVX 5 layers and $|z_0| <$ 47.25 cm at $R = 10.645$.

Figures 15-21 show those variables for side-band events. Figures 22-28 show for zero-silicon region, and figures 29-35 show for OS dilepton events.

5.3 BDT Training, Output and Cross Check

We use the BDT output as the final discriminant for the higgs. First, we check the consistency between training and test samples to check BDT is not overtrained. Those plots are shown in figures 36 and 37.

After that, we derive the final discriminant in each higgs mass point. Figures 38-41 show those distributions in our signal region. As the cross-check, we also show the output in the pilot regions. Figures 43-46 show for the side-band, figures 47-50 for the zero-silicon, and figures 51-54 for the OS region.

For these plots, we can not see significant disagreement between the data and our expected events.

6 Systematic Uncertainties

We estimate several systematic uncertainties for signal and background.

6.1 Rate Systematic Uncertainties for Signal

We estimate several systematic uncertainties for both Wh and Zh samples. For PDF uncertainties, we use "Reweighting Method". For ISR and FSR uncertainties, we use ISR(FSR) more and less samples for Wh and Zh samples. Also, we estimate signal Monte Carlo statistics uncertainties and several scale factor uncertainties (lepton ID scale factors and trigger efficiencies) as rate systematic uncertainties. Moreover, we estimate the uncertainty of the number of Z candidates when we validate MC scale factors (see [4] and tables 16) and also include this (1.98%) as the rate systematic uncertainty. And we assign 5% prediction cross section uncertainties for Wh and Zh (see [10]). The luminosity uncertainties are 6%. Tables 17 and 18 show the summary of rate systematic uncertainties for signals.

6.2 Rate Systematic Uncertainties for Backgrounds

Table 19 show the summary of rate systematic uncertainties of the backgrounds. The fake lepton and residual photon conversion have the weight rate systematic, that is, fake rate and residual conversion rate. The physics backgrounds, that is, WZ and ZZ, are estimated by Monte Carlo samples. We assign Monte Carlo statistical uncertainties, scale factor uncertainties, luminosity uncertainties as the same as the signal MC samples. And we assign prediction cross section uncertainties to those diboson MC samples (see [11]).

6.3 Shape Systematic Uncertainties from Jet Energy Scale

We use some variables related to jet objects as BDT input variables (H_T, number of jets, and Sphericity). So we need to consider the systematics from the jet energy scale. However, we do not apply jet-related variables to the dilepton events, so the systematic uncertainty is only shape systematic, not rate systematic in our BDT discriminant. Figures 55-74 show the shape systematics uncertainty for Jet energy scale in BDT output for fake&residual conversion, WZ, ZZ, Wh and Zh.

7 Limits

We calculate 95% upper limit on the production cross-section times the branching fraction for the higgs mass from 110 to 200 GeV/c^2. For this purpose, we use the Bayesian approach in MCLIMIT (see [12]). We set the number of pseudo-experiment and the sampling to 10K. Tables 20-21 and figures 75-76 show the results including only Wh signal events. The results including both Wh and Zh are shown in tables 22-23 and figures 77-78.

8 Conclusions

We search for the neutral higgs production associated with the vector boson using high-p_T like-sign dilepton events using the data corresponding to the integrated luminosity of 7.6 fb^{-1}. We can not see any significant disagreements between background expectations and the data. The expected number of fermiophobic Wh events for the mass 110 GeV/c^2 is 2.4 events assuming the Standard Model production cross section and 0.24 events for Zh. Also, for the mass 160 GeV/c^2 of the SM higgs, we obtain 0.72 events for Wh and 0.084 events for Zh. The expected number of backgrounds is estimated as 124.35 ± 8.35, while we observe 134 events in the data. To get more search sensitivity, we employed the Boosted Decision Tree technique and deduce the final discriminant in each mass point. We deduce the upper limits on the production cross-section times the branching fraction

$$\sigma(p\bar{p}\to Vh) \times B_F(h\to W^{*+}W^{*-})$$

for the higgs with masses in the region from 110 GeV/c^2 to 200 GeV/c^2. Finally, we obtain the limits on the cross section ratio to be 4.5 for the 110 GeV/c^2 fermiophobic higgs and 10 for the 160 GeV/c^2 Standard Model higgs at the 95% confidence level.

Table 1: Wh Monte Carlo samples.

Mass (GeV/c^2)	$\sigma(p\bar{p}\rightarrow Wh)$ (fb)	$B_F(h_{\rm FP}\rightarrow WW)$	$B_F(h_{\rm SM}\rightarrow WW)$	Dataset	Generated (Events)
110	209.2	0.88	0.05	`fhgp4a`	4198567
120	153.0	0.88	0.13	`fhgp4b`	4198567
130	114.7	0.88	0.30	`fhgp4c`	4198567
140	86.0	0.88	0.49	`fhgp4d`	4198567
150	66.0	0.89	0.69	`fhgp4e`	4198567
160	50.7	0.95	0.91	`fhgp4f`	4198567
170	38.9	0.98	0.96	`fhgp4g`	4198567
180	30.7	0.94	0.93	`fhgp4h`	4198567
190	24.3	0.79	0.79	`fhgp4i`	4198567
200	19.3	0.75	0.74	`fhgp4j`	4198567

Table 2: Zh Monte Carlo samples.

Mass (GeV/c^2)	$\sigma(p\bar{p}\rightarrow Zh)$ (fb)	$B_F(h_{\rm FP}\rightarrow WW)$	$B_F(h_{\rm SM}\rightarrow WW)$	Dataset	Generated (Events)
110	124.3	0.88	0.05	`uhgp4a`	2840191
120	92.7	0.88	0.13	`uhgp4b`	2840191
130	70.9	0.88	0.30	`uhgp4c`	2840191
140	54.2	0.88	0.49	`uhgp4d`	2840191
150	42.5	0.89	0.69	`uhgp4e`	2840191
160	33.3	0.95	0.91	`uhgp4f`	2840191
170	26.1	0.98	0.96	`uhgp4g`	2840191
180	20.8	0.94	0.93	`uhgp4h`	2840191
190	16.6	0.79	0.79	`uhgp4i`	2840191
200	13.5	0.75	0.74	`uhgp4j`	2840191

Table 3: Event pre-selection and lepton selection cuts.

Electron selection	Muon selection
Event pre-selection	
$\lvert z_{\mathrm{pv}}\rvert < 60$ cm	
Cosmic-ray veto	
Geometrical and kinematical cuts	
CEM	CMUP or CMX
Fiducial	CMU, P: (x,z)-fid $< (0,0)$, $(0,-3)$ cm
	CMX: (x,z)-fid $< (0,-3)$ cm, $\rho_{\mathrm{COT}} > 140$ cm
	Blue-beam veto, keystone veto, miniskirt veto
$E_T^{\ell_1} > 20$ GeV ($p_T > 10$ GeV/c)	$p_T^{\ell_1} > 20$ GeV/c
$E_T^{\ell_2} > 6$ GeV ($p_T > 6$ GeV/c)	$p_T^{\ell_2} > 6$ GeV/c
Track quality cuts	
Axial ≥ 3 and stereo ≥ 2 (≥ 5 hits)	
$\lvert z_0 - z_{\mathrm{pv}}\rvert < 2$ cm	
Silicon hits ≥ 3	
$\lvert d_0\rvert < 0.02$ cm	
Isolation cut	
$\mathrm{ISO}_{0.4}^{\mathrm{cal}} < 2$ GeV	
Identification cuts	
Likelihood based on Z leptons	Likelihood based on Z leptons
$\cdot\ L > 0.95$	$\cdot\ L > 0.70$
Other cuts	
Conversion removal	

Table 4: Dilepton selection cuts.

Exactly two leptons
$\lvert z_0^{\ell_1} - z_0^{\ell_2}\rvert < 2$ cm
Dilepton mass > 12 GeV/c^2
Z removal
One like-sign pair

Table 5: Wh acceptance after all selection cuts.

Higgs Mass (GeV/c^2)	Acceptance (%)
110	0.174 ± 0.002
120	0.188 ± 0.002
130	0.202 ± 0.002
140	0.209 ± 0.002
150	0.214 ± 0.002
160	0.207 ± 0.002
170	0.215 ± 0.002
180	0.227 ± 0.002
190	0.247 ± 0.003
200	0.257 ± 0.003

Table 6: Zh acceptance after all selection cuts.

Higgs Mass (GeV/c^2)	Acceptance (%)
110	0.029 ± 0.001
120	0.033 ± 0.001
130	0.035 ± 0.001
140	0.036 ± 0.001
150	0.039 ± 0.001
160	0.036 ± 0.001
170	0.038 ± 0.001
180	0.039 ± 0.001
190	0.042 ± 0.001
200	0.044 ± 0.001

Table 7: Fermiophobic higgs (Wh) expected number of events for the like-sign dilepton events.

	Regions				
	1	2	3	4	Total
Fermiophobic higgs (Wh110)	0.099±0.008	0.034±0.004	0.937±0.058	1.325±0.082	2.394±0.146
(Stat.)	±0.0051	±0.0030	±0.0161	±0.0188	±0.0254
(Syst.)	±0.0001	±0.0000	±0.0010	±0.0017	±0.0030
(Luminosity)	±0.0059	±0.0020	±0.0562	±0.0795	±0.1437
Fermiophobic higgs (Wh120)	0.083±0.006	0.028±0.003	0.708±0.044	1.072±0.066	1.892±0.115
(Stat.)	±0.0040	±0.0024	±0.0119	±0.0145	±0.0194
(Syst.)	±0.0001	±0.0000	±0.0008	±0.0014	±0.0024
(Luminosity)	±0.0050	±0.0017	±0.0425	±0.0643	±0.1135
Fermiophobic higgs (Wh130)	0.073±0.005	0.017±0.002	0.509±0.032	0.919±0.056	1.518±0.092
(Stat.)	±0.0033	±0.0016	±0.0088	±0.0116	±0.0150
(Syst.)	±0.0001	±0.0000	±0.0006	±0.0012	±0.0019
(Luminosity)	±0.0044	±0.0010	±0.0305	±0.0552	±0.0911
Fermiophobic higgs (Wh140)	0.052±0.004	0.019±0.002	0.369±0.023	0.755±0.046	1.195±0.073
(Stat.)	±0.0024	±0.0015	±0.0065	±0.0091	±0.0115
(Syst.)	±0.0001	±0.0000	±0.0004	±0.0010	±0.0015
(Luminosity)	±0.0031	±0.0011	±0.0221	±0.0453	±0.0717
Fermiophobic higgs (Wh150)	0.040±0.003	0.010±0.001	0.276±0.017	0.633±0.039	0.958±0.058
(Stat.)	±0.0018	±0.0009	±0.0049	±0.0074	±0.0091
(Syst.)	±0.0001	±0.0000	±0.0003	±0.0008	±0.0012
(Luminosity)	±0.0024	±0.0006	±0.0165	±0.0380	±0.0575
Fermiophobic higgs (Wh160)	0.032±0.002	0.006±0.001	0.200±0.013	0.524±0.032	0.762±0.046
(Stat.)	±0.0015	±0.0007	±0.0038	±0.0061	±0.0074
(Syst.)	±0.0000	±0.0000	±0.0002	±0.0007	±0.0010
(Luminosity)	±0.0019	±0.0004	±0.0120	±0.0314	±0.0457
Fermiophobic higgs (Wh170)	0.024±0.002	0.005±0.001	0.157±0.010	0.435±0.027	0.620±0.038
(Stat.)	±0.0011	±0.0005	±0.0030	±0.0049	±0.0059
(Syst.)	±0.0000	±0.0000	±0.0002	±0.0006	±0.0008
(Luminosity)	±0.0014	±0.0003	±0.0094	±0.0261	±0.0372
Fermiophobic higgs (Wh180)	0.017±0.001	0.003±0.000	0.117±0.007	0.362±0.022	0.500±0.030
(Stat.)	±0.0008	±0.0004	±0.0023	±0.0039	±0.0046
(Syst.)	±0.0000	±0.0000	±0.0001	±0.0005	±0.0006
(Luminosity)	±0.0010	±0.0002	±0.0070	±0.0217	±0.0300
Fermiophobic higgs (Wh190)	0.012±0.001	0.002±0.000	0.083±0.005	0.266±0.016	0.364±0.022
(Stat.)	±0.0006	±0.0002	±0.0016	±0.0027	±0.0032
(Syst.)	±0.0000	±0.0000	±0.0001	±0.0004	±0.0005
(Luminosity)	±0.0007	±0.0001	±0.0050	±0.0160	±0.0218
Fermiophobic higgs (Wh200)	0.008±0.001	0.002±0.000	0.061±0.004	0.212±0.013	0.282±0.017
(Stat.)	±0.0004	±0.0002	±0.0011	±0.0021	±0.0024
(Syst.)	±0.0000	±0.0000	±0.0001	±0.0003	±0.0004
(Luminosity)	±0.0005	±0.0001	±0.0036	±0.0127	±0.0169

Table 8: Fermiophobic higgs (Zh) expected number of events for the like-sign dilepton events.

	Regions				
	1	2	3	4	Total
Fermiophobic higgs (Zh110)	0.010±0.002	0.003±0.001	0.102±0.008	0.126±0.009	0.241±0.016
(Stat.)	±0.0015	±0.0009	±0.0049	±0.0053	±0.0075
(Syst.)	±0.0000	±0.0000	±0.0001	±0.0002	±0.0004
(Luminosity)	±0.0006	±0.0002	±0.0061	±0.0076	±0.0145
Fermiophobic higgs (Zh120)	0.007±0.001	0.004±0.001	0.078±0.006	0.114±0.008	0.203±0.014
(Stat.)	±0.0011	±0.0009	±0.0037	±0.0044	±0.0059
(Syst.)	±0.0000	±0.0000	±0.0001	±0.0002	±0.0003
(Luminosity)	±0.0004	±0.0003	±0.0047	±0.0069	±0.0122
Fermiophobic higgs (Zh130)	0.007±0.001	0.002±0.001	0.063±0.005	0.094±0.007	0.166±0.011
(Stat.)	±0.0009	±0.0005	±0.0029	±0.0035	±0.0047
(Syst.)	±0.0000	±0.0000	±0.0001	±0.0001	±0.0002
(Luminosity)	±0.0004	±0.0001	±0.0038	±0.0056	±0.0099
Fermiophobic higgs (Zh140)	0.005±0.001	0.002±0.000	0.044±0.003	0.079±0.006	0.130±0.009
(Stat.)	±0.0007	±0.0004	±0.0021	±0.0028	±0.0036
(Syst.)	±0.0000	±0.0000	±0.0001	±0.0001	±0.0002
(Luminosity)	±0.0003	±0.0001	±0.0026	±0.0048	±0.0078
Fermiophobic higgs (Zh150)	0.003±0.001	0.001±0.000	0.037±0.003	0.072±0.005	0.113±0.007
(Stat.)	±0.0005	±0.0003	±0.0017	±0.0024	±0.0030
(Syst.)	±0.0000	±0.0000	±0.0000	±0.0001	±0.0002
(Luminosity)	±0.0002	±0.0001	±0.0022	±0.0043	±0.0068
Fermiophobic higgs (Zh160)	0.003±0.001	0.001±0.000	0.025±0.002	0.060±0.004	0.088±0.006
(Stat.)	±0.0005	±0.0002	±0.0013	±0.0020	±0.0024
(Syst.)	±0.0000	±0.0000	±0.0000	±0.0001	±0.0001
(Luminosity)	±0.0002	±0.0000	±0.0015	±0.0036	±0.0053
Fermiophobic higgs (Zh170)	0.003±0.000	0.001±0.000	0.021±0.002	0.049±0.003	0.074±0.005
(Stat.)	±0.0004	±0.0003	±0.0011	±0.0016	±0.0020
(Syst.)	±0.0000	±0.0000	±0.0000	±0.0001	±0.0001
(Luminosity)	±0.0002	±0.0001	±0.0013	±0.0029	±0.0044
Fermiophobic higgs (Zh180)	0.002±0.000	0.000±0.000	0.016±0.001	0.041±0.003	0.059±0.004
(Stat.)	±0.0003	±0.0001	±0.0008	±0.0013	±0.0016
(Syst.)	±0.0000	±0.0000	±0.0000	±0.0001	±0.0001
(Luminosity)	±0.0001	±0.0000	±0.0010	±0.0025	±0.0035
Fermiophobic higgs (Zh190)	0.001±0.000	0.000±0.000	0.011±0.001	0.030±0.002	0.043±0.003
(Stat.)	±0.0002	±0.0001	±0.0006	±0.0009	±0.0011
(Syst.)	±0.0000	±0.0000	±0.0000	±0.0000	±0.0001
(Luminosity)	±0.0001	±0.0000	±0.0006	±0.0018	±0.0026
Fermiophobic higgs (Zh200)	0.001±0.000	0.000±0.000	0.009±0.001	0.024±0.002	0.034±0.002
(Stat.)	±0.0001	±0.0001	±0.0004	±0.0007	±0.0008
(Syst.)	±0.0000	±0.0000	±0.0000	±0.0000	±0.0001
(Luminosity)	±0.0001	±0.0000	±0.0005	±0.0014	±0.0020

Table 9: Standard Model higgs (Wh) expected number of events for the like-sign dilepton events.

	Regions				
	1	2	3	4	Total
Standard Model higgs (Wh110)	0.005±0.000	0.002±0.000	0.049±0.003	0.069±0.004	0.125±0.008
(Stat.)	±0.0003	±0.0002	±0.0008	±0.0010	±0.0013
(Syst.)	±0.0000	±0.0000	±0.0001	±0.0001	±0.0002
(Luminosity)	±0.0003	±0.0001	±0.0029	±0.0042	±0.0075
Standard Model higgs (Wh120)	0.013±0.001	0.004±0.000	0.110±0.007	0.166±0.010	0.293±0.018
(Stat.)	±0.0006	±0.0004	±0.0018	±0.0022	±0.0030
(Syst.)	±0.0000	±0.0000	±0.0001	±0.0002	±0.0004
(Luminosity)	±0.0008	±0.0003	±0.0066	±0.0100	±0.0176
Standard Model higgs (Wh130)	0.025±0.002	0.006±0.001	0.172±0.011	0.310±0.019	0.512±0.031
(Stat.)	±0.0011	±0.0005	±0.0030	±0.0039	±0.0051
(Syst.)	±0.0000	±0.0000	±0.0002	±0.0004	±0.0006
(Luminosity)	±0.0015	±0.0003	±0.0103	±0.0186	±0.0307
Standard Model higgs (Wh140)	0.029±0.002	0.011±0.001	0.208±0.013	0.426±0.026	0.674±0.041
(Stat.)	±0.0014	±0.0008	±0.0036	±0.0051	±0.0065
(Syst.)	±0.0000	±0.0000	±0.0002	±0.0006	±0.0008
(Luminosity)	±0.0018	±0.0006	±0.0125	±0.0255	±0.0404
Standard Model higgs (Wh150)	0.031±0.002	0.008±0.001	0.214±0.013	0.491±0.030	0.743±0.045
(Stat.)	±0.0014	±0.0007	±0.0038	±0.0057	±0.0071
(Syst.)	±0.0000	±0.0000	±0.0003	±0.0006	±0.0009
(Luminosity)	±0.0018	±0.0005	±0.0128	±0.0295	±0.0446
Standard Model higgs (Wh160)	0.030±0.002	0.006±0.001	0.190±0.012	0.497±0.030	0.723±0.044
(Stat.)	±0.0014	±0.0006	±0.0036	±0.0058	±0.0070
(Syst.)	±0.0000	±0.0000	±0.0002	±0.0007	±0.0009
(Luminosity)	±0.0018	±0.0004	±0.0114	±0.0298	±0.0434
Standard Model higgs (Wh170)	0.024±0.002	0.005±0.001	0.155±0.010	0.429±0.026	0.612±0.037
(Stat.)	±0.0011	±0.0005	±0.0030	±0.0048	±0.0058
(Syst.)	±0.0000	±0.0000	±0.0002	±0.0006	±0.0008
(Luminosity)	±0.0014	±0.0003	±0.0093	±0.0258	±0.0367
Standard Model higgs (Wh180)	0.017±0.001	0.003±0.000	0.116±0.007	0.359±0.022	0.496±0.030
(Stat.)	±0.0008	±0.0004	±0.0022	±0.0039	±0.0046
(Syst.)	±0.0000	±0.0000	±0.0001	±0.0005	±0.0006
(Luminosity)	±0.0010	±0.0002	±0.0070	±0.0216	±0.0297
Standard Model higgs (Wh190)	0.012±0.001	0.002±0.000	0.083±0.005	0.265±0.016	0.362±0.022
(Stat.)	±0.0006	±0.0002	±0.0015	±0.0027	±0.0032
(Syst.)	±0.0000	±0.0000	±0.0001	±0.0004	±0.0005
(Luminosity)	±0.0007	±0.0001	±0.0050	±0.0159	±0.0217
Standard Model higgs (Wh200)	0.008±0.001	0.001±0.000	0.060±0.004	0.211±0.013	0.281±0.017
(Stat.)	±0.0004	±0.0002	±0.0011	±0.0021	±0.0024
(Syst.)	±0.0000	±0.0000	±0.0001	±0.0003	±0.0004
(Luminosity)	±0.0005	±0.0001	±0.0036	±0.0127	±0.0169

Table 10: Standard Model higgs (Zh) expected number of events for the like-sign dilepton events.

	Regions				
	1	2	3	4	Total
Standard Model higgs (Zh110)	0.001±0.000	0.000±0.000	0.005±0.000	0.007±0.000	0.013±0.001
(Stat.)	±0.0001	±0.0000	±0.0003	±0.0003	±0.0004
(Syst.)	±0.0000	±0.0000	±0.0000	±0.0000	±0.0000
(Luminosity)	±0.0000	±0.0000	±0.0003	±0.0004	±0.0008
Standard Model higgs (Zh120)	0.001±0.000	0.001±0.000	0.012±0.001	0.018±0.001	0.031±0.002
(Stat.)	±0.0002	±0.0001	±0.0006	±0.0007	±0.0009
(Syst.)	±0.0000	±0.0000	±0.0000	±0.0000	±0.0000
(Luminosity)	±0.0001	±0.0000	±0.0007	±0.0011	±0.0019
Standard Model higgs (Zh130)	0.002±0.000	0.001±0.000	0.021±0.002	0.032±0.002	0.056±0.004
(Stat.)	±0.0003	±0.0002	±0.0010	±0.0012	±0.0016
(Syst.)	±0.0000	±0.0000	±0.0000	±0.0000	±0.0001
(Luminosity)	±0.0001	±0.0000	±0.0013	±0.0019	±0.0034
Standard Model higgs (Zh140)	0.003±0.000	0.001±0.000	0.025±0.002	0.045±0.003	0.074±0.005
(Stat.)	±0.0004	±0.0003	±0.0012	±0.0016	±0.0020
(Syst.)	±0.0000	±0.0000	±0.0000	±0.0001	±0.0001
(Luminosity)	±0.0002	±0.0001	±0.0015	±0.0027	±0.0044
Standard Model higgs (Zh150)	0.003±0.000	0.001±0.000	0.028±0.002	0.056±0.004	0.088±0.006
(Stat.)	±0.0004	±0.0003	±0.0013	±0.0019	±0.0023
(Syst.)	±0.0000	±0.0000	±0.0000	±0.0001	±0.0001
(Luminosity)	±0.0002	±0.0001	±0.0017	±0.0033	±0.0053
Standard Model higgs (Zh160)	0.003±0.000	0.001±0.000	0.023±0.002	0.057±0.004	0.084±0.006
(Stat.)	±0.0004	±0.0002	±0.0012	±0.0019	±0.0023
(Syst.)	±0.0000	±0.0000	±0.0000	±0.0001	±0.0001
(Luminosity)	±0.0002	±0.0000	±0.0014	±0.0034	±0.0050
Standard Model higgs (Zh170)	0.003±0.000	0.001±0.000	0.021±0.002	0.048±0.003	0.073±0.005
(Stat.)	±0.0004	±0.0002	±0.0011	±0.0016	±0.0020
(Syst.)	±0.0000	±0.0000	±0.0000	±0.0001	±0.0001
(Luminosity)	±0.0002	±0.0001	±0.0013	±0.0029	±0.0044
Standard Model higgs (Zh180)	0.002±0.000	0.000±0.000	0.016±0.001	0.041±0.003	0.059±0.004
(Stat.)	±0.0003	±0.0001	±0.0008	±0.0013	±0.0015
(Syst.)	±0.0000	±0.0000	±0.0000	±0.0001	±0.0001
(Luminosity)	±0.0001	±0.0000	±0.0010	±0.0024	±0.0035
Standard Model higgs (Zh190)	0.001±0.000	0.000±0.000	0.011±0.001	0.030±0.002	0.043±0.003
(Stat.)	±0.0002	±0.0001	±0.0006	±0.0009	±0.0011
(Syst.)	±0.0000	±0.0000	±0.0000	±0.0000	±0.0001
(Luminosity)	±0.0001	±0.0000	±0.0006	±0.0018	±0.0026
Standard Model higgs (Zh200)	0.001±0.000	0.000±0.000	0.009±0.001	0.024±0.002	0.034±0.002
(Stat.)	±0.0001	±0.0001	±0.0004	±0.0007	±0.0008
(Syst.)	±0.0000	±0.0000	±0.0000	±0.0000	±0.0001
(Luminosity)	±0.0001	±0.0000	±0.0005	±0.0014	±0.0020

Table 11: Summary of the Monte Carlo samples.

Process	Datasets	Events	$\sigma \cdot B_F$ (pb)	K factor	Filter-efficiency	Luminosity (fb^{-1})	Notes
Electron channels							
$W \to e\nu$	`wewkge`	4036290	1960	1.4	—	1.47	
$Z/\gamma^* \to ee$	`zewkad`	1594110	355 ± 3	1.4	—	3.21	$M > 20$ GeV/c^2
Muon channels							
$W \to \mu\nu$	`wewk8m`	1608588	1960	1.4	—	0.586	
$Z/\gamma^* \to \mu\mu$	`zewk9m`	6701700	355 ± 3	1.4	—	13.5	$M > 20$ GeV/c^2
Both channels							
$Z/\gamma^* \to \tau\tau$	`zewkat`	6849882	238 ± 3	1.4	—	19.0	$M > 30$ GeV/c^2
$t\bar{t}$	`ttop75`	1111652	7.3	—	—	152.3	
WW	`wewkbd`	1596781	1.27	—	—	1.26×10^3	
WZ	`wewkcd`	3598792	0.365	—	0.76	1.19×10^4	
ZZ	`wewkdd`	761342	2.01	—	0.23	1.65×10^3	$M > 15$ GeV/c^2

Table 12: Background expectation and observed number of events for the like-sign dilepton events.

	Regions				
	1	2	3	4	Total
Fakes	0.54	13.63	74.38	1.99	90.54
Photon-conversions	1.76	1.99	20.54	2.91	27.21
Total	2.30±0.47	15.62±1.74	94.92±6.97	4.90±0.91	117.75±8.32
(Stat.)	±0.42	±1.26	±3.35	±0.59	±3.69
(Syst.)	±0.21	±1.19	±6.11	±0.70	±7.46
WZ	0.27	0.08	1.99	3.29	5.63
ZZ	0.05	0.02	0.40	0.50	0.98
Total MC	0.32±0.04	0.10±0.01	2.39±0.25	3.79±0.41	6.60±0.70
(Stat.)	±0.01	±0.01	±0.04	±0.04	±0.06
(Syst.)	±0.00	±0.00	±0.00	±0.01	±0.01
(Cross section)	±0.03	±0.01	±0.20	±0.33	±0.57
(Luminosity)	±0.02	±0.01	±0.14	±0.23	±0.40
Fermiophobic higgs (Wh110)	0.099±0.009	0.034±0.004	0.937±0.075	1.325±0.105	2.394±0.189
Fermiophobic higgs (Zh110)	0.010±0.002	0.003±0.001	0.102±0.009	0.126±0.011	0.241±0.020
Total	0.109±0.010	0.037±0.004	1.039±0.080	1.451±0.111	2.636±0.201
(Stat.)	±0.005	±0.003	±0.017	±0.020	±0.027
(Syst.)	±0.000	±0.000	±0.001	±0.002	±0.003
(Cross section)	±0.005	±0.002	±0.047	±0.067	±0.120
(Luminosity)	±0.007	±0.002	±0.062	±0.087	±0.158
SM higgs (Wh160)	0.030±0.003	0.006±0.001	0.190±0.015	0.497±0.039	0.723±0.057
SM higgs (Zh160)	0.003±0.001	0.001±0.000	0.023±0.002	0.057±0.005	0.084±0.007
Total	0.033±0.003	0.007±0.001	0.213±0.016	0.554±0.042	0.807±0.061
(Stat.)	±0.001	±0.001	±0.004	±0.006	±0.007
(Syst.)	±0.000	±0.000	±0.000	±0.001	±0.001
(Cross section)	±0.002	±0.000	±0.010	±0.025	±0.036
(Luminosity)	±0.002	±0.000	±0.013	±0.033	±0.048
Total expected	2.62±0.47	15.73±1.74	97.31±6.97	8.69±1.00	124.35±8.35
Data	3	9	114	8	134

Table 13: Background expectation and observed number of events for opposite-sign dilepton events.

	Regions				
	1	2	3	4	Total
Fakes	24.41	20.45	77.23	22.22	144.31
Photon-conversions	28.70	31.78	42.85	18.09	121.42
Total	53.11±20.53	52.23±4.67	120.07±8.61	40.32±35.08	265.73±57.32
(Stat.)	±3.73	±2.72	±4.10	±5.82	±8.51
(Syst.)	±20.19	±3.80	±7.57	±34.59	±56.68
$Z/\gamma^* \to ee$	4332.23	2936.03	3159.69	2328.85	12756.80
$Z/\gamma^* \to \mu\mu$	4997.50	1051.32	768.94	1877.48	8695.21
$Z/\gamma^* \to \tau\tau$	389.48	544.58	574.72	126.00	1634.79
$t\bar{t}$	3.69	1.13	27.16	90.26	122.24
WW	15.01	4.15	49.20	110.07	178.43
WZ	0.76	0.30	3.73	6.95	11.74
ZZ	0.78	0.52	4.40	7.93	13.63
Total MC	9739.45±587.96	4538.02±276.07	4587.84±279.08	4547.54±276.40	23412.83±1408.45
(Stat.)	±64.88	±45.58	±45.96	±44.10	±101.71
(Syst.)	±0.00	±0.00	±0.00	±0.00	±0.00
(Cross section)	±0.11	±0.06	±0.58	±1.05	±1.80
(Luminosity)	±584.37	±272.28	±275.27	±272.85	±1404.77
Fermiophobic higgs (Wh110)	0.099±0.009	0.064±0.007	1.275±0.101	1.518±0.120	2.957±0.233
Fermiophobic higgs (Zh110)	0.021±0.003	0.024±0.003	0.480±0.039	0.569±0.046	1.094±0.087
Total	0.120±0.010	0.088±0.008	1.755±0.127	2.087±0.151	4.051±0.292
(Stat.)	±0.006	±0.005	±0.022	±0.023	±0.033
(Syst.)	±0.000	±0.000	±0.000	±0.000	±0.000
(Cross section)	±0.005	±0.003	±0.068	±0.081	±0.158
(Luminosity)	±0.007	±0.005	±0.105	±0.125	±0.243
SM higgs (Wh160)	0.034±0.003	0.010±0.001	0.285±0.023	0.877±0.069	1.206±0.095
SM higgs (Zh160)	0.010±0.001	0.005±0.001	0.124±0.010	0.422±0.033	0.562±0.044
Total	0.045±0.004	0.015±0.001	0.409±0.030	1.299±0.092	1.768±0.126
(Stat.)	±0.002	±0.001	±0.005	±0.009	±0.011
(Syst.)	±0.000	±0.000	±0.000	±0.000	±0.000
(Cross section)	±0.002	±0.001	±0.016	±0.049	±0.067
(Luminosity)	±0.003	±0.001	±0.025	±0.078	±0.106
Total expected	9792.56±588.32	4590.25±276.11	4707.91±279.21	4587.86±278.61	23678.56±1409.61
Data	9046	4311	4243	4283	21883

Table 14: Background expectation and observed number of events for opposite-sign and like-sign dilepton events.

	Opposite-Sign	Like-Sign
Fakes	144.31	90.54
Photon-conversions	121.42	27.21
Total	265.66±57.32	117.75±8.32
(Stat.)	±8.51	±3.69
(Syst.)	±56.69	±7.46
$Z/\gamma^* \to ee$	12754.32	-
$Z/\gamma^* \to \mu\mu$	8615.39	-
$Z/\gamma^* \to \tau\tau$	1627.39	-
$t\bar{t}$	121.71	-
WW	177.63	-
WZ	11.69	5.63
ZZ	13.58	0.98
Total MC	23321.70±1403.17	6.60±0.70
(Stat.)	±101.54	±0.06
(Syst.)	±23.25	±0.01
(Cross section)	±1.79	±0.57
(Luminosity)	±1399.30	±0.40
Fermiophobic higgs (Wh110)	2.943±0.232	2.394±0.189
Fermiophobic higgs (Zh110)	1.088±0.086	0.241±0.020
Total	4.031±0.290	2.636±0.201
(Stat.)	±0.033	±0.027
(Syst.)	±0.005	±0.003
(Cross section)	±0.157	±0.120
(Luminosity)	±0.242	±0.158
SM higgs (Wh160)	1.200±0.094	0.723±0.057
SM higgs (Zh160)	0.559±0.044	0.084±0.007
Total	1.759±0.125	0.807±0.061
(Stat.)	±0.011	±0.007
(Syst.)	±0.002	±0.001
(Cross section)	±0.066	±0.036
(Luminosity)	±0.106	±0.048
Total expected	23587.36±1404.35	124.35±8.35
Data	21773	134

Table 15: BDT input parameters.

BDT Input Parameter	Value
Boost Algorithm	AdaBoost
Separation Type	Gini Index
Tree Prune Method	Cost-Complexity
Minimum number of events required in a leaf node	10
Number of steps during node cut optimisation	20
Tree Prune Strength	-1
Number of Trees	10000

Table 16: Summary of observed events, expected events, and the difference between those for $Z\rightarrow\ell^{\pm}\ell^{\mp}$ pairs in period 0 through 34.

Dilepton Type	Observed Events (O)	Expected Events (E)	(O-E)/O
CEM-CEM	69853	71647 $\pm$ 2200	-0.0257
CMUP-CMUP	17987	17885 $\pm$ 581	-0.0057
CMX-CMUP	10550	11144 $\pm$ 379	-0.0563
CMUP-CMX	10781	11473 $\pm$ 389	-0.0642
CMX-CMX	7883	7216 $\pm$ 254	0.0846
Overall	117054	119365 $\pm$ 2400	0.0198

Table 17: Wh Systematic uncertainty(%).

Mass (GeV/c^2)	110	120	130	140	150	160	170	180	190	200
MC statistics	1.06	1.03	0.99	0.96	0.95	0.97	0.95	0.93	0.88	0.85
MC scale factors	0.14	0.13	0.13	0.13	0.13	0.12	0.13	0.12	0.14	0.14
PDF	2.38	1.98	1.82	1.86	1.51	1.08	1.60	1.00	0.99	0.61
ISR	2.68	2.68	2.68	2.68	3.51	3.51	3.51	3.51	3.51	3.51
FSR	4.90	4.90	4.90	4.90	4.44	4.44	4.44	4.44	4.44	4.44
Cross Section	5.00	5.00	5.00	5.00	5.00	5.00	5.00	5.00	5.00	5.00
Z Cross Section	1.98	1.98	1.98	1.98	1.98	1.98	1.98	1.98	1.98	1.98
Luminosity	6.00	6.00	6.00	6.00	6.00	6.00	6.00	6.00	6.00	6.00
Total	10.1	10.1	10.0	10.0	10.0	10.0	10.0	9.94	9.94	9.90

Table 18: Zh Systematic uncertainty(%).

Mass (GeV/c^2)	110	120	130	140	150	160	170	180	190	200
MC statistics	3.11	2.91	2.83	2.77	2.65	2.74	2.74	2.54	2.56	2.35
MC scale factors	0.17	0.15	0.12	0.15	0.18	0.12	0.14	0.17	0.23	0.29
PDF	2.84	2.06	1.87	2.00	2.40	1.43	1.04	1.50	1.08	0.84
ISR	3.86	3.86	3.86	3.86	3.86	3.86	3.86	3.86	3.86	3.86
FSR	1.40	1.40	1.40	1.40	1.40	1.40	1.40	1.40	1.40	1.40
Cross Section	5.00	5.00	5.00	5.00	5.00	5.00	5.00	5.00	5.00	5.00
Z Cross Section	1.98	1.98	1.98	1.98	1.98	1.98	1.98	1.98	1.98	1.98
Luminosity	6.00	6.00	6.00	6.00	6.00	6.00	6.00	6.00	6.00	6.00
Total	9.98	9.72	9.66	9.67	9.73	9.56	9.51	9.51	9.46	9.39

Table 19: Systematic uncertainty(%) for background.

	Fake leptons	Residual photon-conversion	WZ	ZZ
Statistics	2.71	1.01	0.89	3.06
Fake rate	8.06	-	-	-
Residual conversion rate	-	0.59	-	-
MC scale factors	-	-	0.14	0.13
Cross Section	-	-	10.00	10.00
Luminosity	-	-	6.00	6.00
Total	8.50	1.17	16.5	16.5

Table 20: The 95 % C.L. relative cross section limit to fermiophobic higgs. Only Wh signal.

Mass (GeV/c^2)	Expected limit					Observed limit
	-2σ	-1σ	Median	$+1\sigma$	$+2\sigma$	
110	2.56	3.47	4.98	7.08	9.63	4.97
120	2.97	4.02	5.68	8.04	11.0	5.76
130	3.42	4.64	6.56	9.25	12.7	7.24
140	4.19	5.55	7.83	11.2	15.1	8.40
150	4.83	6.35	8.93	12.7	17.5	10.9
160	5.87	7.65	10.6	15.1	21.1	11.1
170	6.87	8.85	12.3	17.3	23.9	13.8
180	8.23	10.6	14.5	20.5	28.5	16.7
190	11.1	14.2	19.7	28.0	38.9	22.1
200	13.8	17.6	24.1	33.8	47.5	29.3

Table 21: The 95 % C.L. relative cross section limit to the Standard Model higgs. Only Wh signal.

Mass (GeV/c^2)	Expected limit					Observed limit
	-2σ	-1σ	Median	$+1\sigma$	$+2\sigma$	
110	42.7	55.9	76.7	108.7	150.5	95.1
120	17.2	22.4	31.3	44.3	60.8	37.2
130	9.63	12.5	17.5	24.7	34.2	21.5
140	7.12	9.40	13.1	18.4	25.5	14.9
150	6.15	7.99	11.2	15.8	21.9	14.1
160	6.12	8.00	11.1	15.8	21.9	11.7
170	6.94	8.91	12.4	17.5	24.0	14.0
180	8.29	10.7	14.7	20.6	28.4	16.8
190	11.2	14.4	19.9	28.1	39.0	22.2
200	13.9	17.6	24.2	34.0	47.8	29.4

Table 22: The 95 % C.L. relative cross section limit to fermiophobic higgs. Including both Wh and Zh signals.

Mass (GeV/c^2)	Expected limit					Observed limit
	-2σ	-1σ	Median	$+1\sigma$	$+2\sigma$	
110	2.33	3.25	4.61	6.51	8.83	4.54
120	2.71	3.68	5.28	7.47	10.2	5.22
130	3.16	4.28	6.05	8.60	11.5	6.55
140	3.79	5.06	7.18	10.1	13.7	7.61
150	4.42	5.76	8.15	11.6	15.8	9.83
160	5.23	6.90	9.70	13.8	19.0	9.93
170	6.16	8.08	11.1	15.8	21.9	12.4
180	7.43	9.51	13.1	18.5	25.5	15.0
190	10.0	12.8	17.9	25.4	34.8	19.8
200	12.5	15.7	21.4	30.3	42.1	26.3

Table 23: The 95 % C.L. relative cross section limit to the Standard Model higgs. Including both Wh and Zh signals.

Mass (GeV/c^2)	Expected limit					Observed limit
	-2σ	-1σ	Median	$+1\sigma$	$+2\sigma$	
110	38.5	50.2	69.8	100.2	138.6	86.9
120	15.8	20.5	28.4	40.0	55.5	33.7
130	8.69	11.5	15.8	22.5	30.8	19.4
140	6.46	8.53	11.9	16.9	23.4	13.5
150	5.56	7.31	10.1	14.4	19.7	12.7
160	5.50	7.20	10.1	14.3	19.9	10.5
170	6.22	8.17	11.2	15.9	22.1	12.6
180	7.47	9.56	13.2	18.7	25.7	15.1
190	10.1	12.9	18.0	25.5	34.8	19.9
200	12.5	15.8	21.6	30.5	42.3	26.4

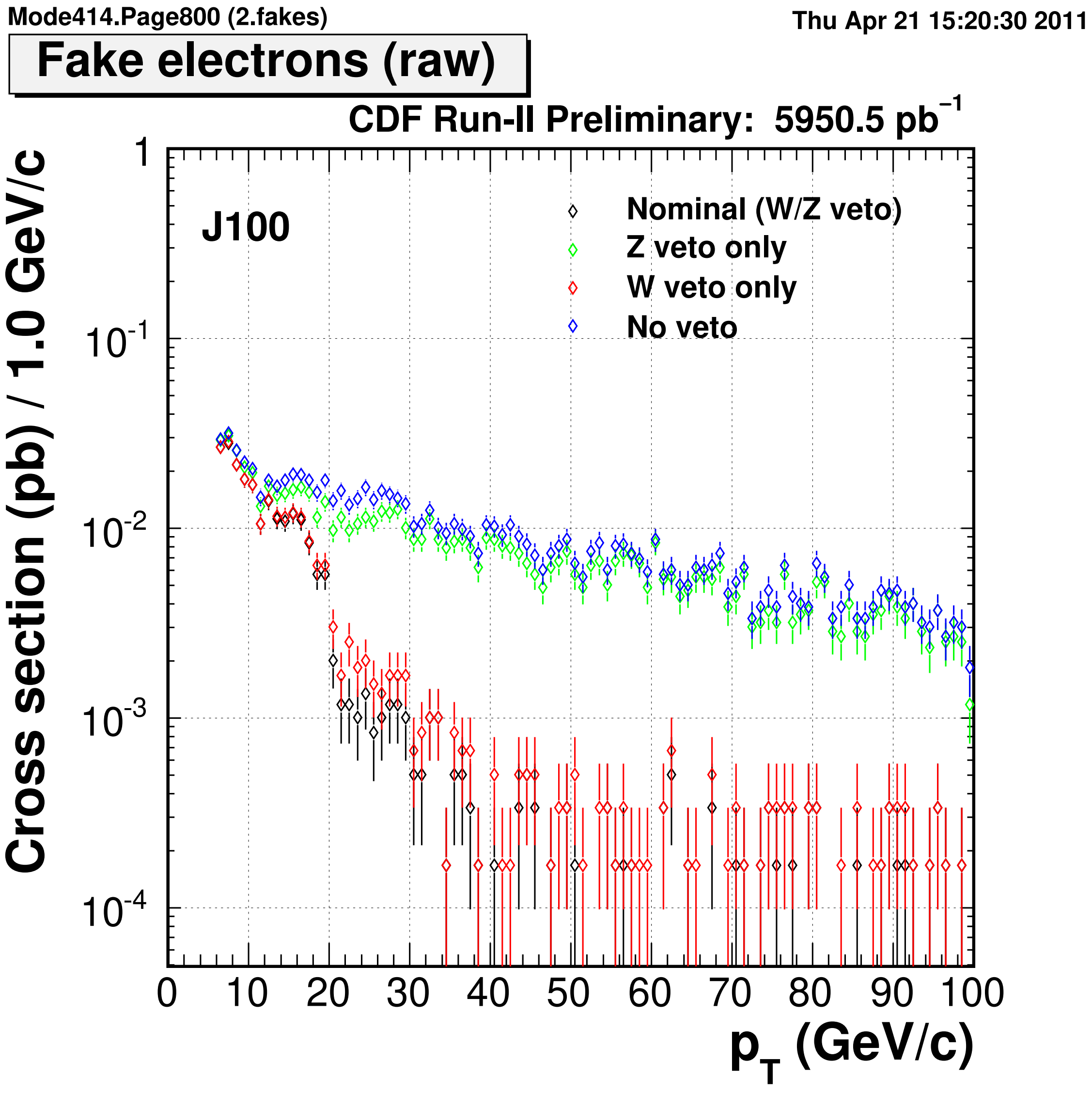

Figure 1: W veto bias for jet 100 sample.

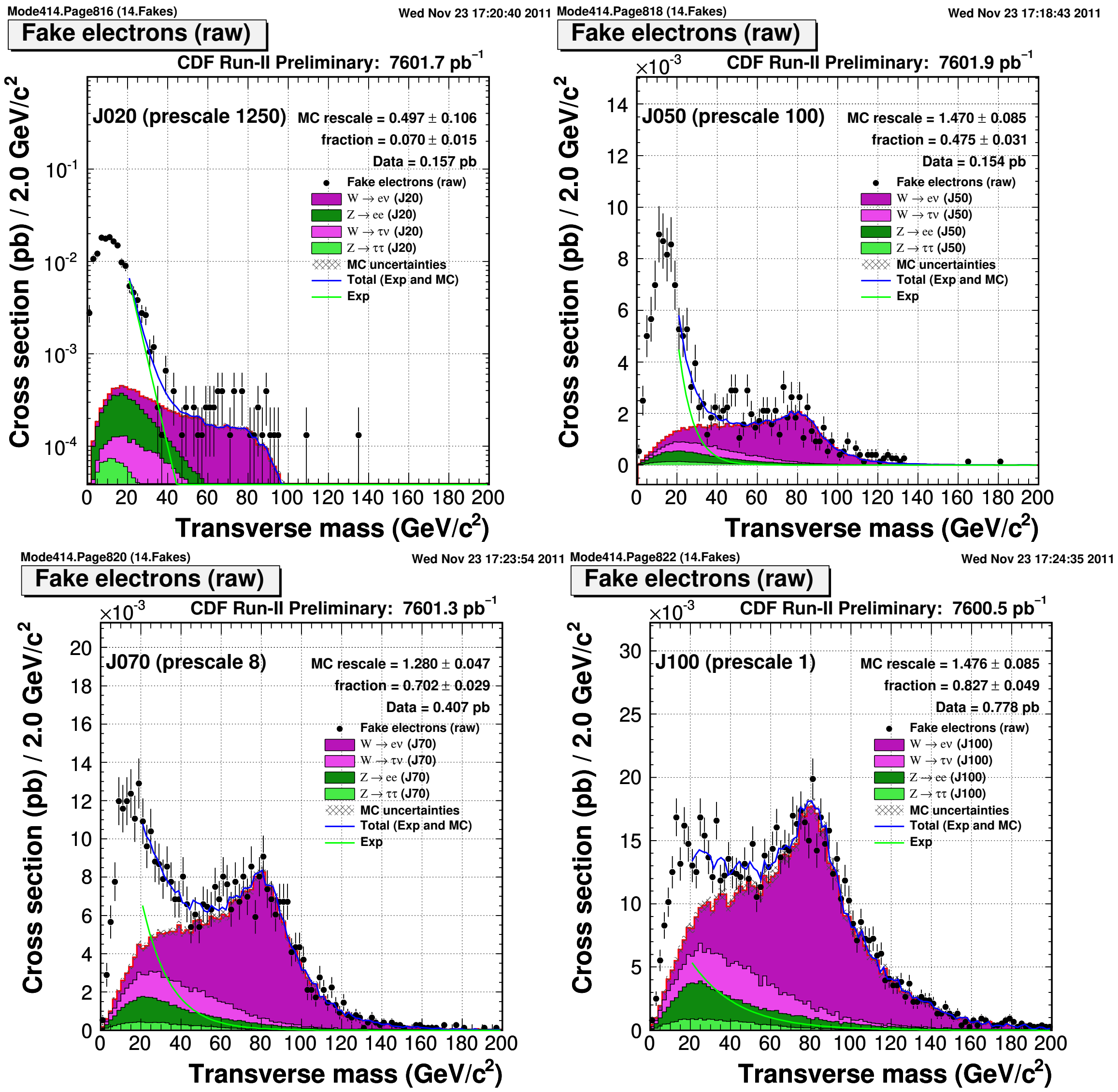

Figure 2: Fake electron transverse mass distributions for each jet samples. We fit MCs to data, and then, we use the parameter to subtract MCs from data to estimate fake leptons.

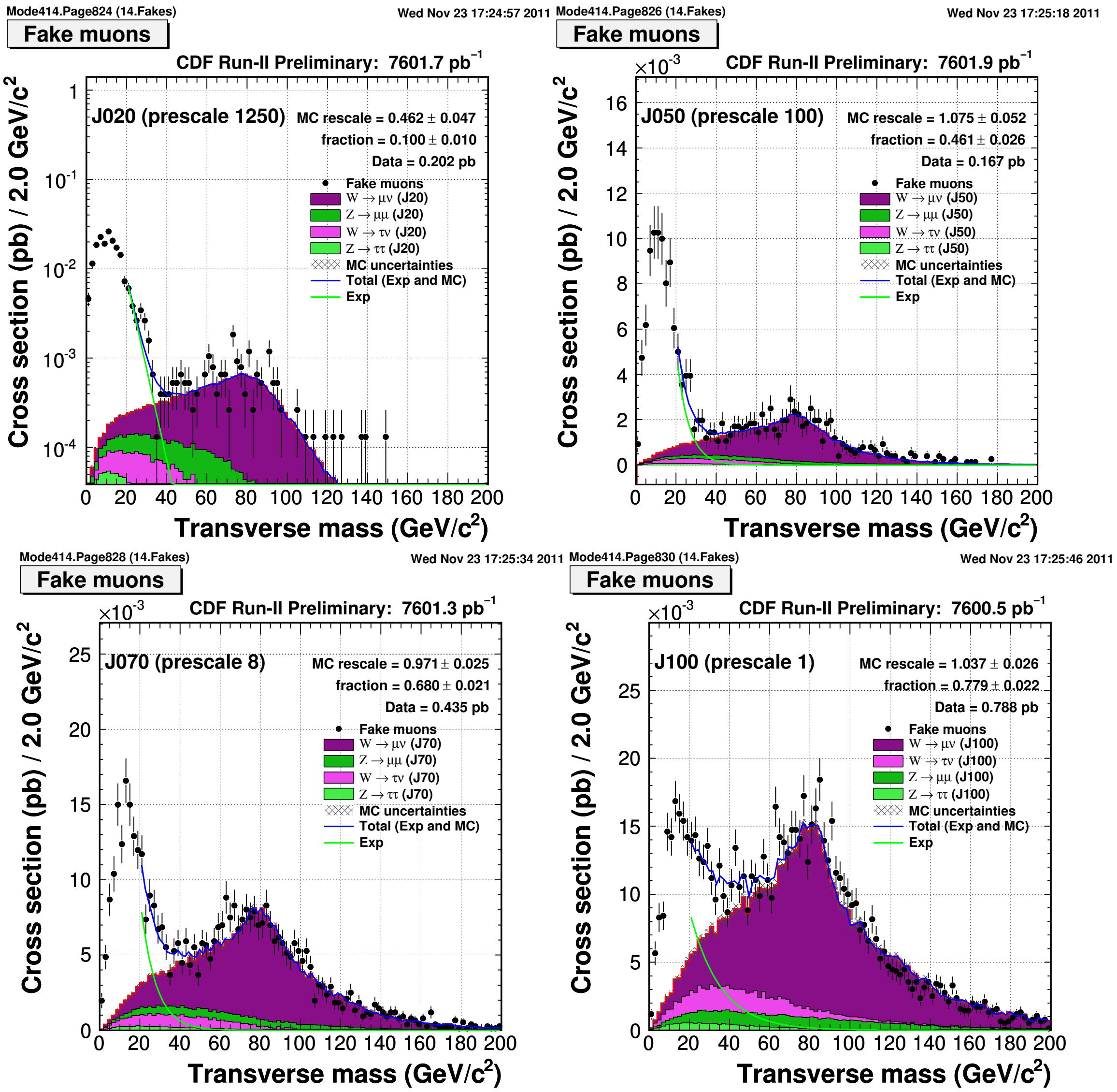

Figure 3: Fake muon transverse mass distributions for each jet samples. We fit MCs to data, and then, we use the parameter to subtract MCs from data to estimate fake leptons.

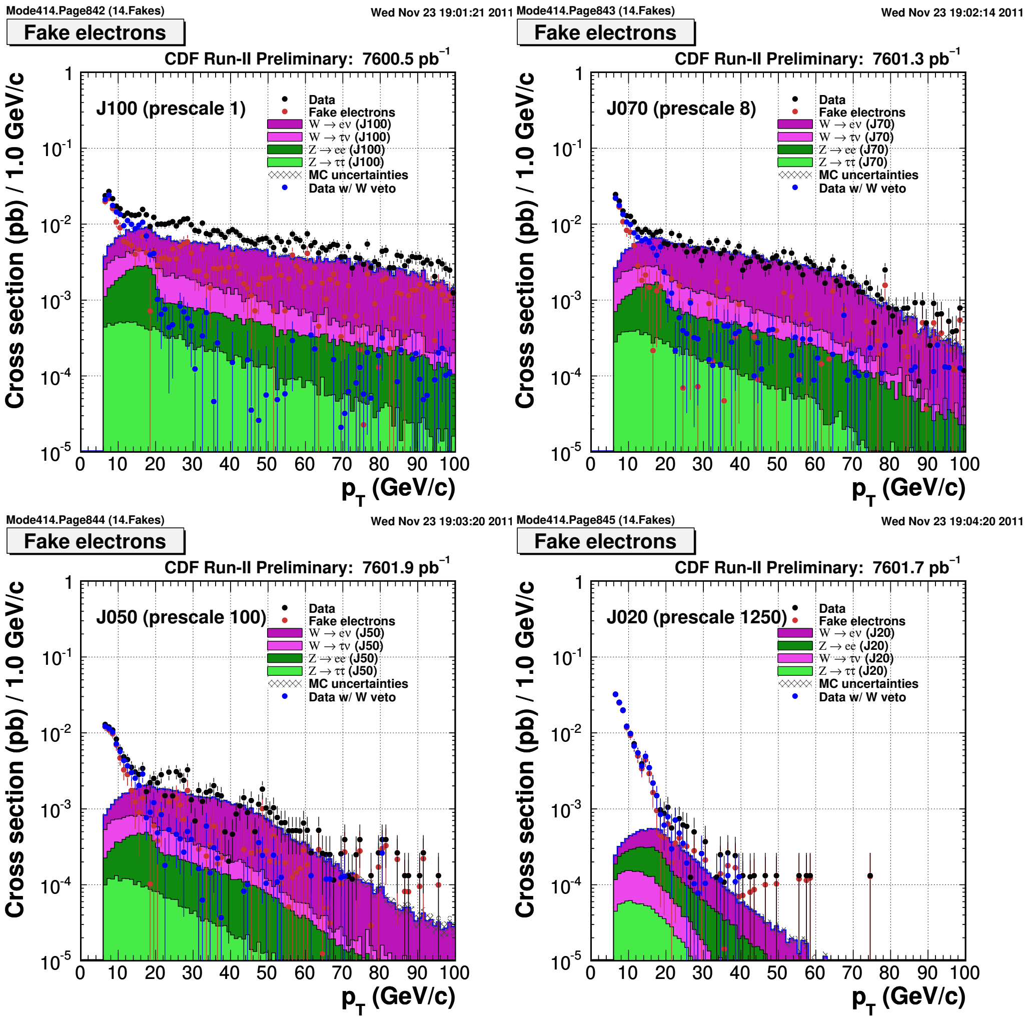

Figure 4: p_T distributions for fake electrons in each jet sample.

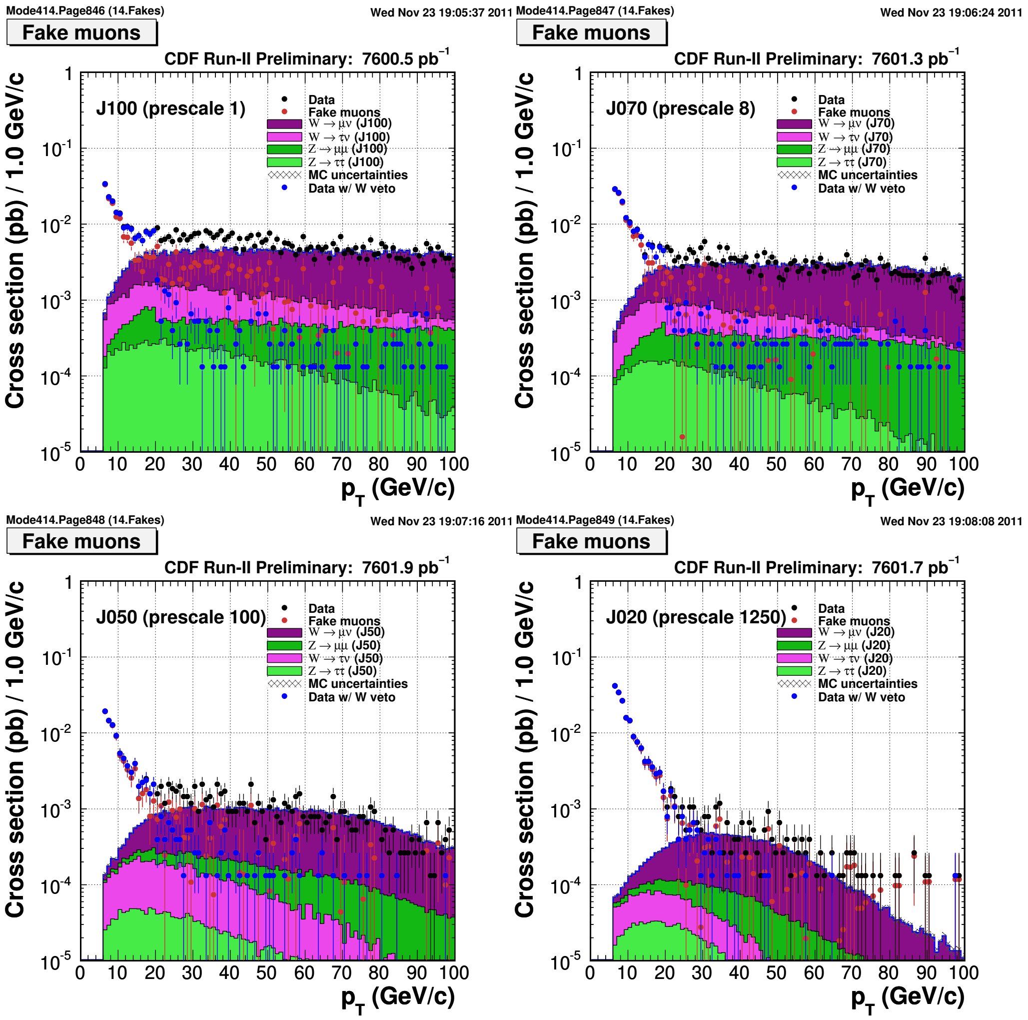

Figure 5: p_T distributions for fake muons in each jet sample.

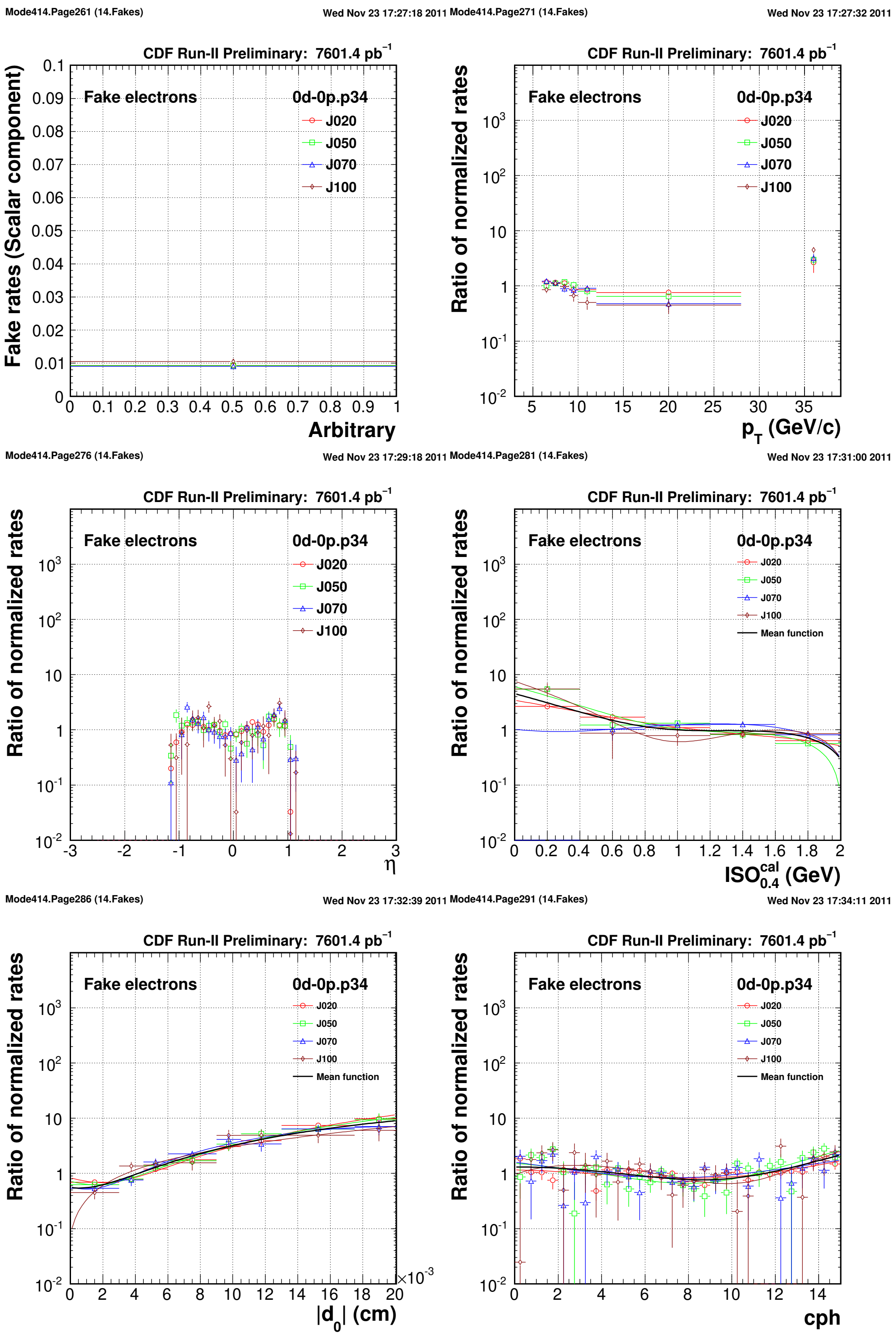

Figure 6: Fake rate and normalized rates for electrons.

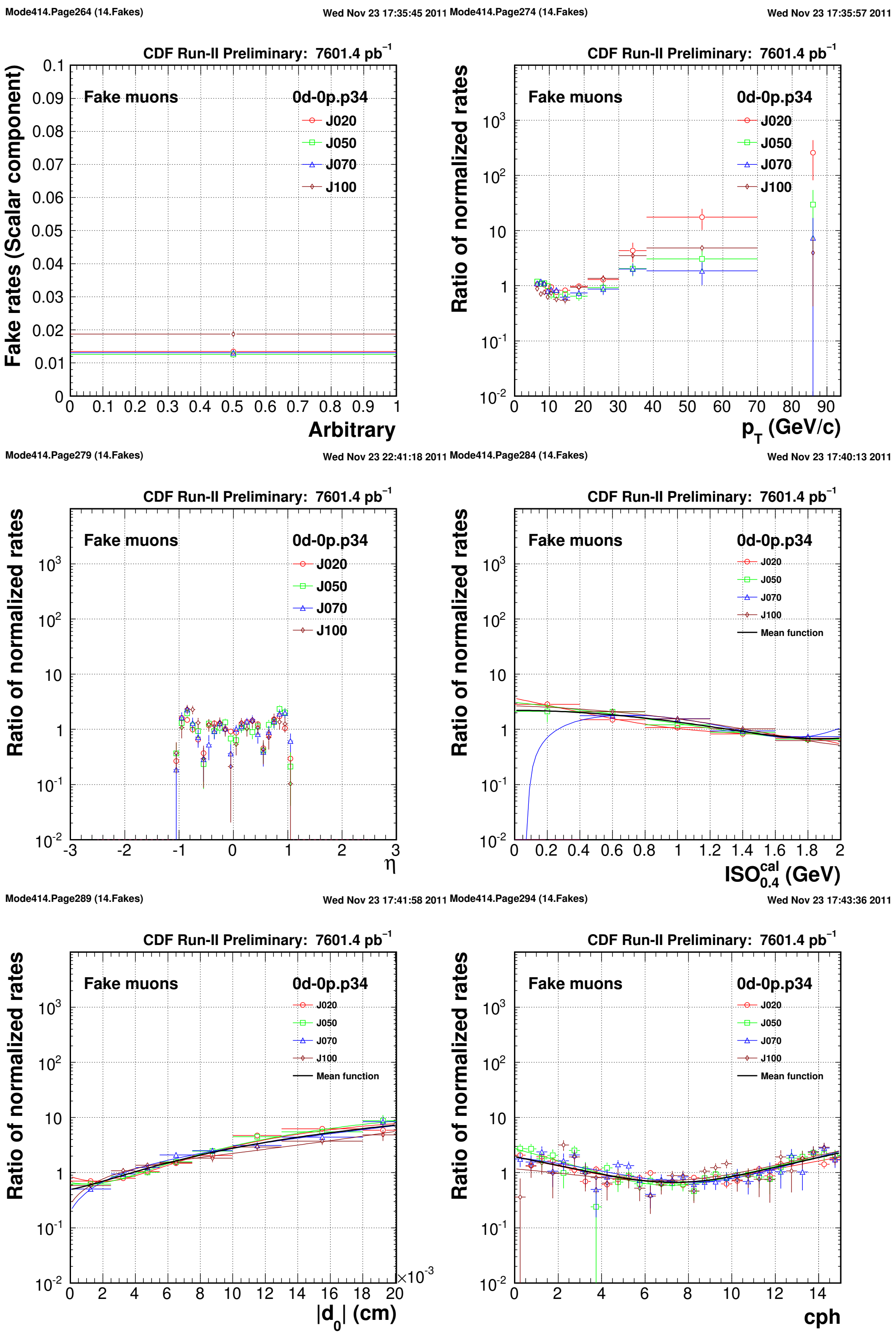

Figure 7: Fake rate and normalized rates for muons.

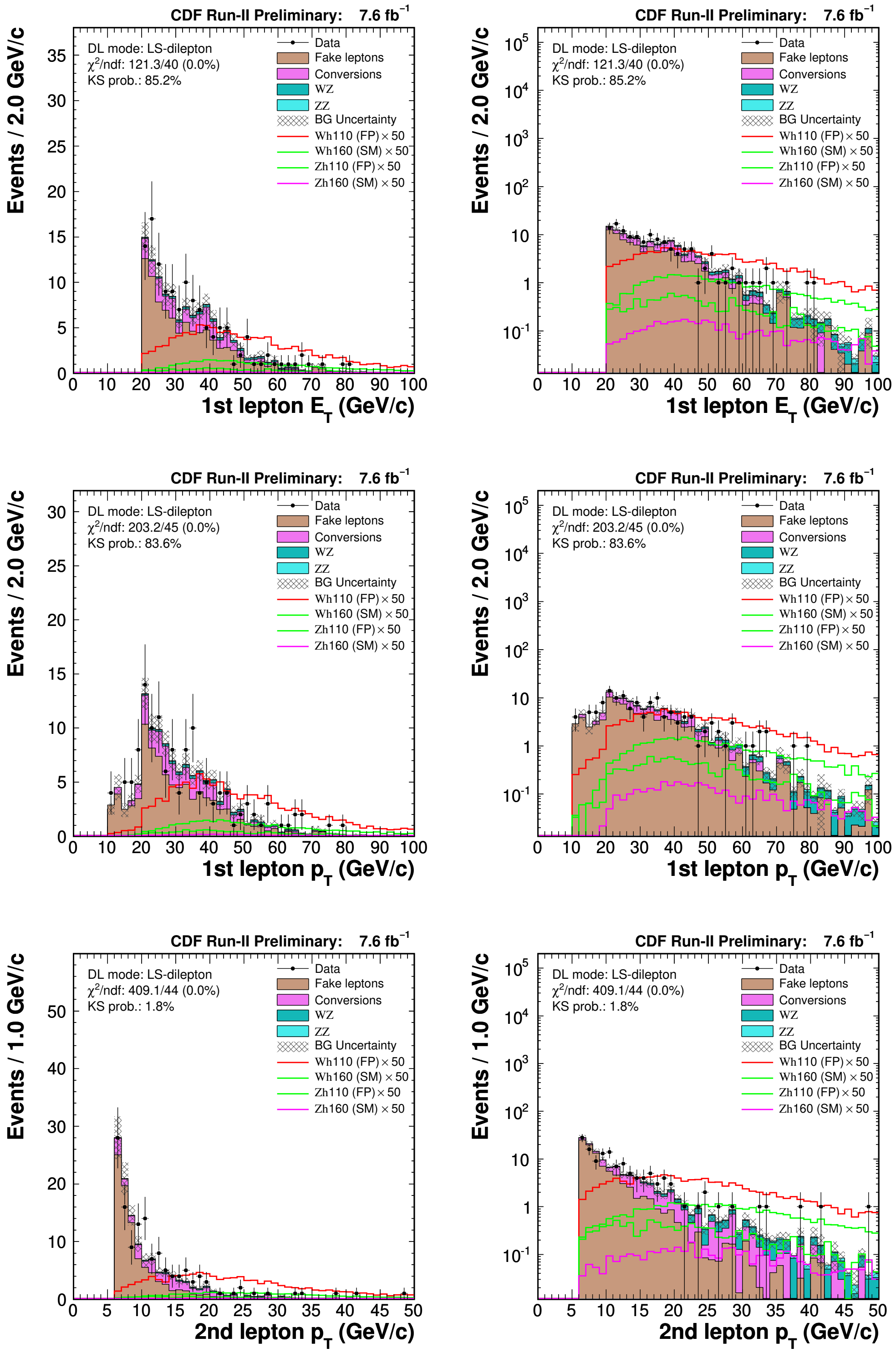

Figure 8: 1st lepton E_T, 1st lepton p_T, and 2nd lepton p_T distributions in the signal region (left: linear, right: log).

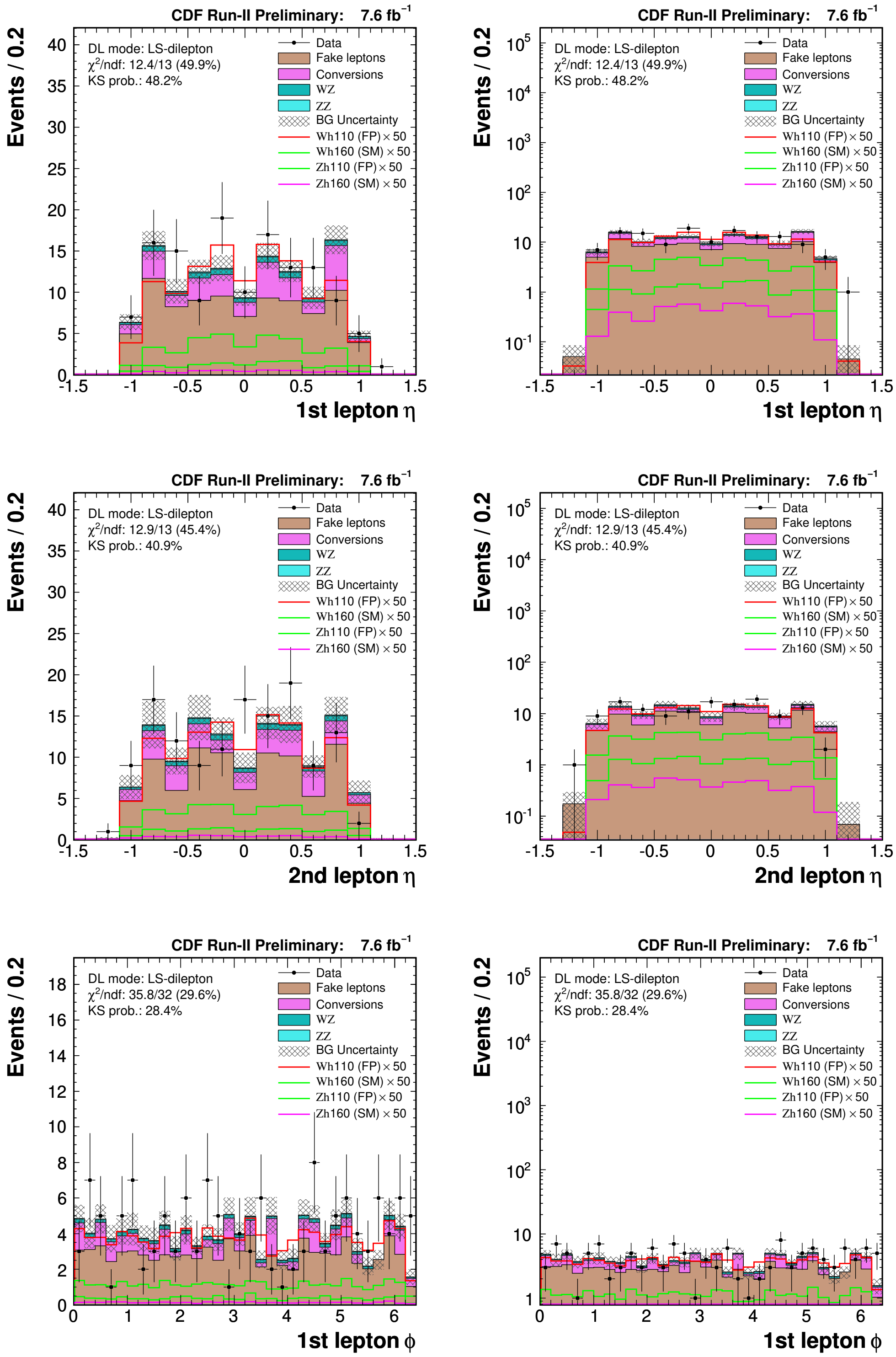

Figure 9: 1st lepton η, 2nd lepton η, and 1st lepton ϕ distributions in the signal region (left: linear, right: log).

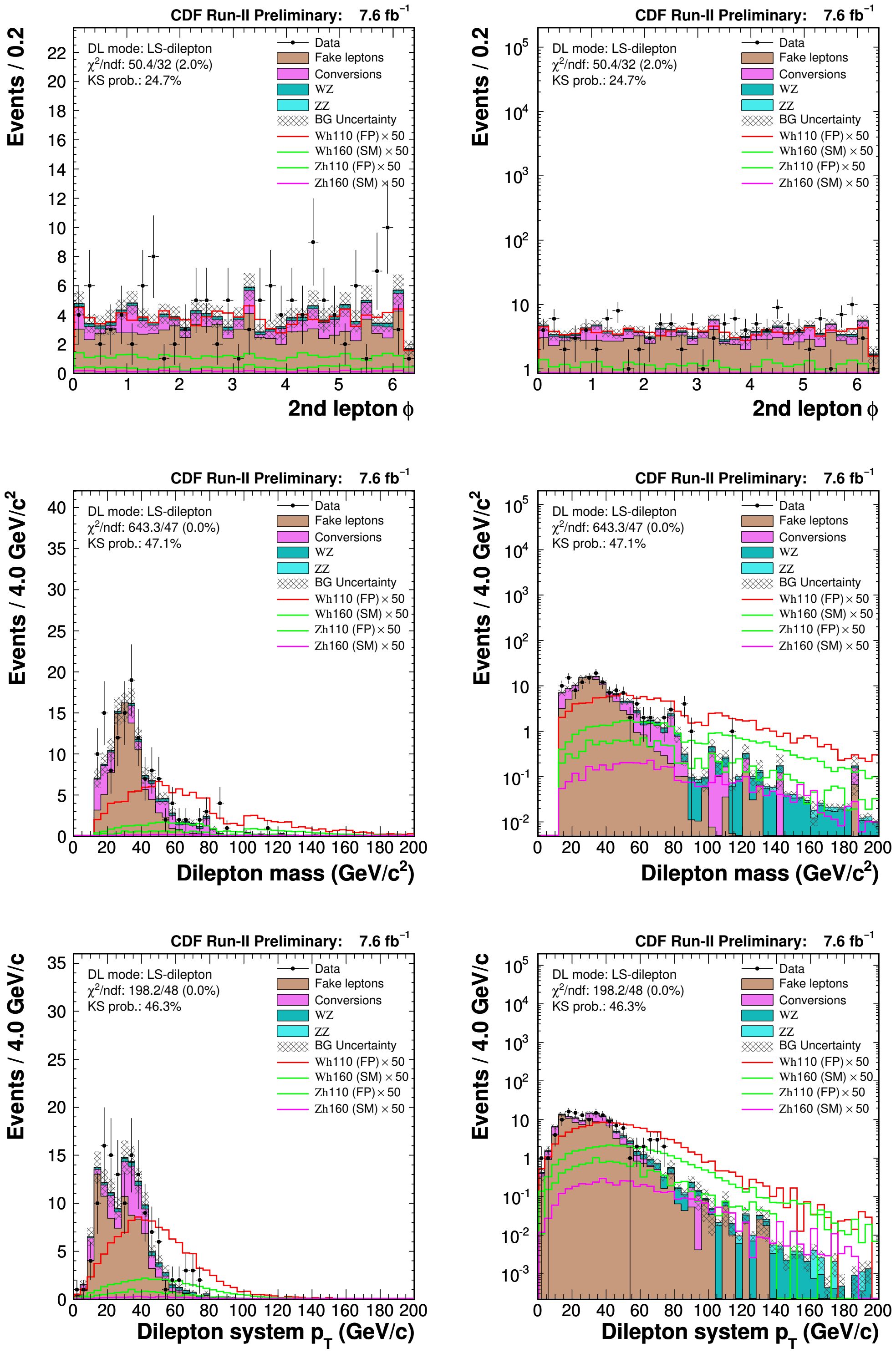

Figure 10: 2nd lepton ϕ, dilepton mass, and dilepton system p_T distributions in the signal region (left: linear, right: log).

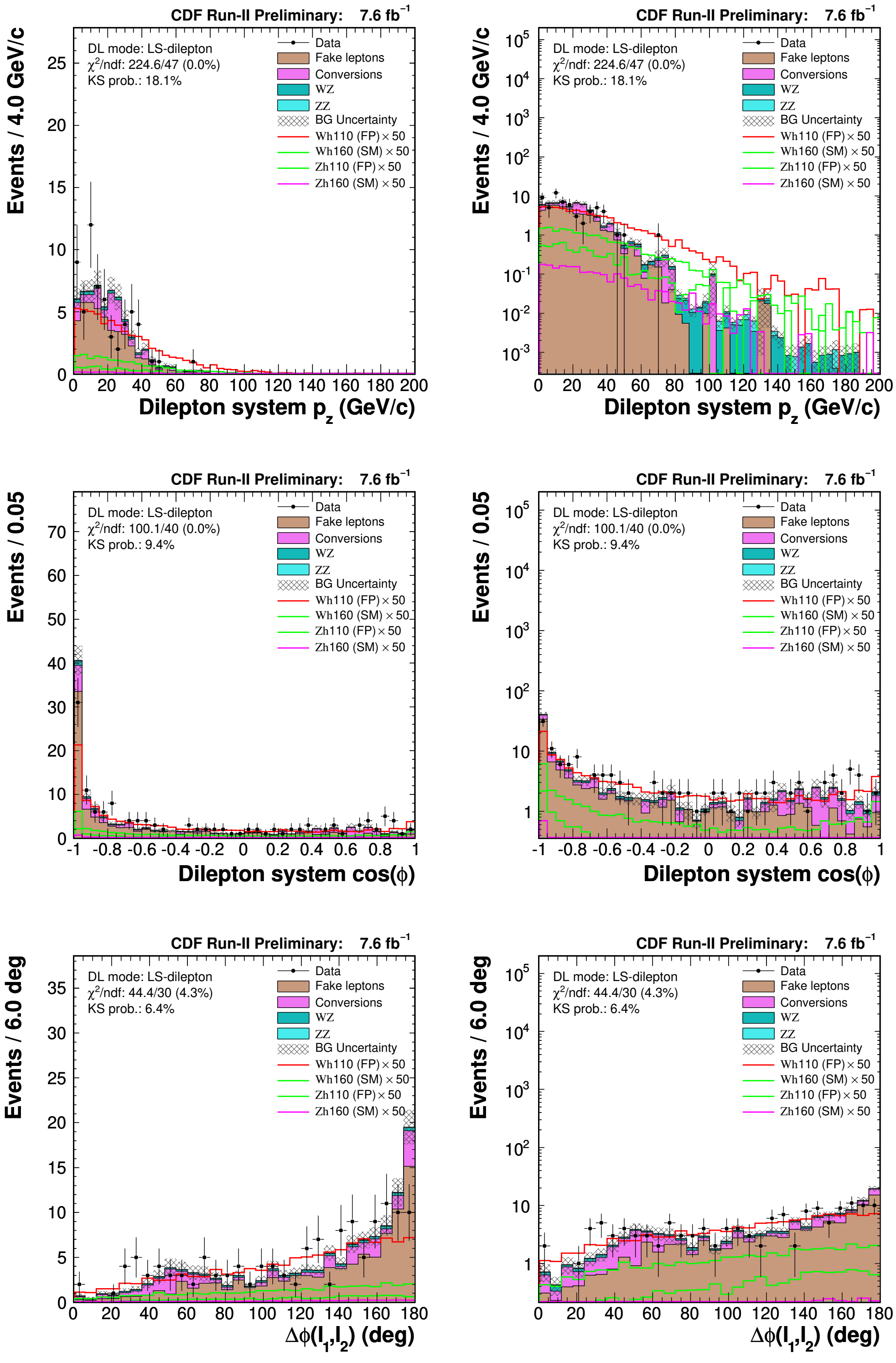

Figure 11: Dilepton system p_z, dilepton system $\cos(\phi)$, and $\Delta\phi(\ell_1, \ell_2)$ distributions in the signal region (left: linear, right: log).

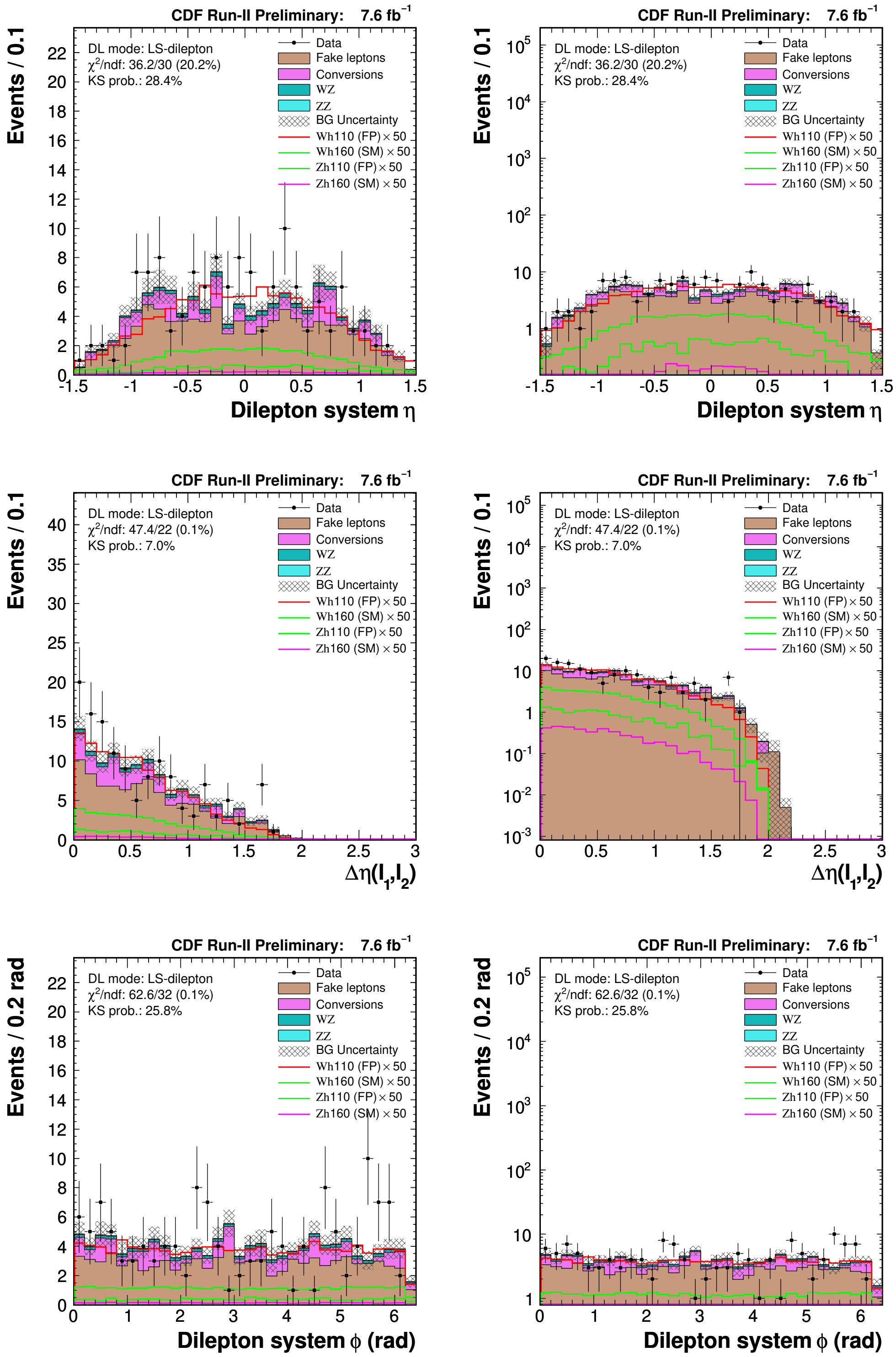

Figure 12: Dilepton system η, $\Delta\eta(\ell_1, \ell_2)$, and dilepton system ϕ distributions in the signal region (left: linear, right: log).

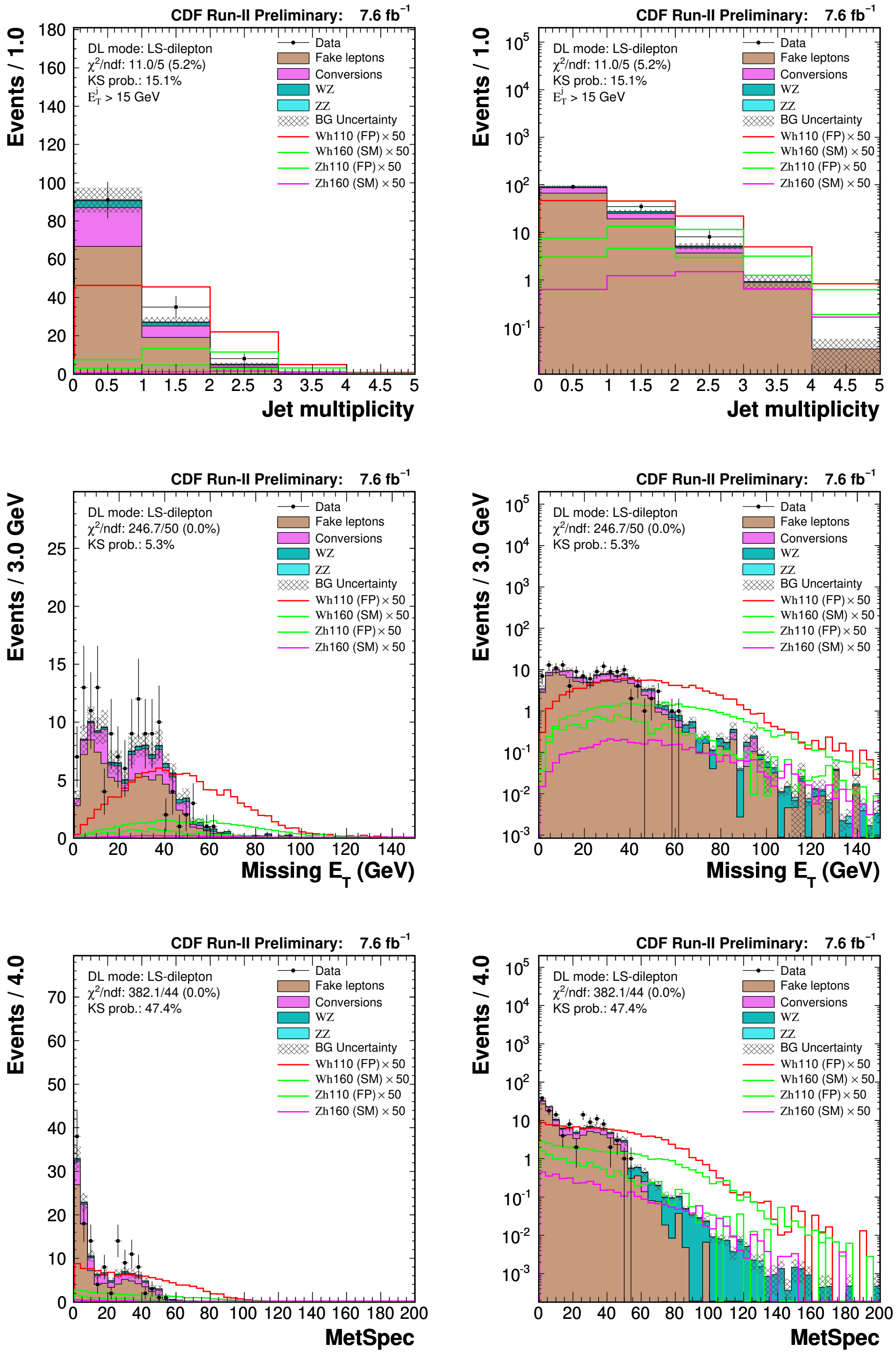

Figure 13: Jet multiplicity, missing E_T, and MetSpec distributions in the signal region (left: linear, right: log).

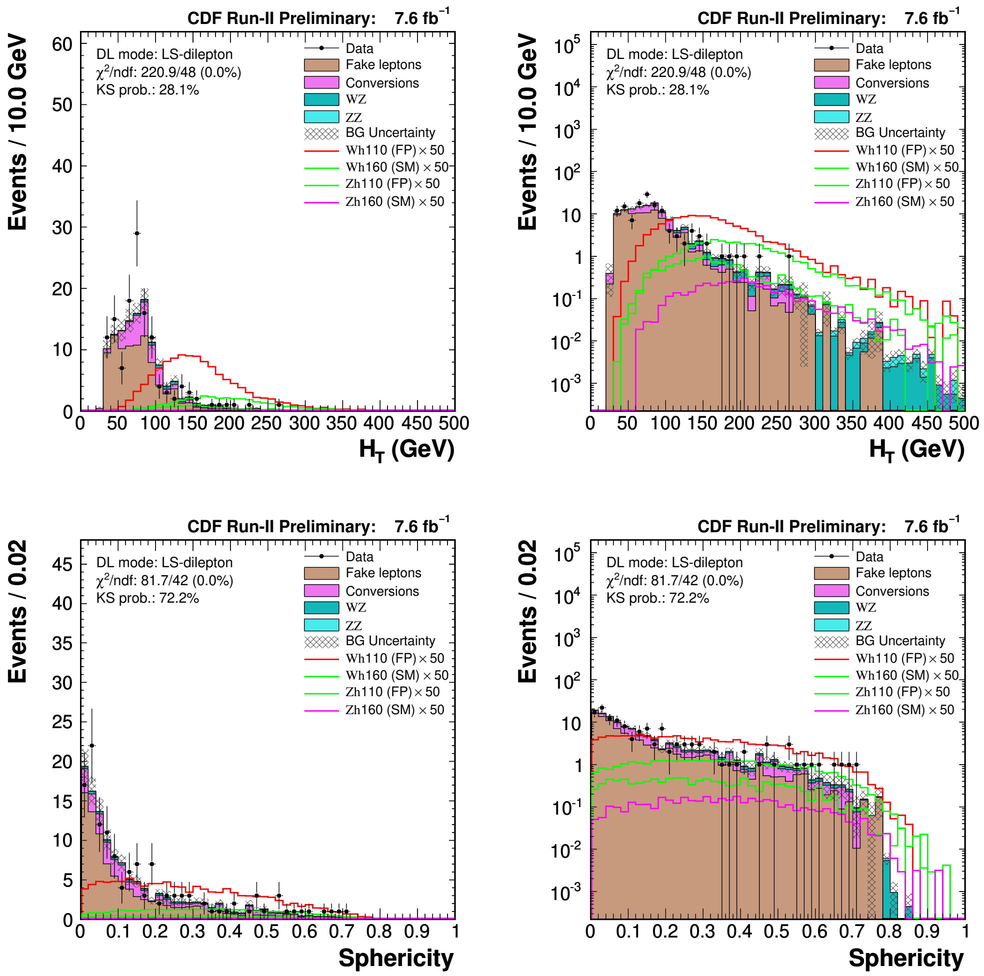

Figure 14: H_T and sphericity distributions in the signal region (left: linear, right: log).

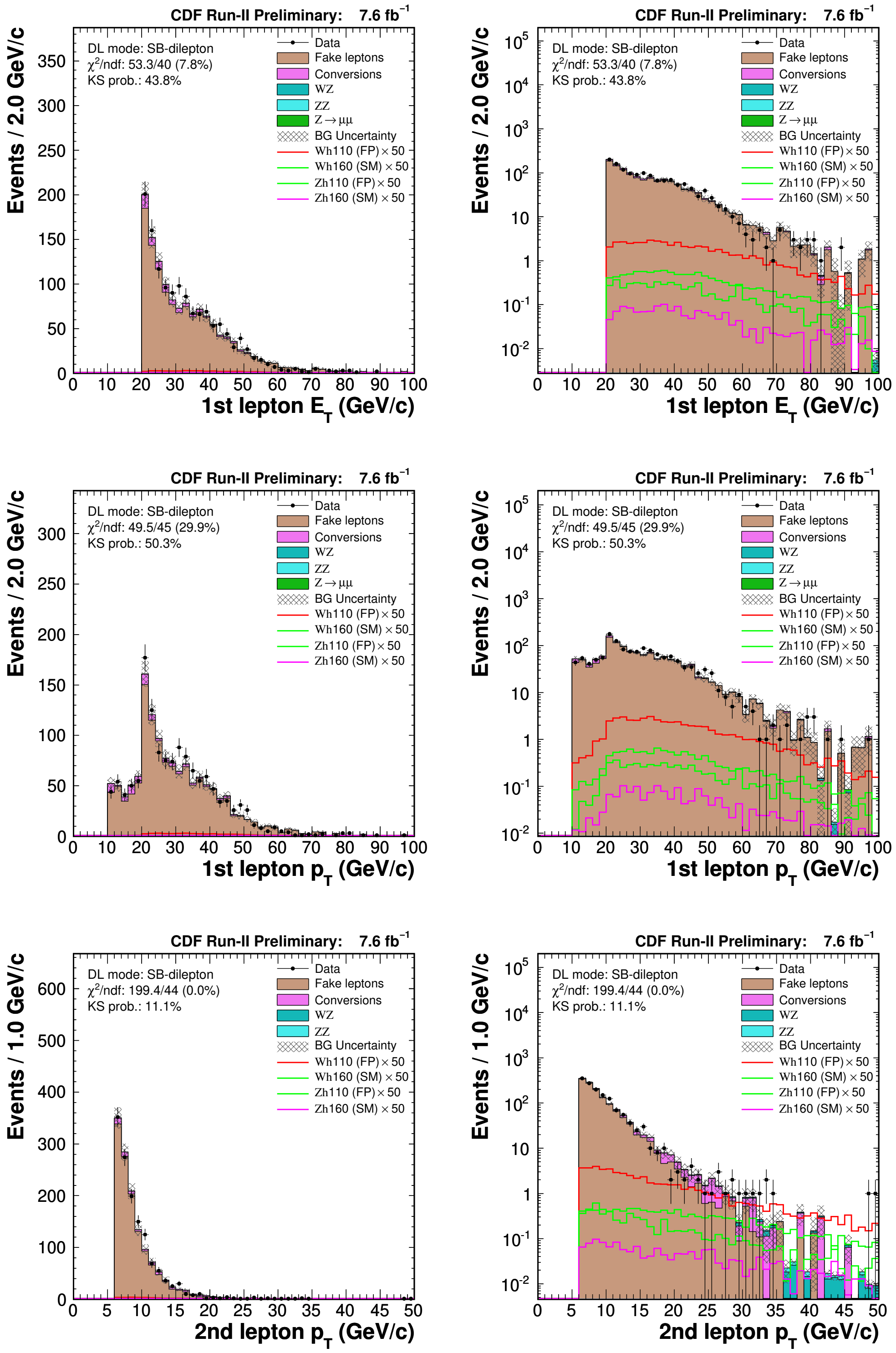

Figure 15: 1st lepton E_T, 1st lepton p_T, and 2nd lepton p_T distributions in the side-band region (left: linear, right: log).

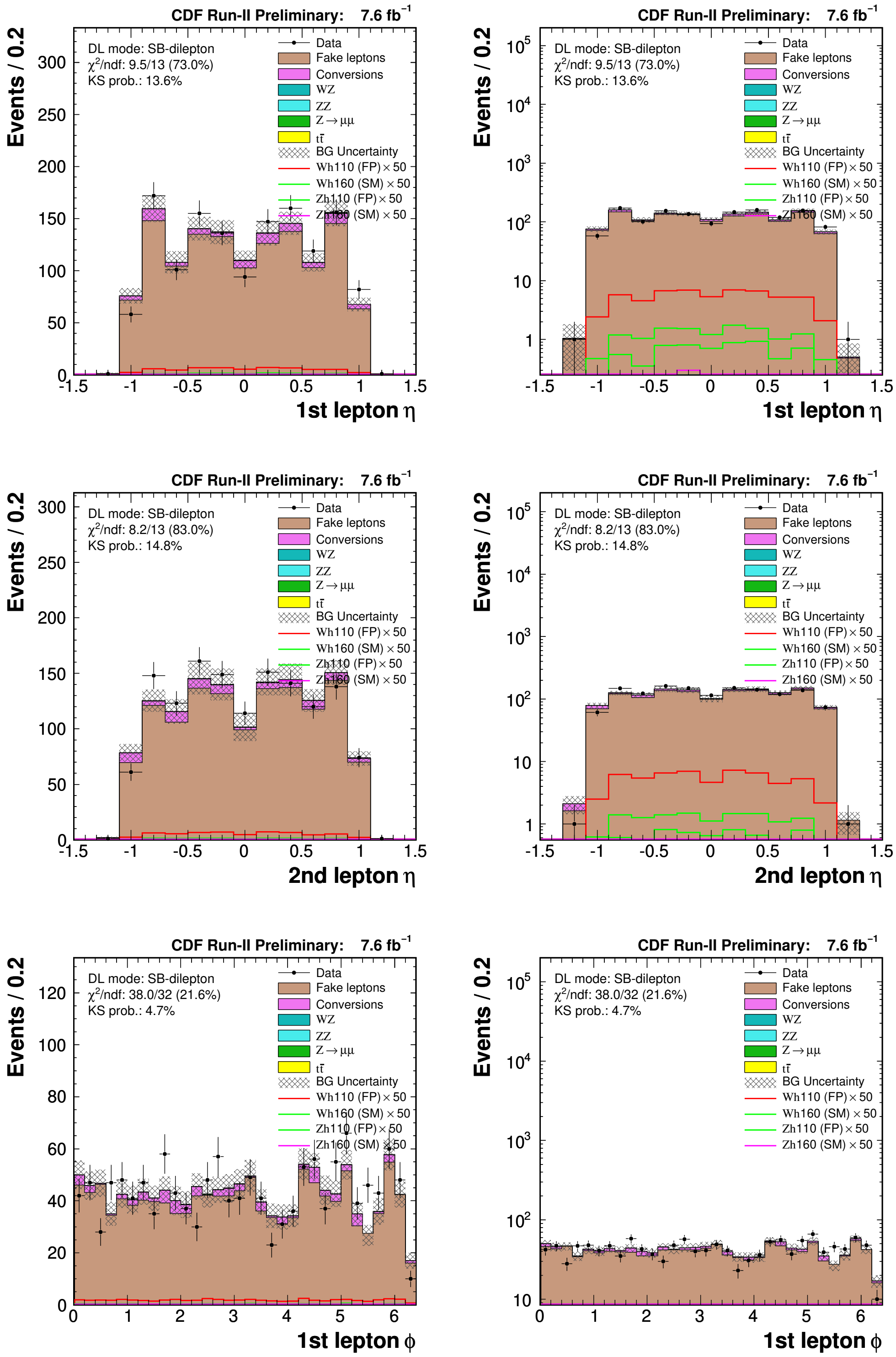

Figure 16: 1st lepton η, 2nd lepton η, and 1st lepton ϕ distributions in the side-band region (left: linear, right: log).

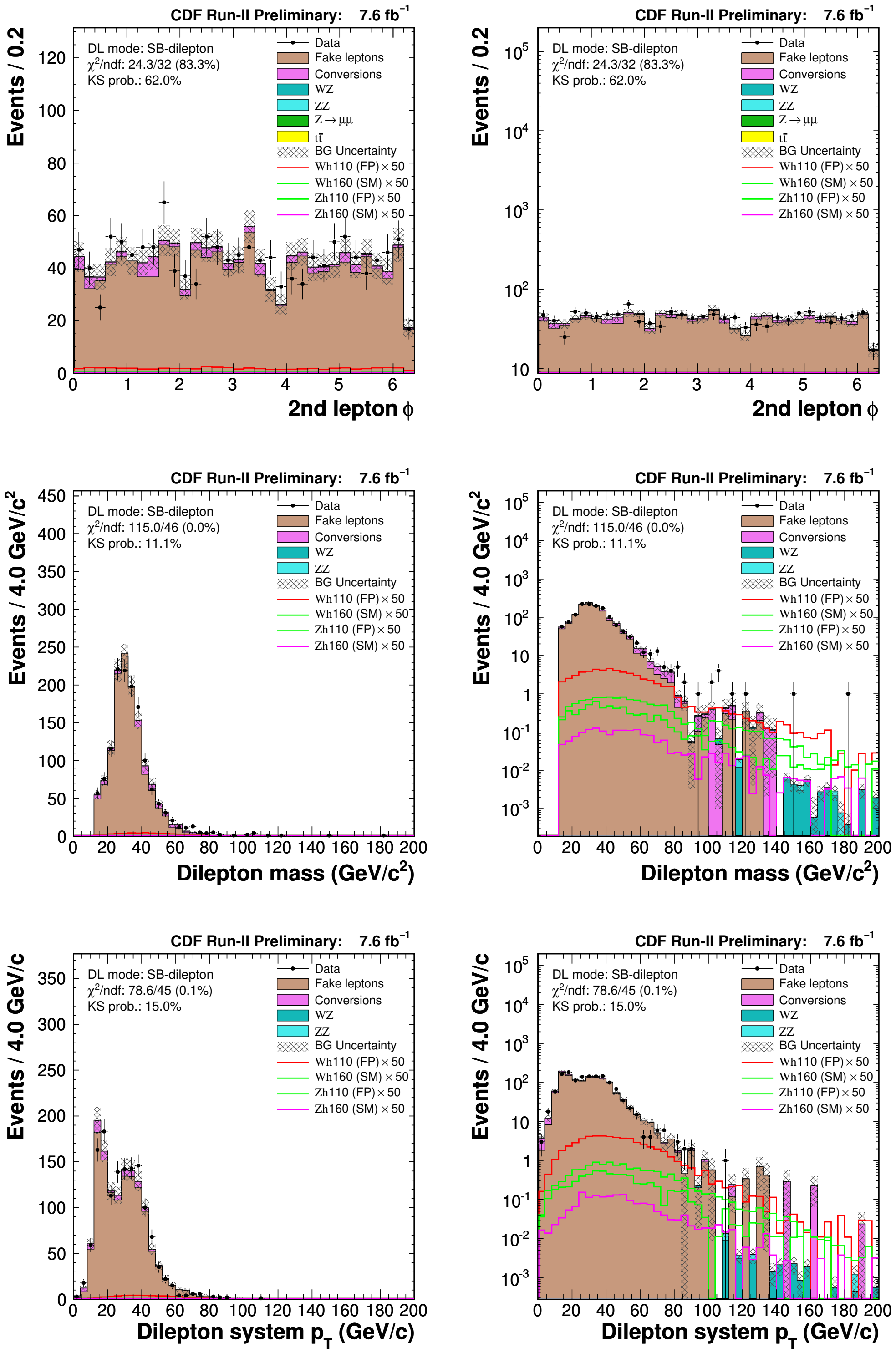

Figure 17: 2nd lepton ϕ, dilepton mass, and dilepton system p_T distributions in the side-band region (left: linear, right: log).

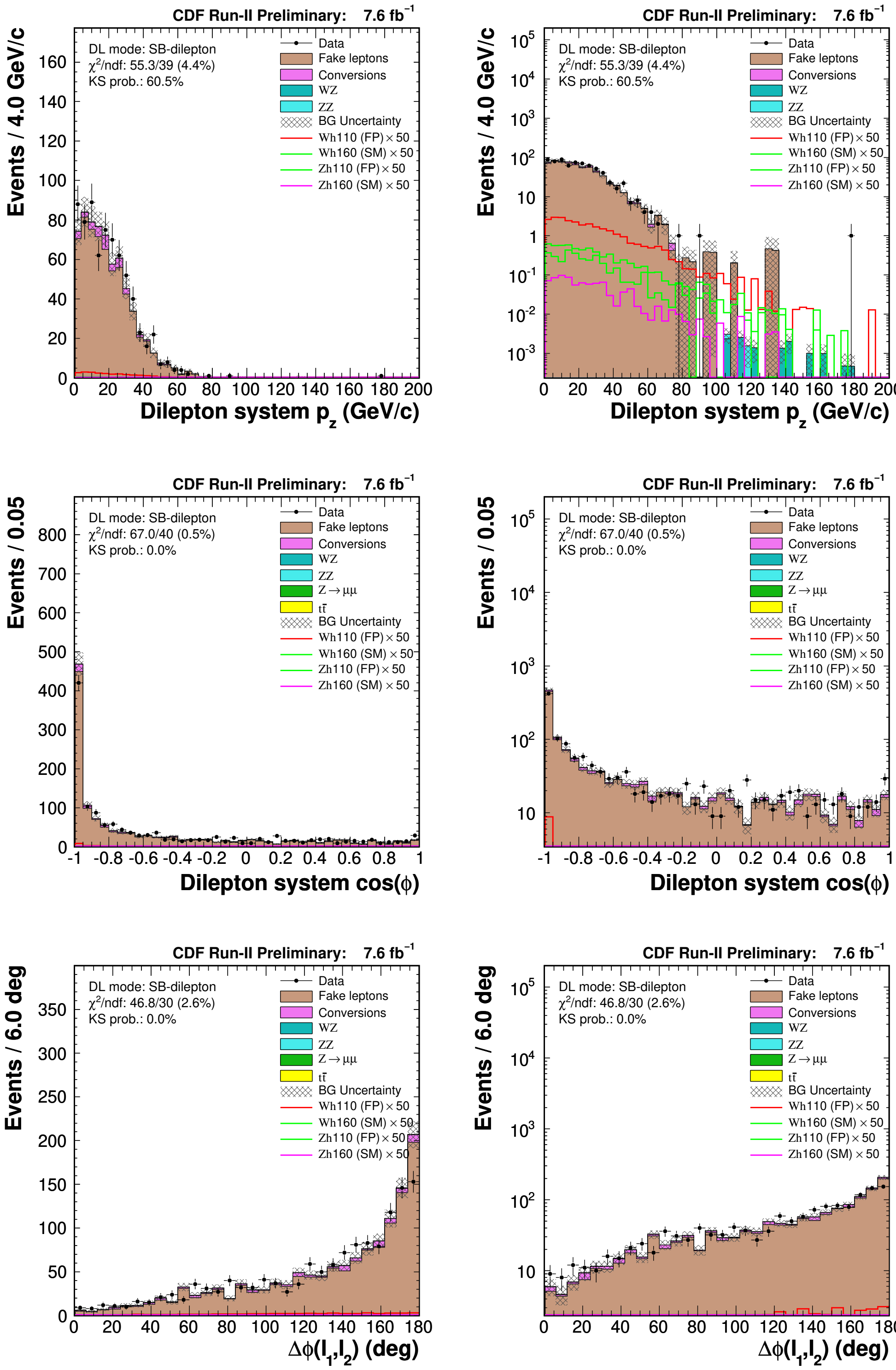

Figure 18: Dilepton system p_z, dilepton system $\cos(\phi)$, and $\Delta\phi(\ell_1, \ell_2)$ distributions in the side-band region (left: linear, right: log).

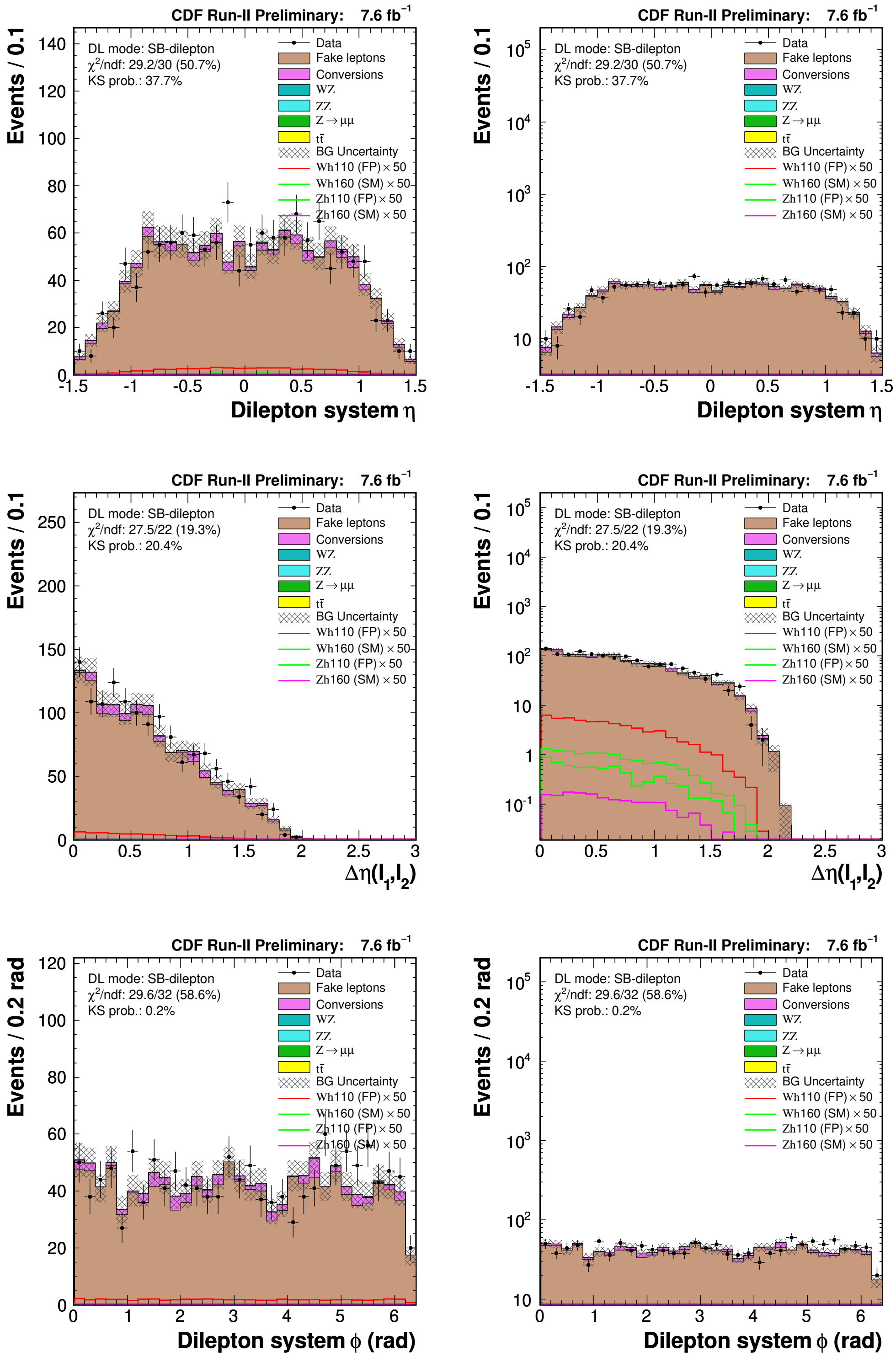

Figure 19: Dilepton system η, $\Delta\eta(\ell_1, \ell_2)$, and dilepton system ϕ distributions in the side-band region (left: linear, right: log).

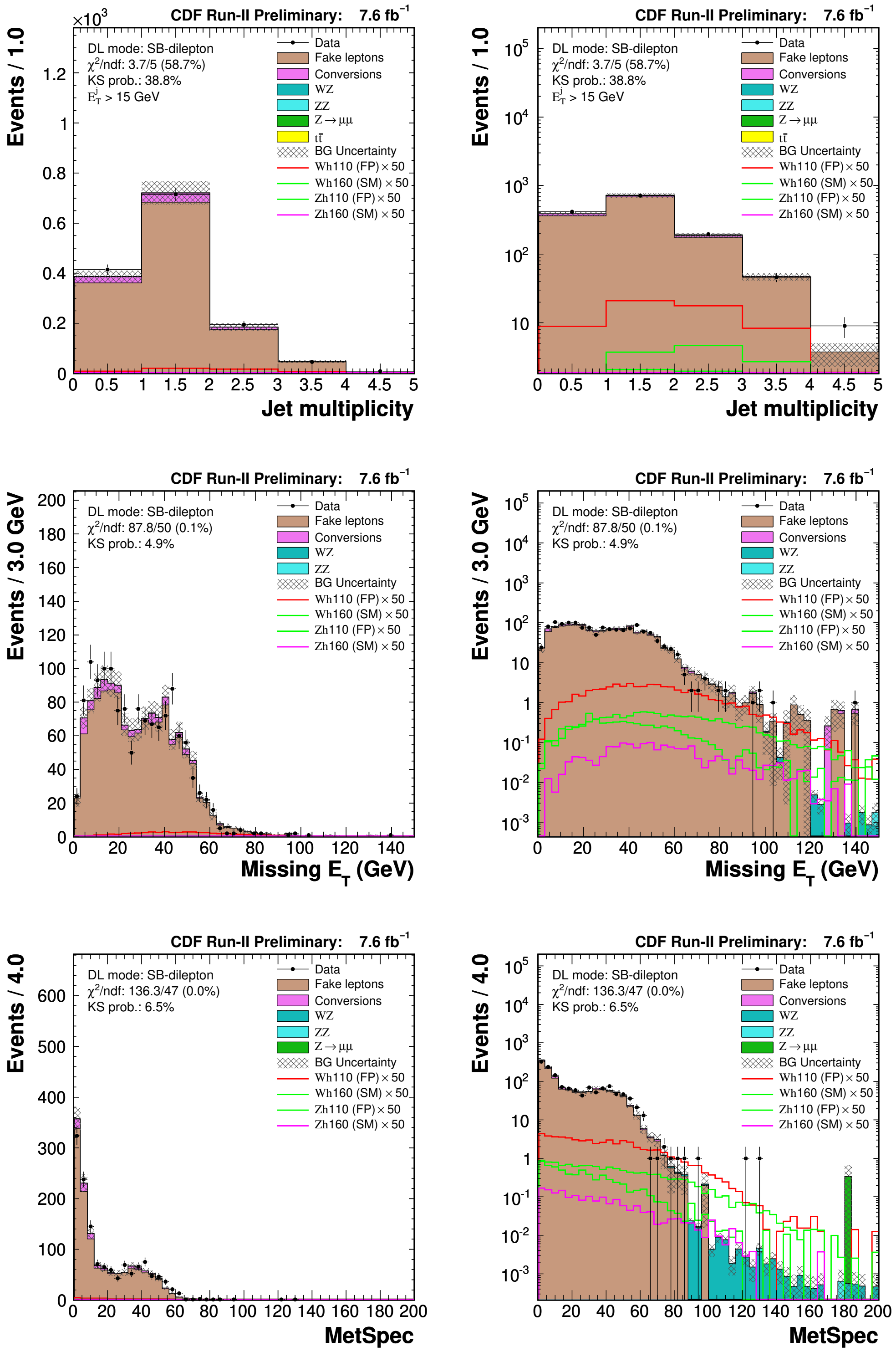

Figure 20: Jet multiplicity, missing E_T, and MetSpec distributions in the signal region (left: linear, right: log).

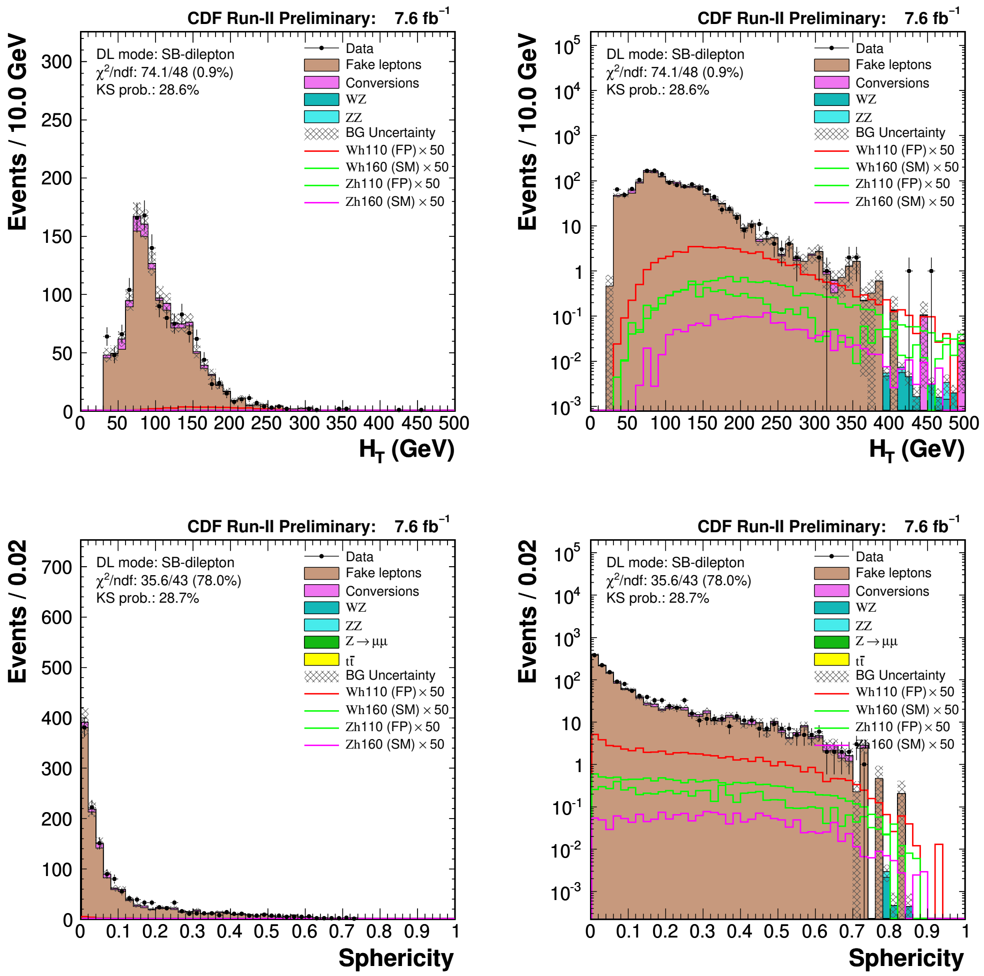

Figure 21: H_T and sphericity distributions in the signal region (left: linear, right: log).

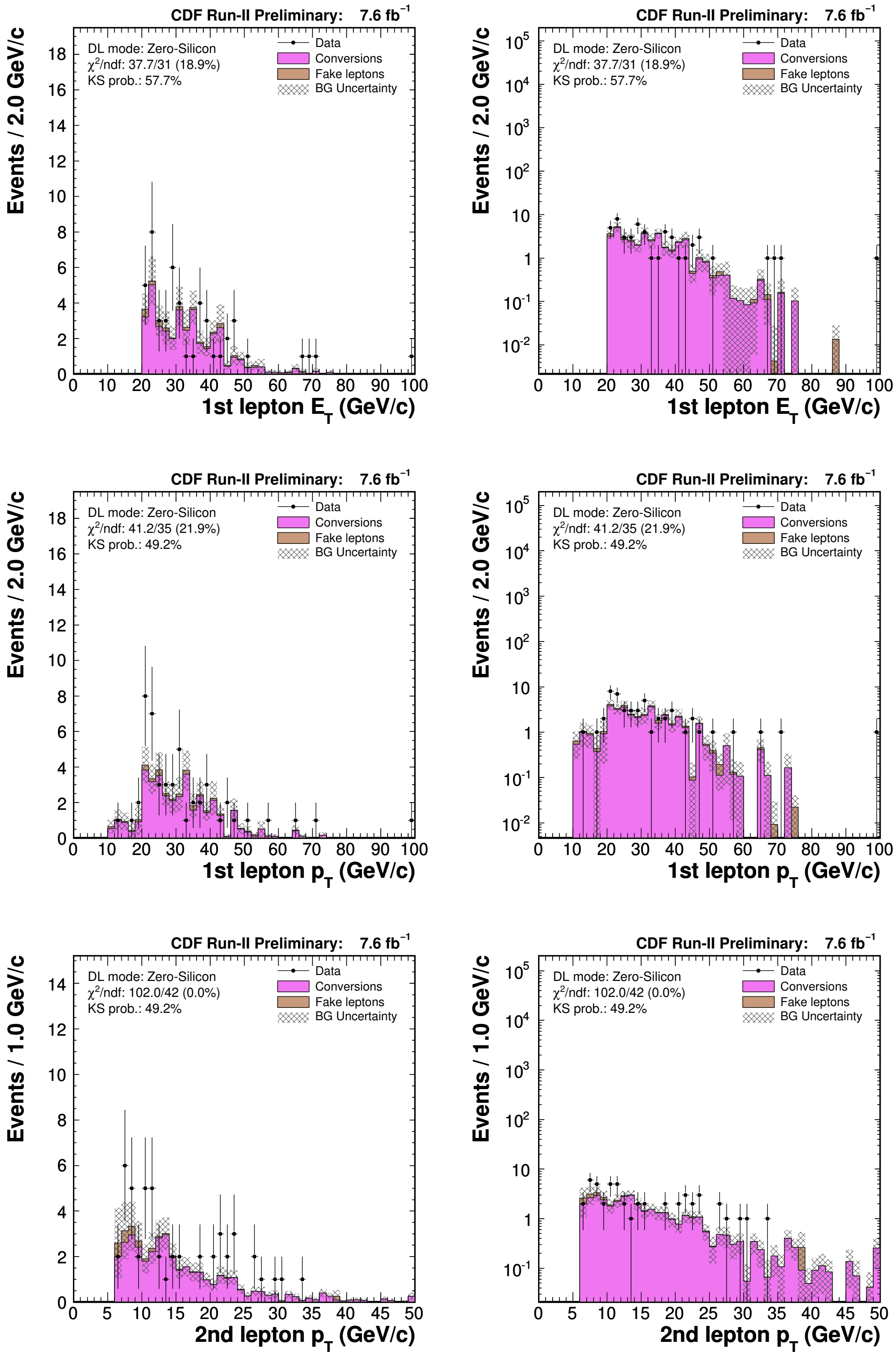

Figure 22: 1st lepton E_T, 1st lepton p_T, and 2nd lepton p_T distributions in the zero-silicon region (left: linear, right: log).

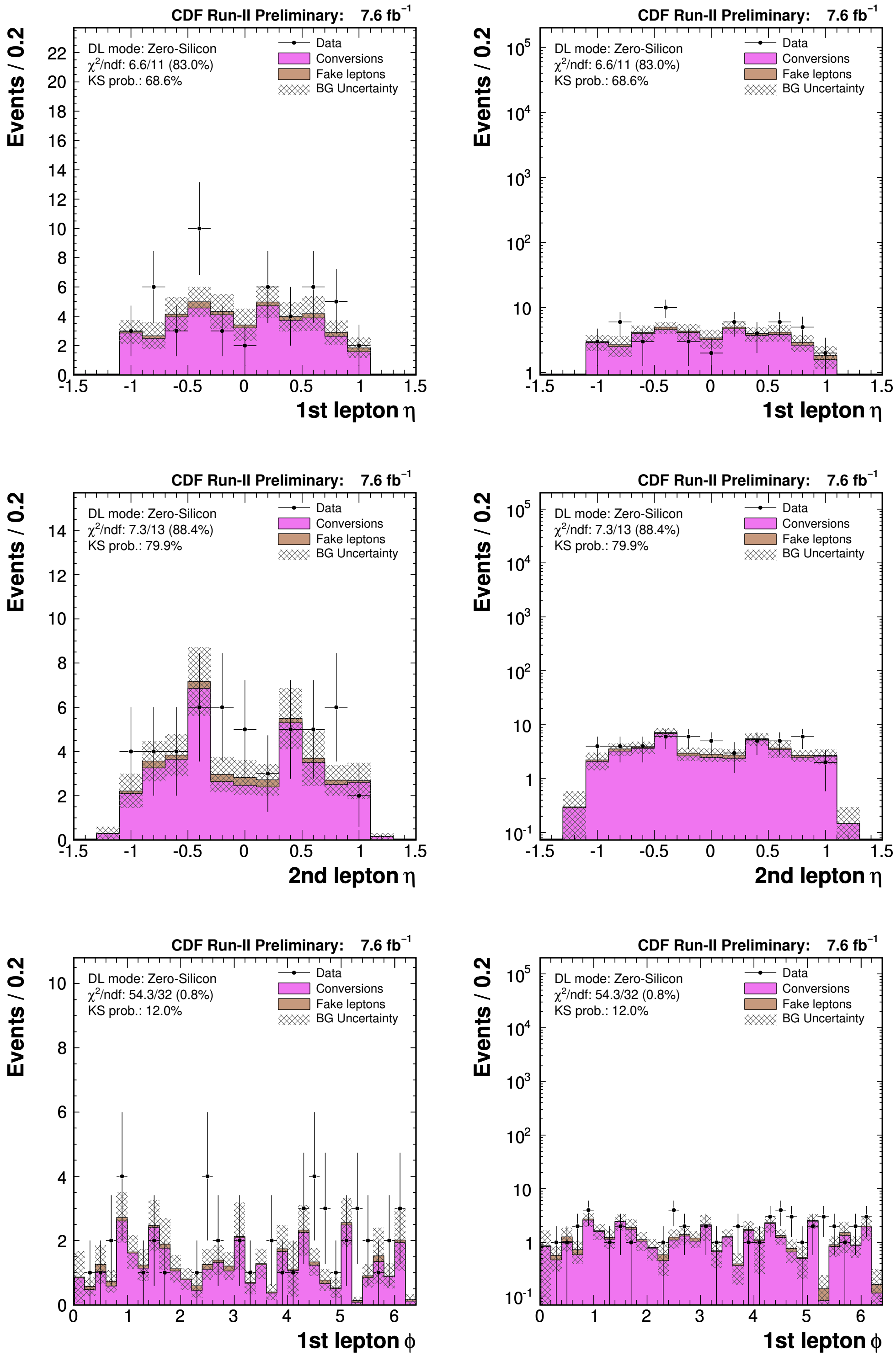

Figure 23: 1st lepton η, 2nd lepton η, and 1st lepton ϕ distributions in the zero-silicon region (left: linear, right: log).

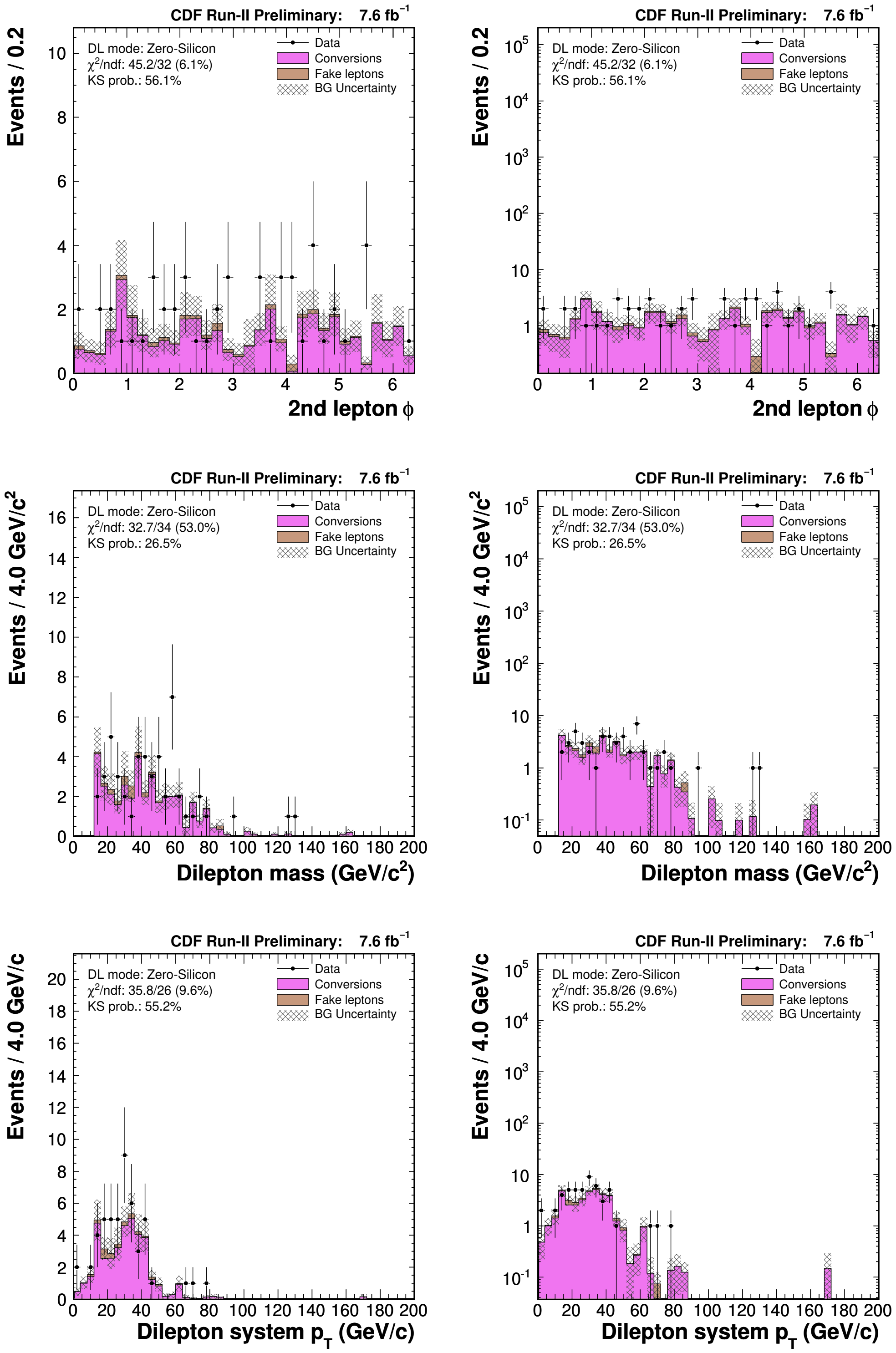

Figure 24: 2nd lepton ϕ, dilepton mass, and dilepton system p_T distributions in the zero-silicon region (left: linear, right: log).

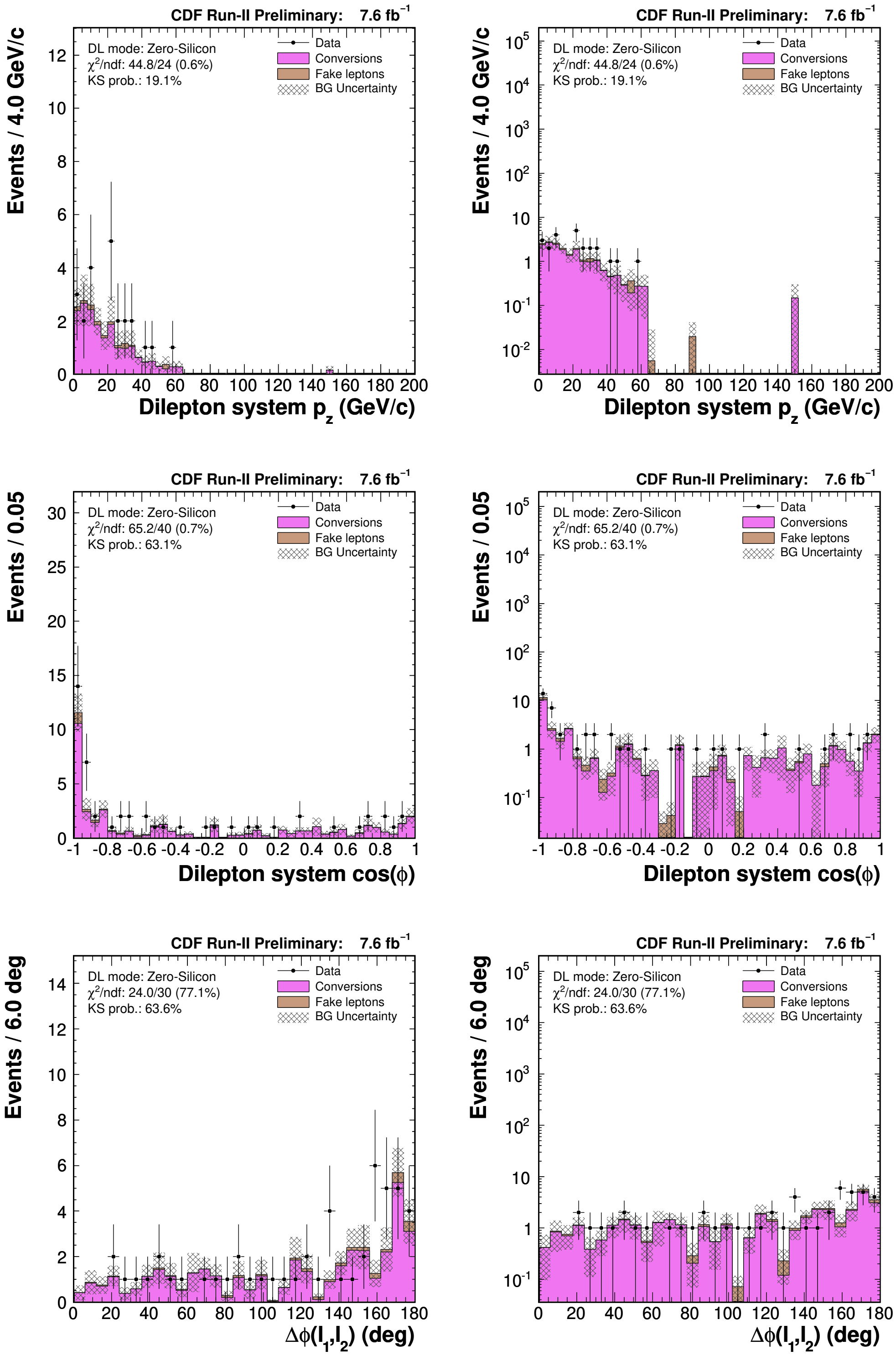

Figure 25: Dilepton system p_z, dilepton system $\cos(\phi)$, and $\Delta\phi(\ell_1, \ell_2)$ distributions in the zero-silicon region (left: linear, right: log).

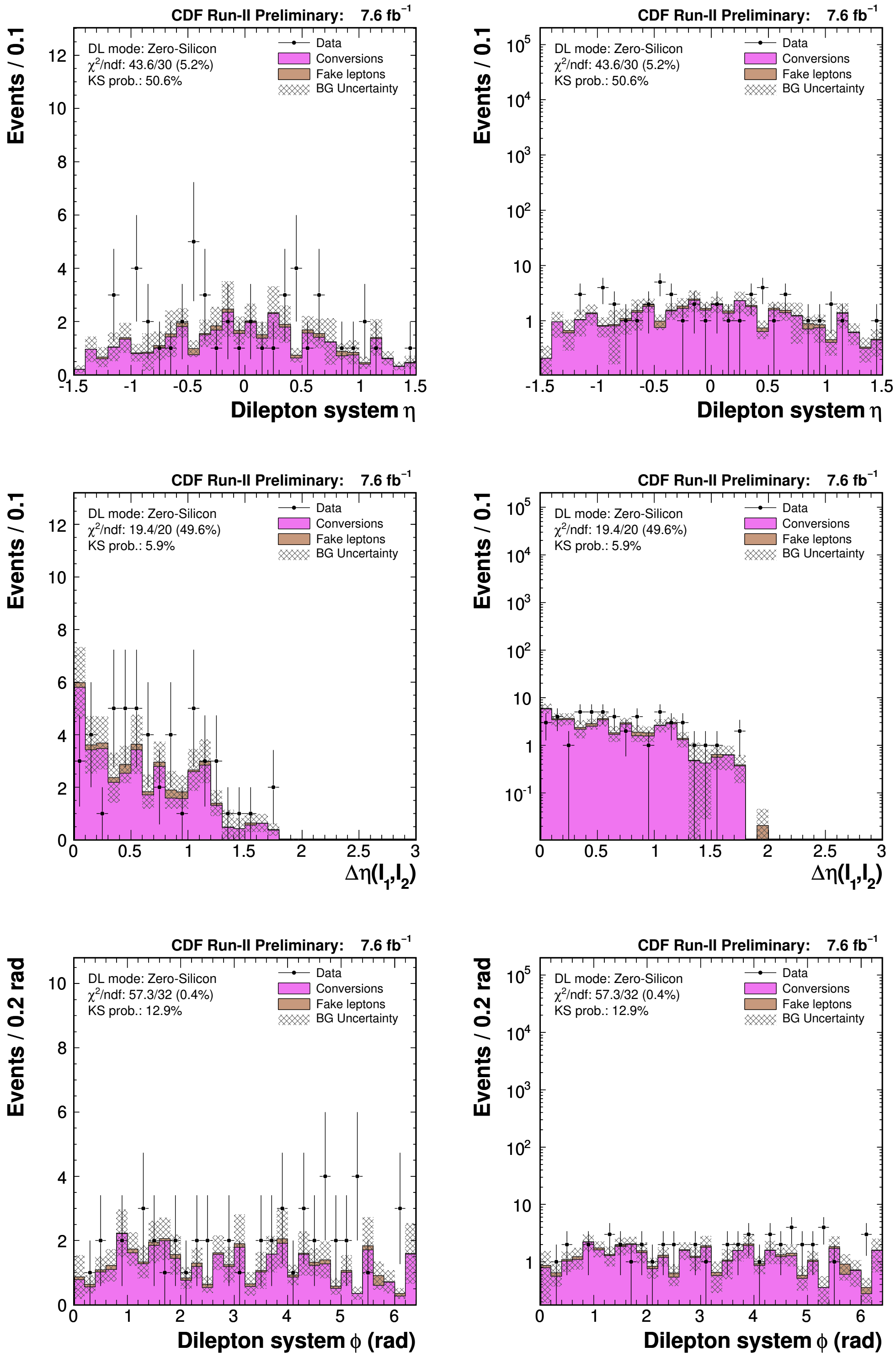

Figure 26: Dilepton system η, $\Delta\eta(\ell_1, \ell_2)$, and dilepton system ϕ distributions in the zero-silicon region (left: linear, right: log).

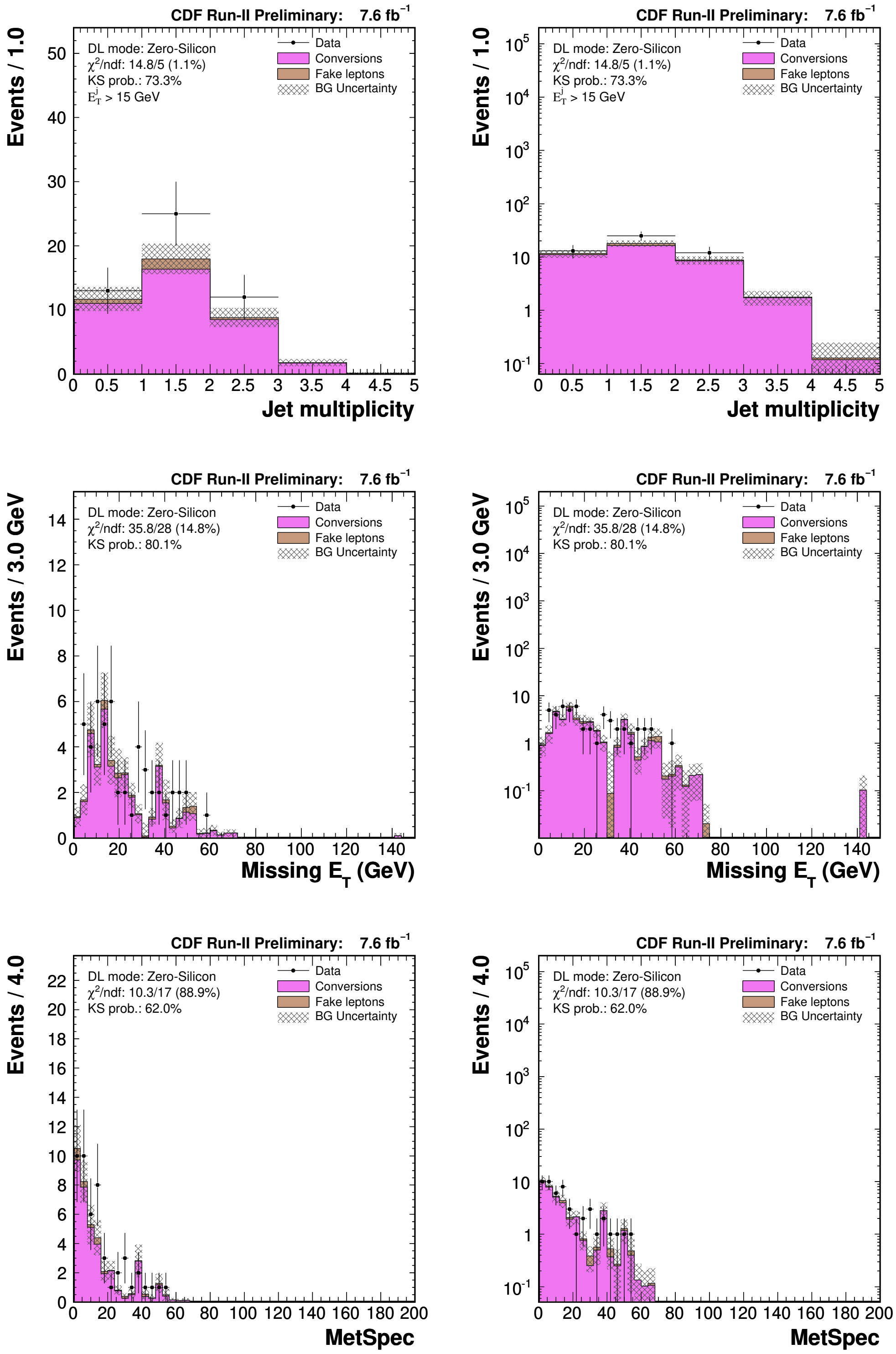

Figure 27: Jet multiplicity, missing E_T, and MetSpec distributions in the zero-silicon region (left: linear, right: log).

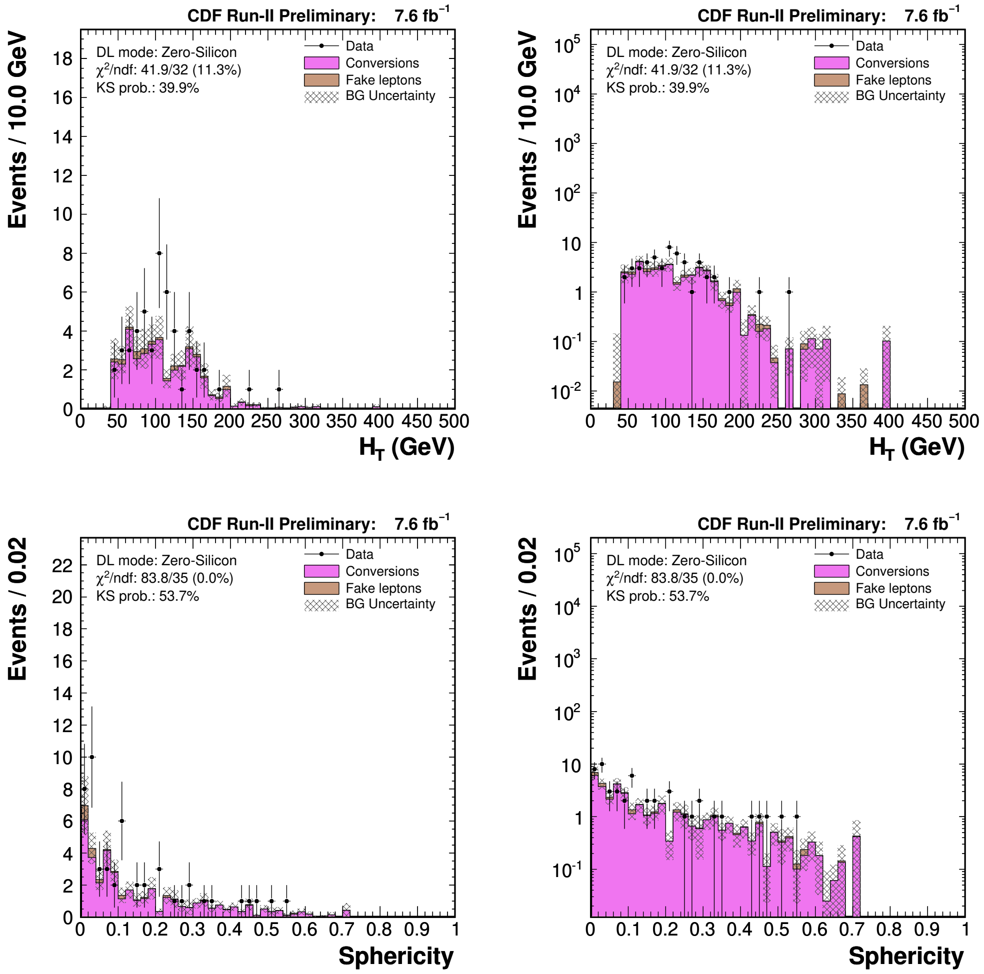

Figure 28: H_T and sphericity distributions in the zero-silicon region (left: linear, right: log).

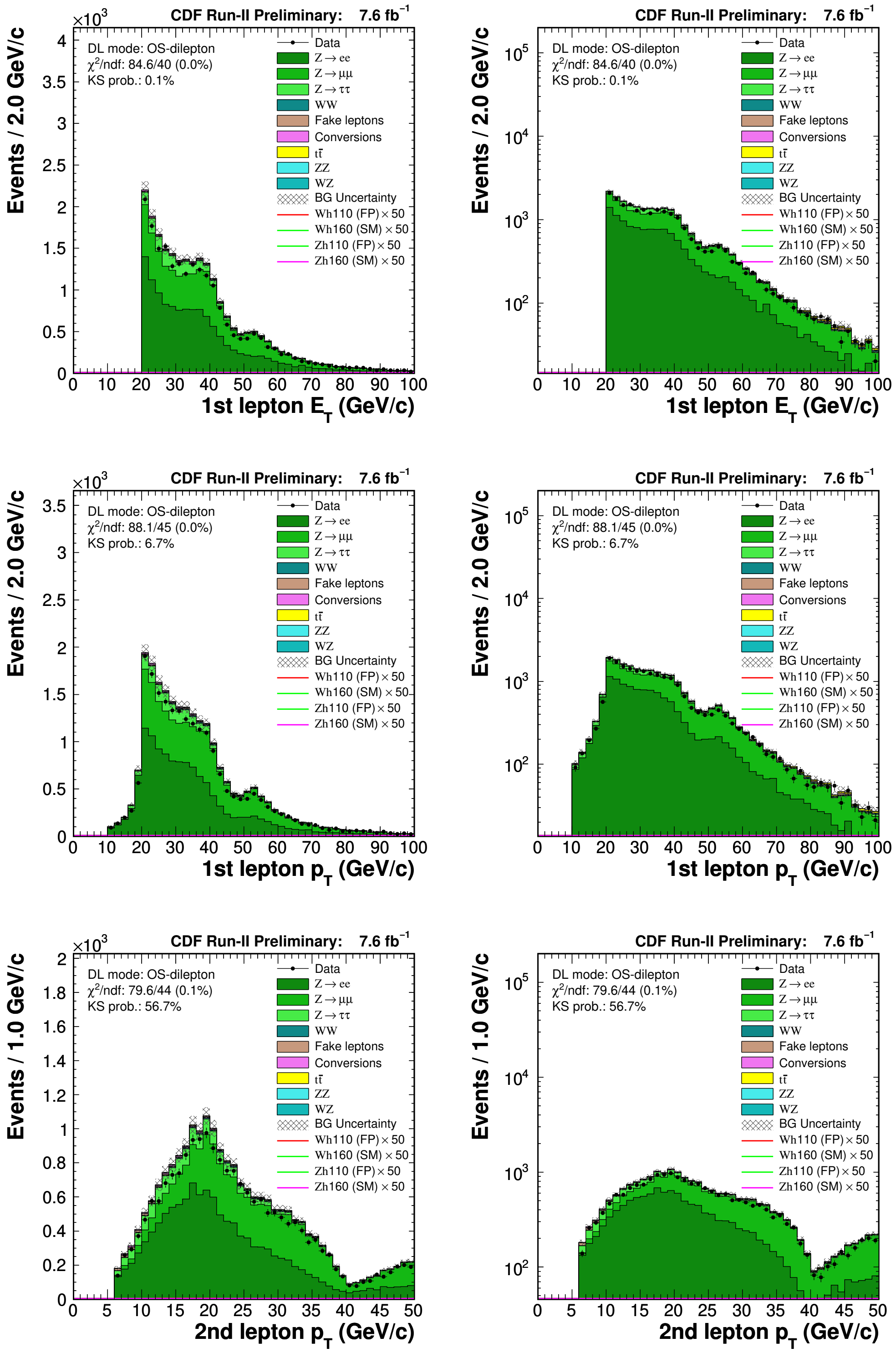

Figure 29: 1st lepton E_T, 1st lepton p_T, and 2nd lepton p_T distributions in the OS region (left: linear, right: log).

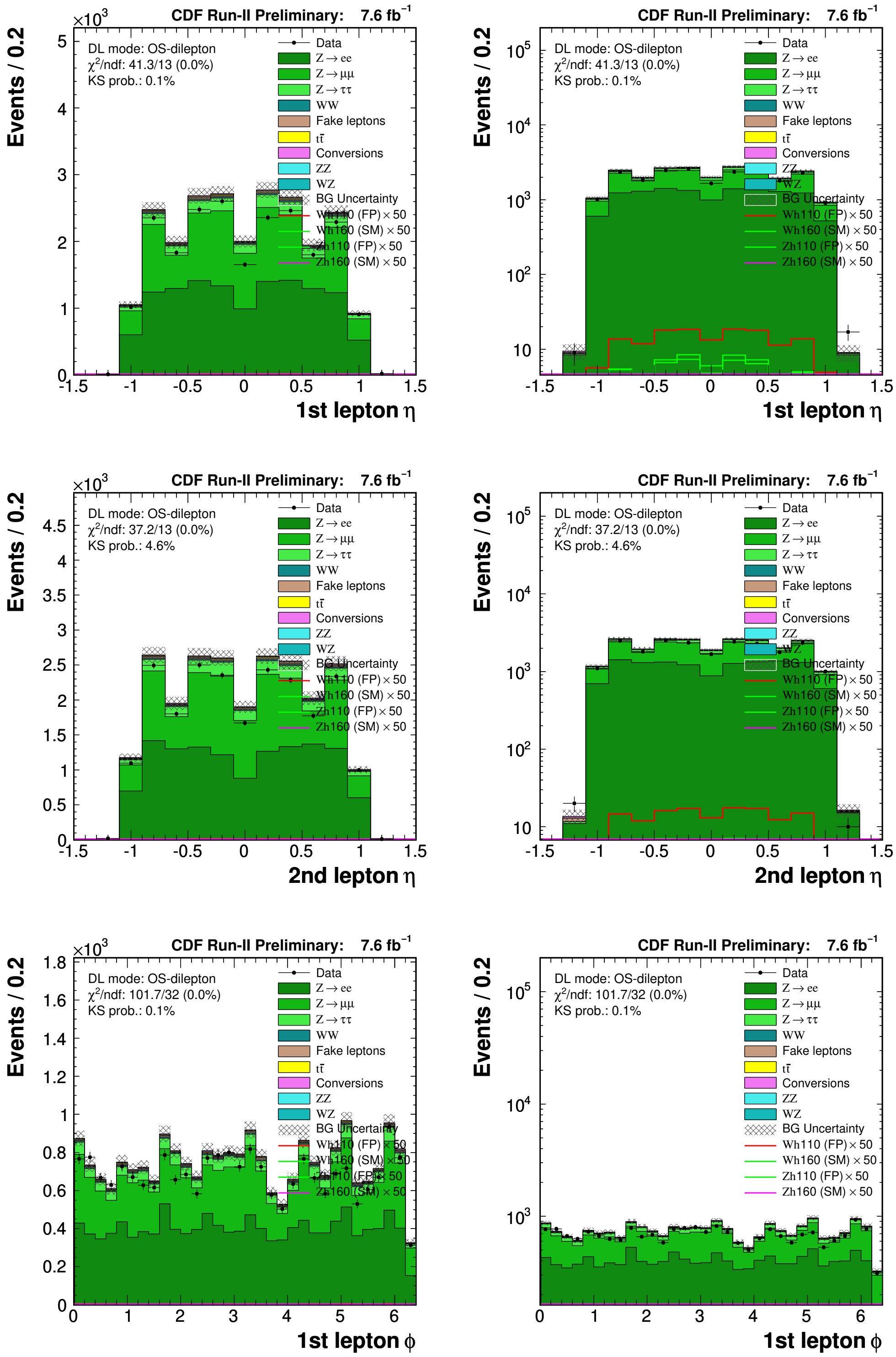

Figure 30: 1st lepton η, 2nd lepton η, and 1st lepton ϕ distributions in the OS region (left: linear, right: log).

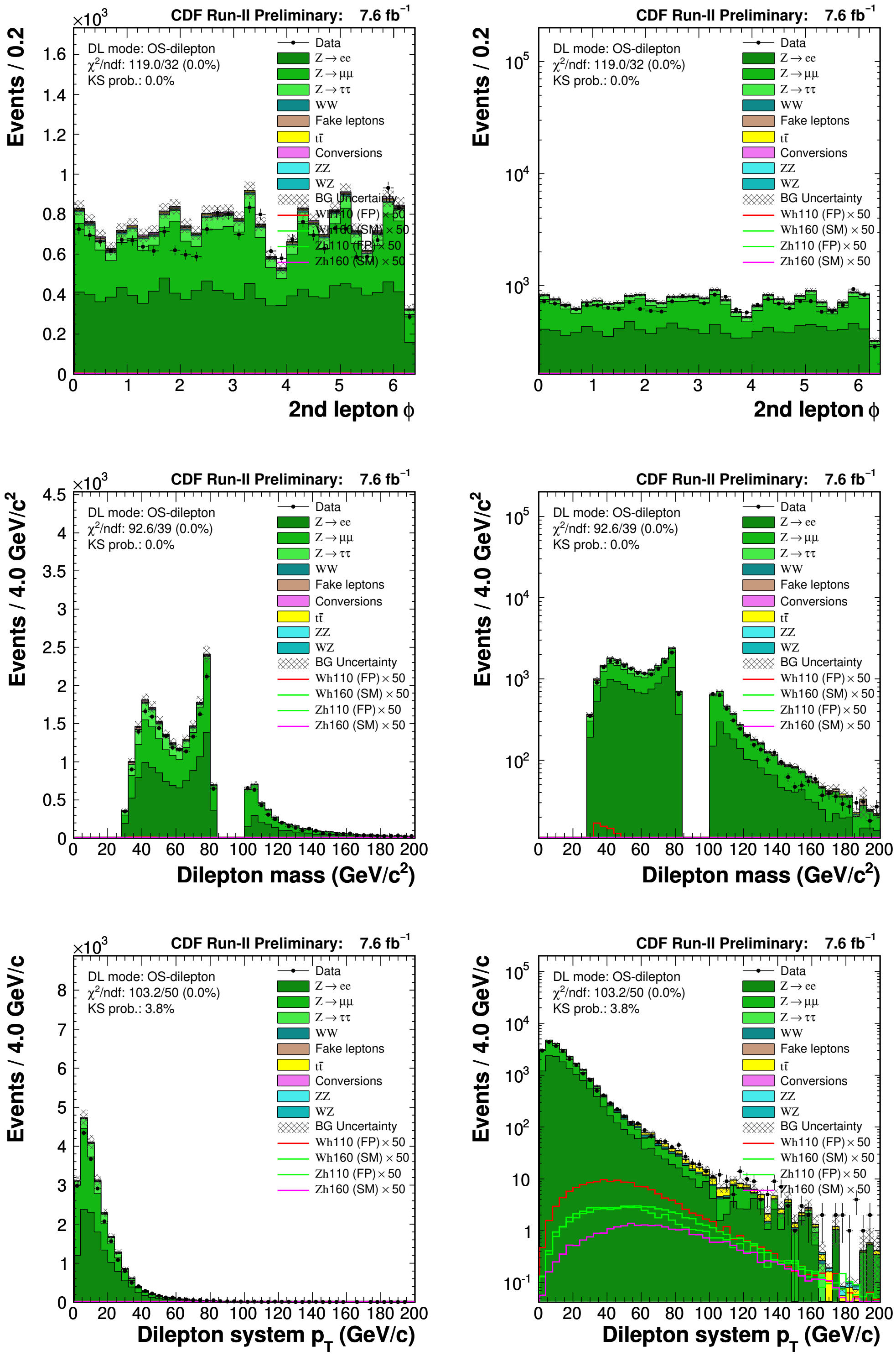

Figure 31: 2nd lepton ϕ, dilepton mass, and dilepton system p_T distributions in the OS region (left: linear, right: log).

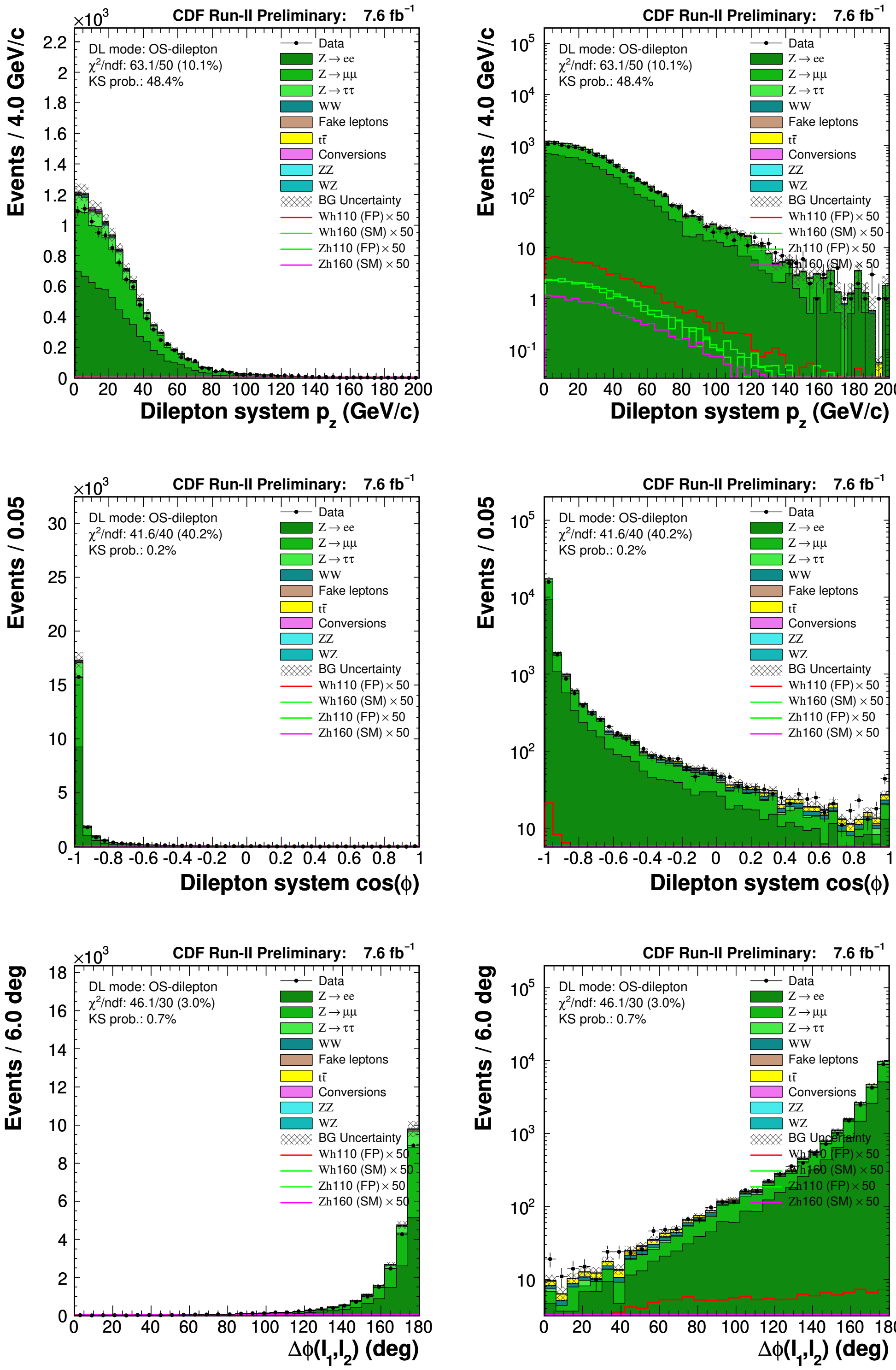

Figure 32: Dilepton system p_z, dilepton system $\cos(\phi)$, and $\Delta\phi(\ell_1, \ell_2)$ distributions in the OS region (left: linear, right: log).

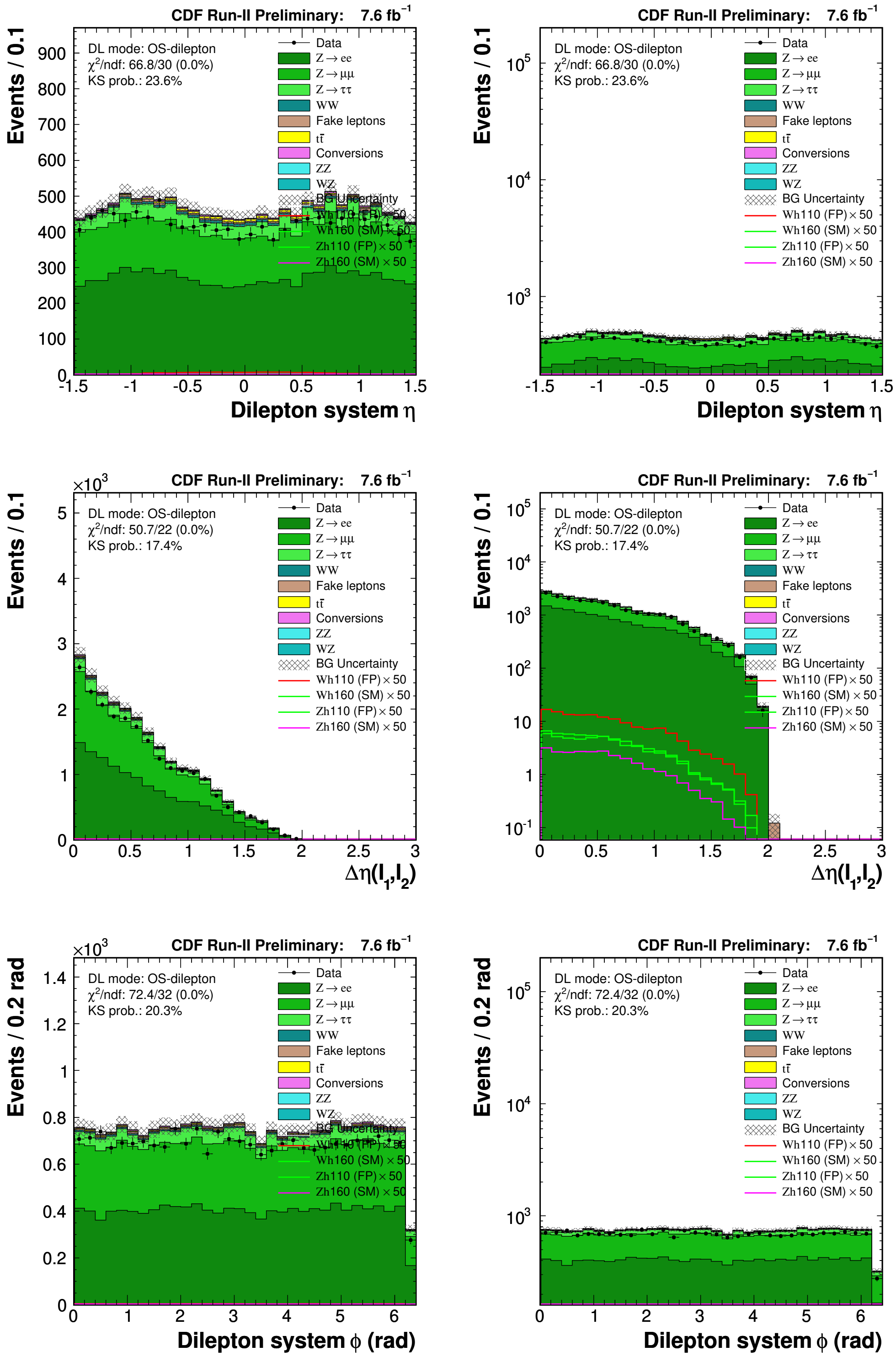

Figure 33: Dilepton system η, $\Delta\eta(\ell_1, \ell_2)$, and dilepton system ϕ distributions in the OS region (left: linear, right: log).

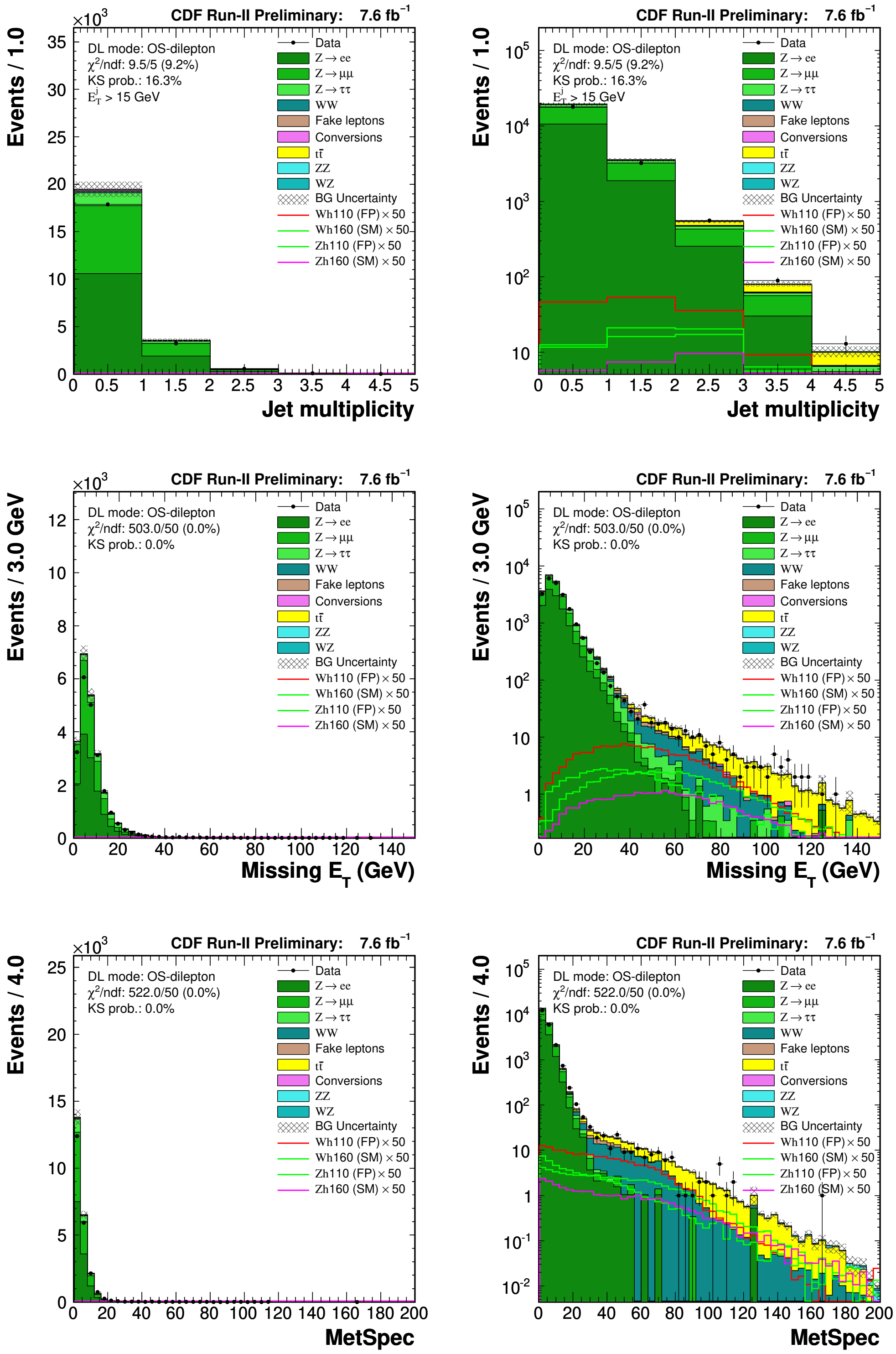

Figure 34: Jet multiplicity, missing E_T, and MetSpec distributions in the OS region (left: linear, right: log).

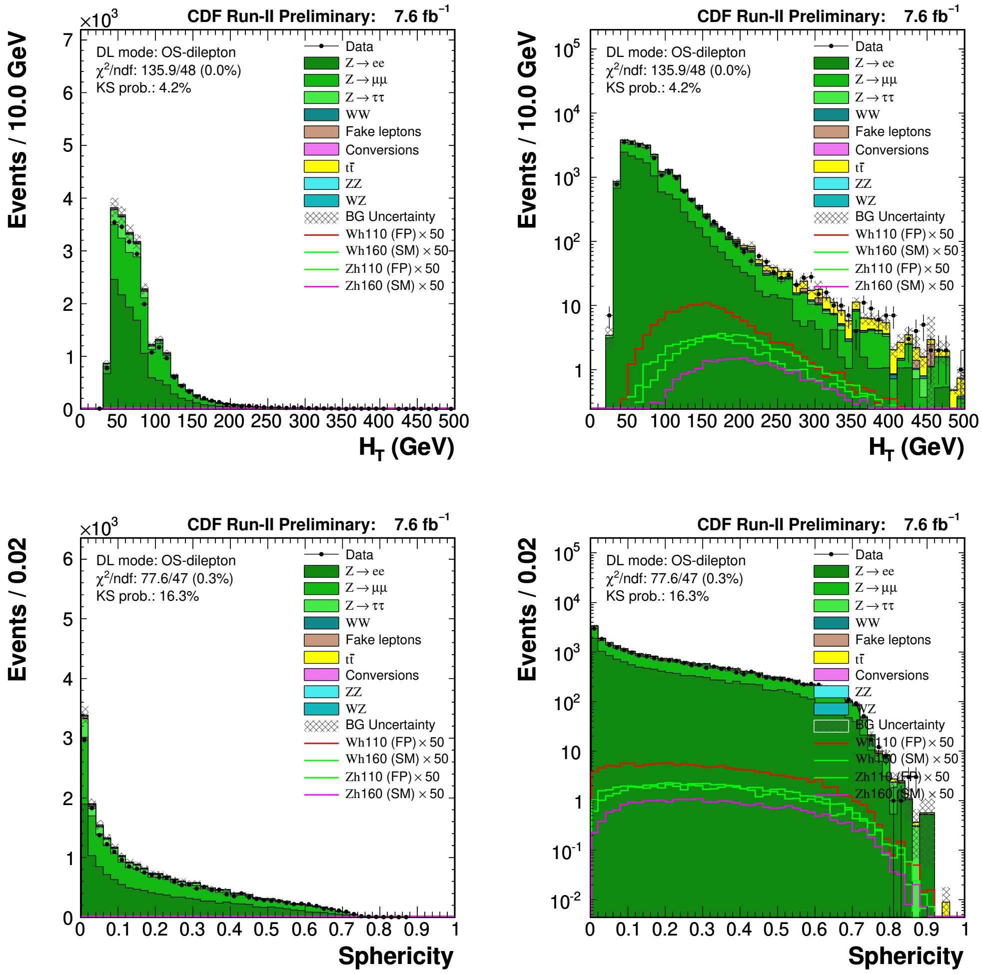

Figure 35: H_T and sphericity distributions in the OS region (left: linear, right: log).

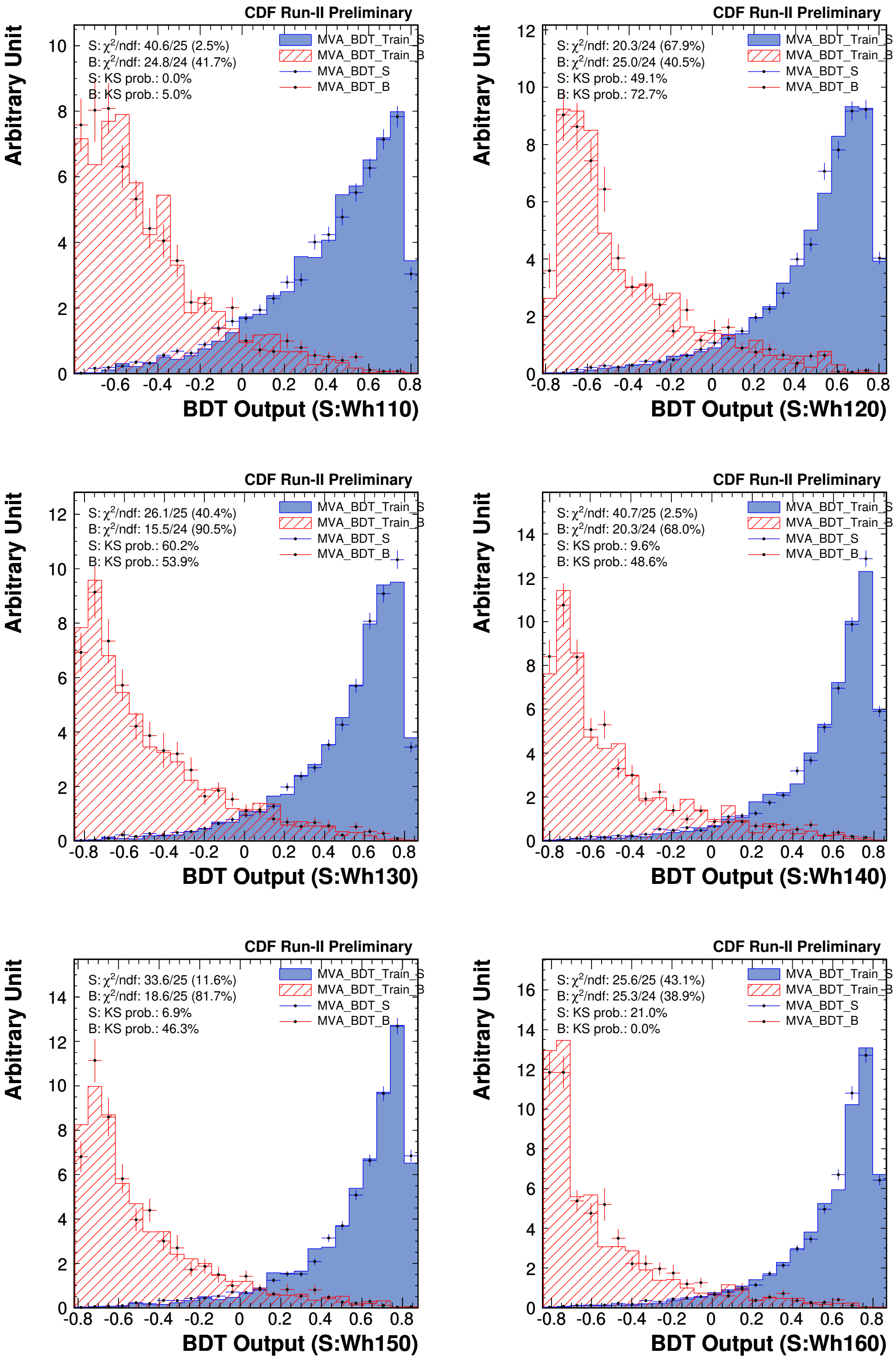

Figure 36: BDT training and test sample plots.

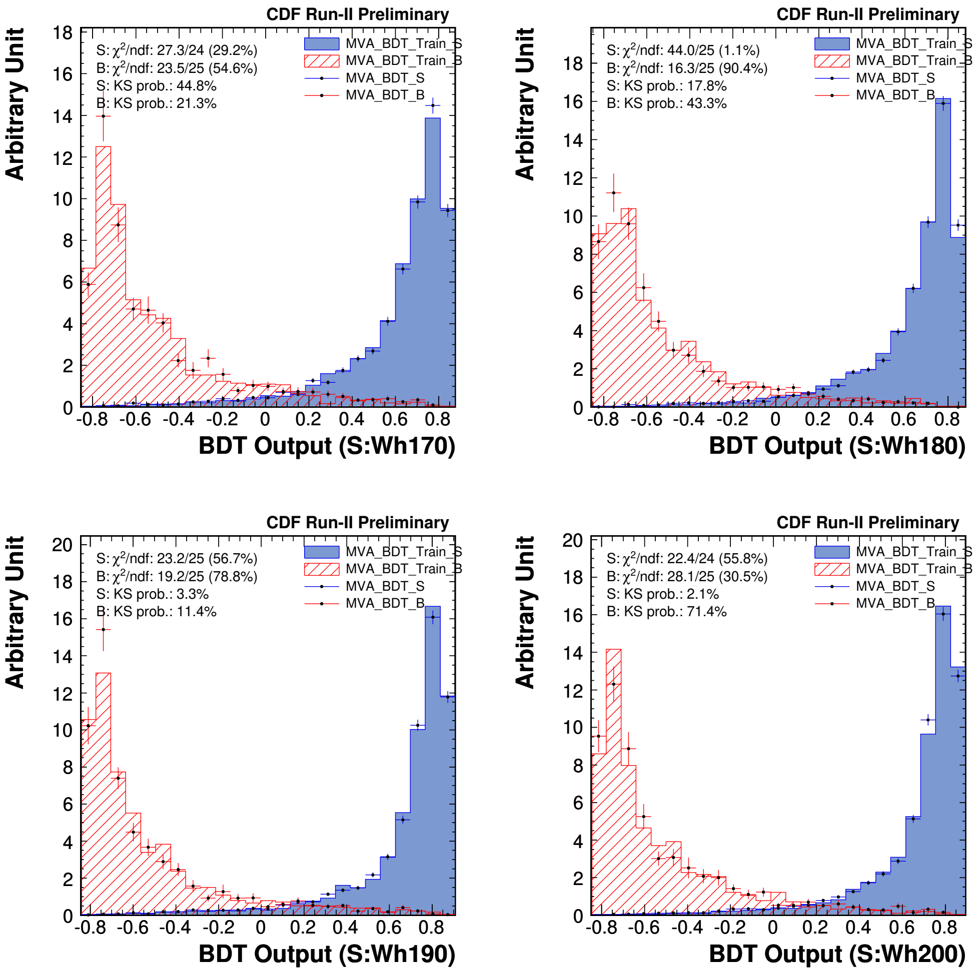

Figure 37: BDT training and test sample plots.

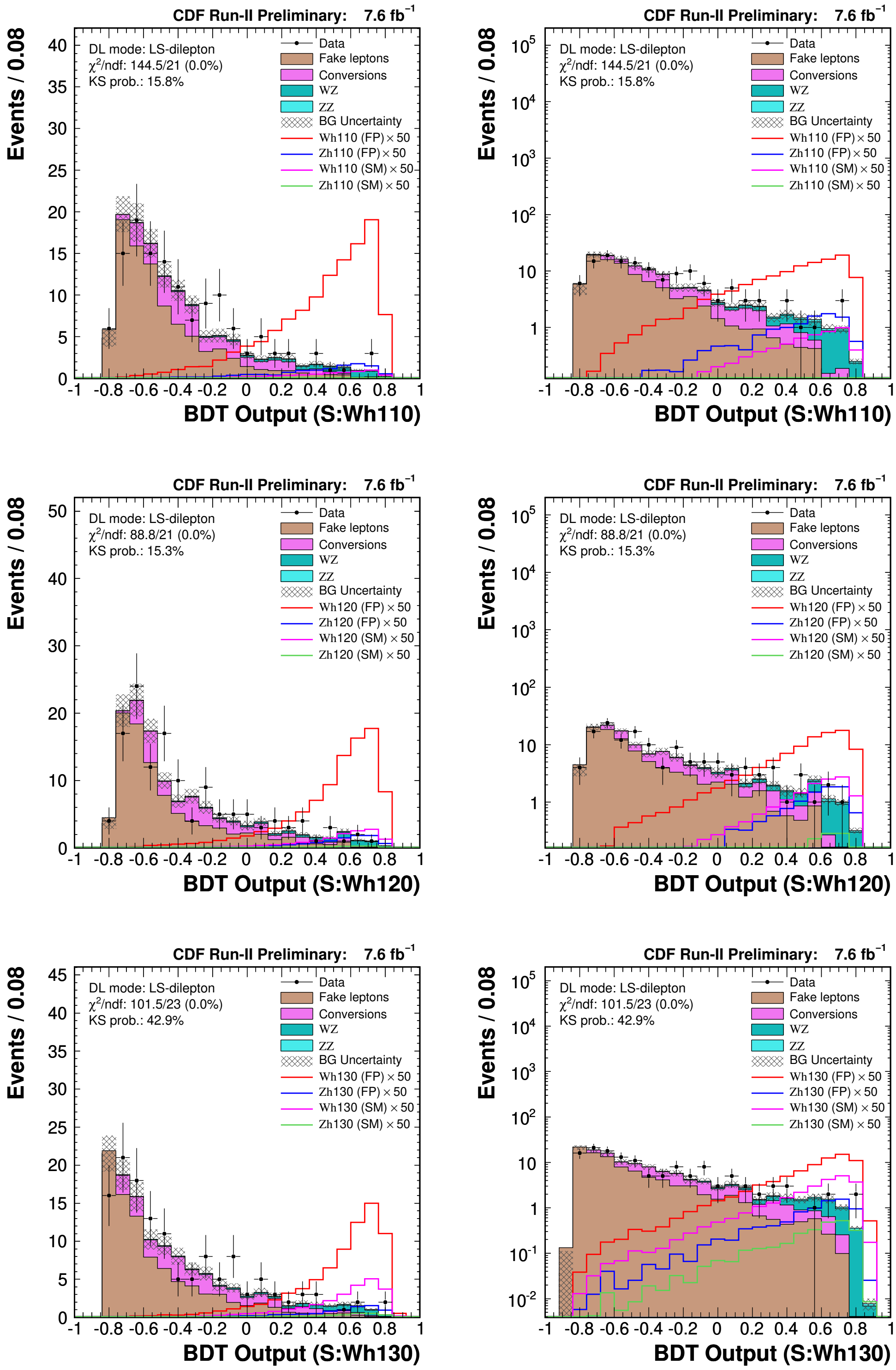

Figure 38: BDT output for like-sign dilepton events in the signal region (left: linear, right: log).

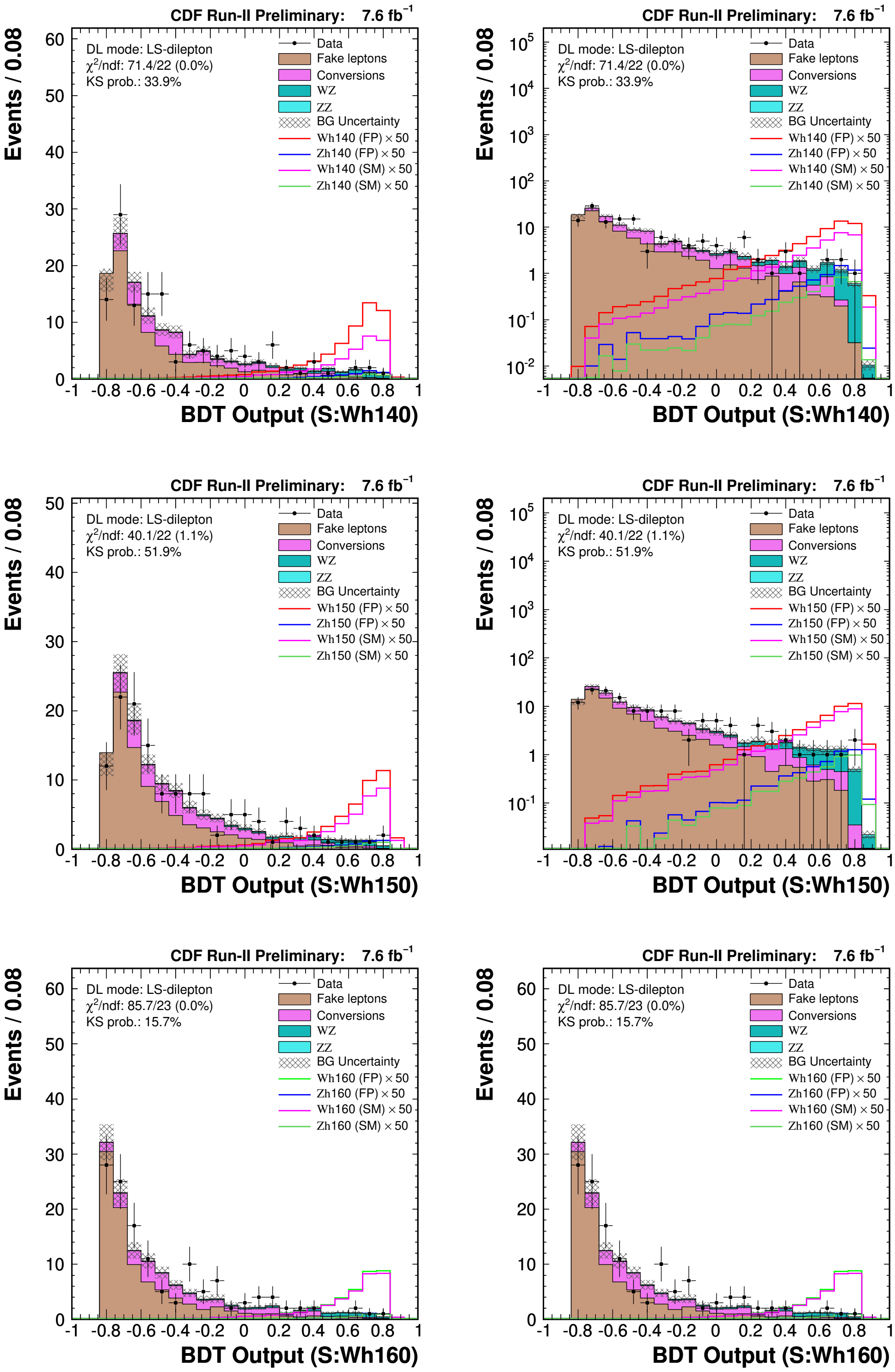

Figure 39: BDT output for like-sign dilepton events in the signal region (left: linear, right: log).

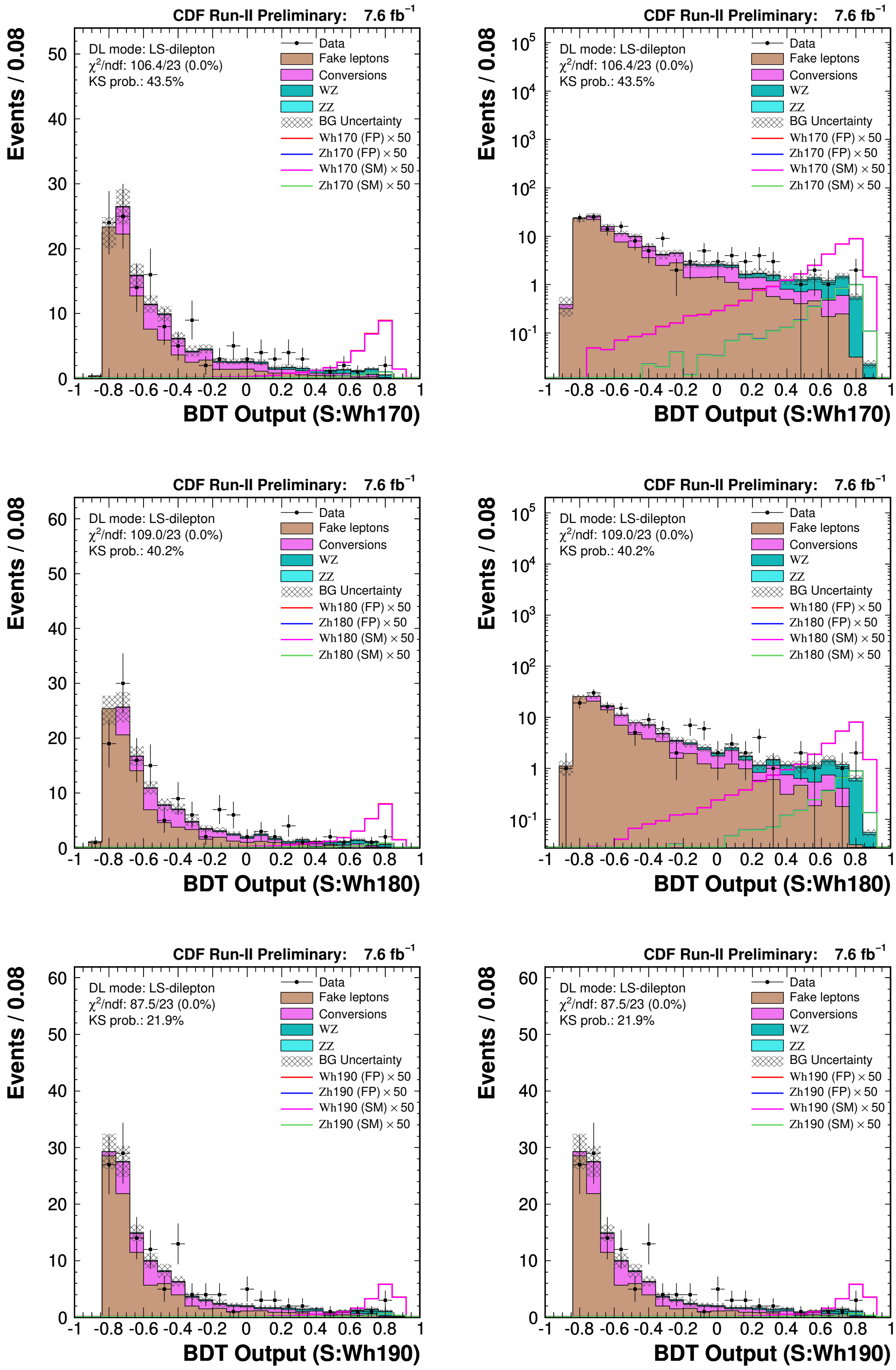

Figure 40: BDT output for like-sign dilepton events in the signal region (left: linear, right: log).

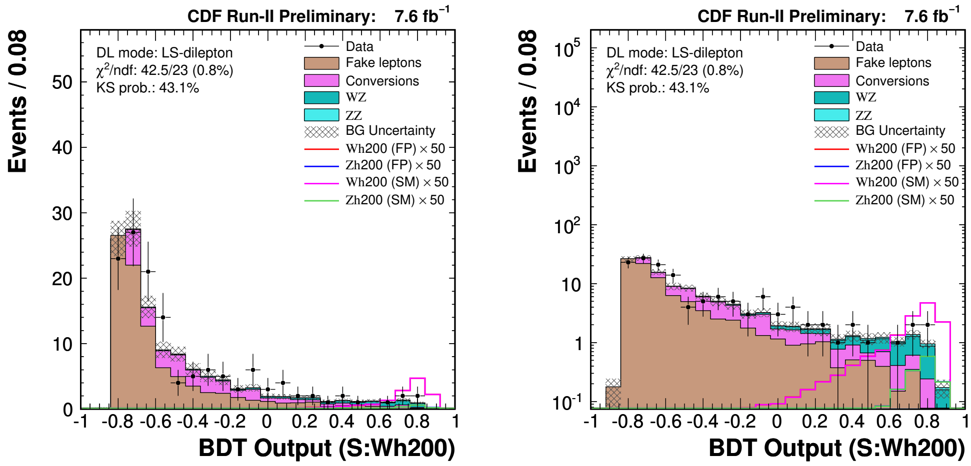

Figure 41: BDT output for like-sign dilepton events in the signal region (left: linear, right: log).

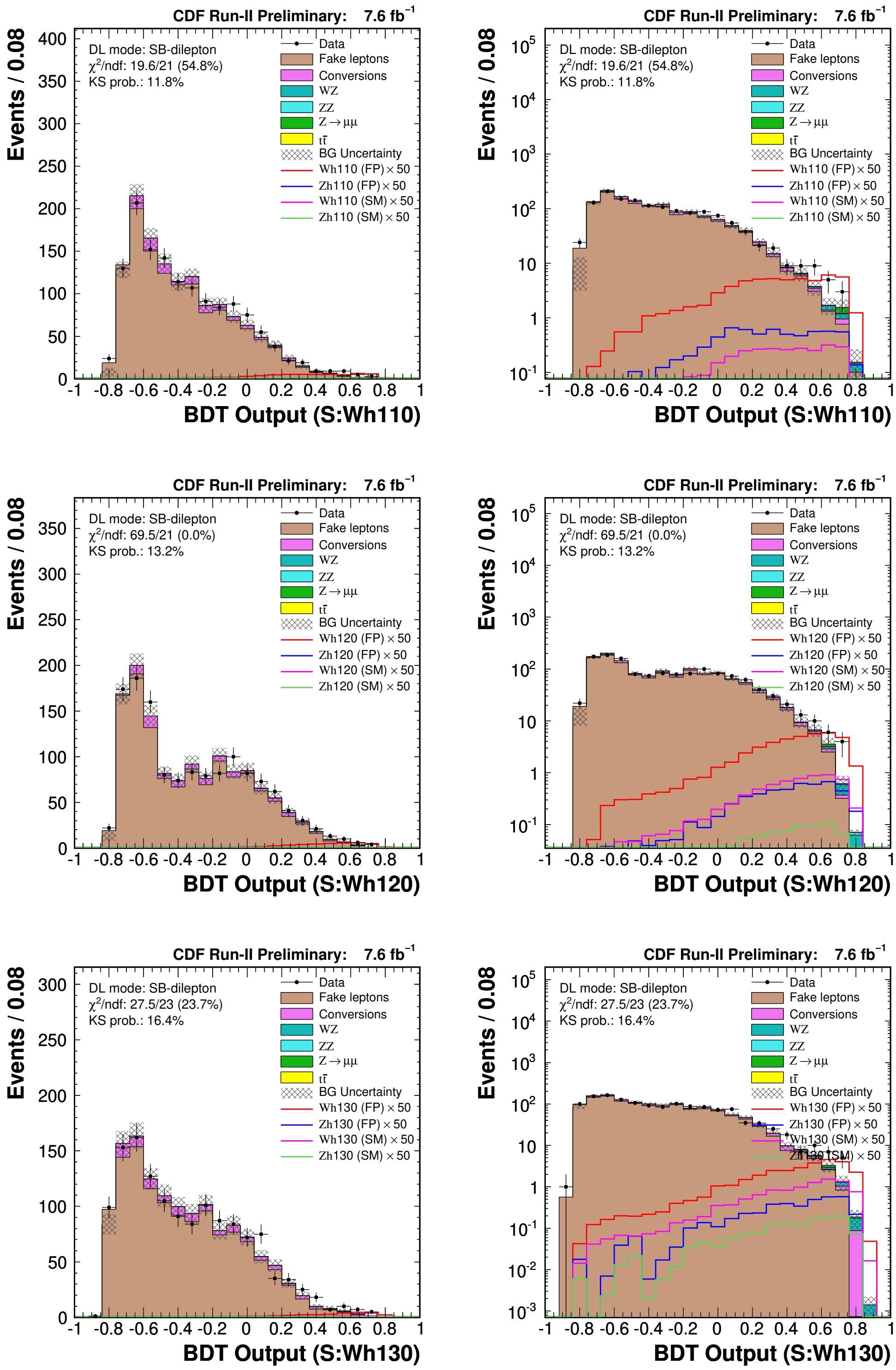

Figure 42: BDT output for in the side-band region (left: linear, right: log).

Figure 43: Zero silicon variables.

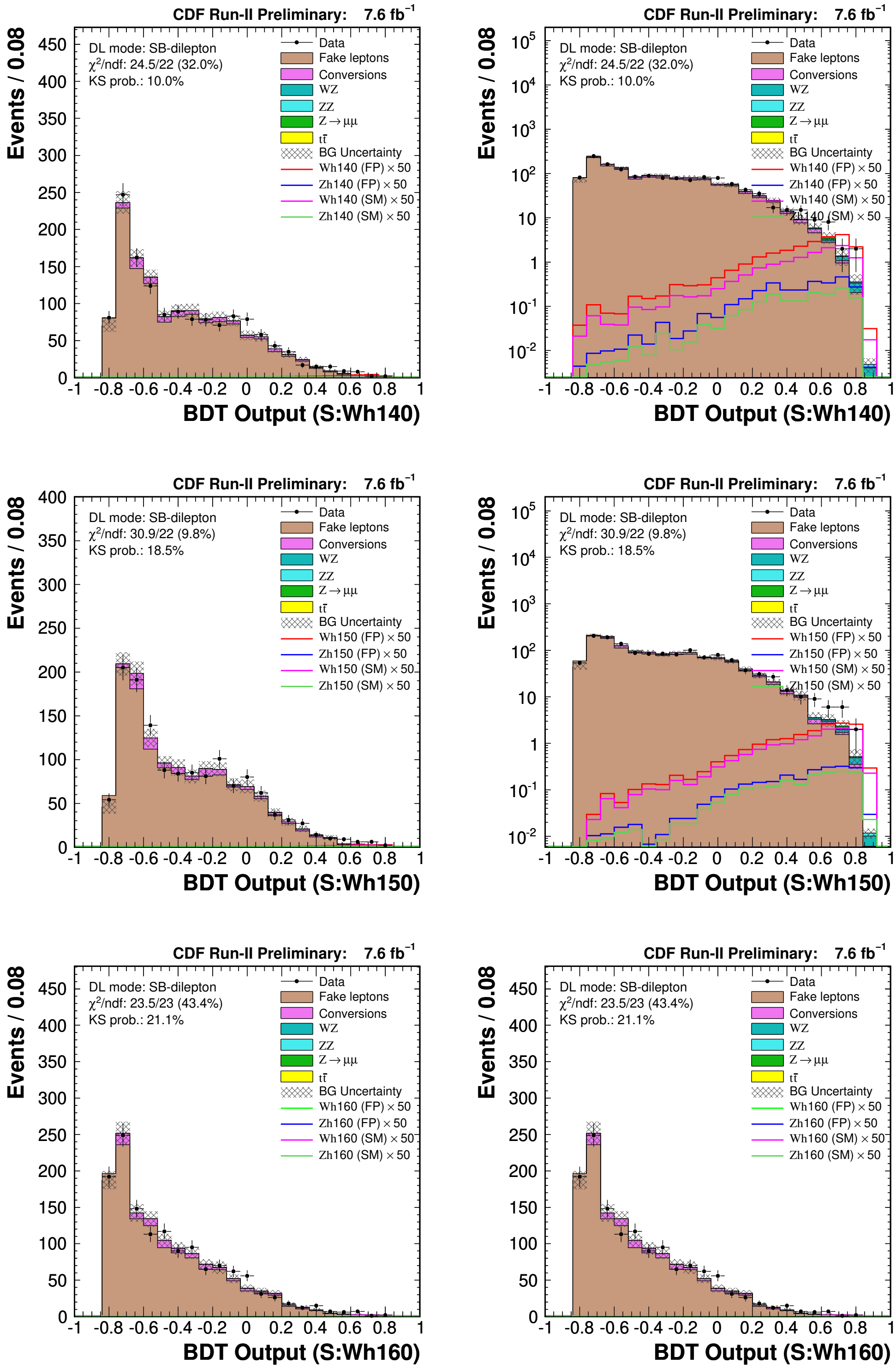

Figure 44: BDT output for in the side-band region (left: linear, right: log).

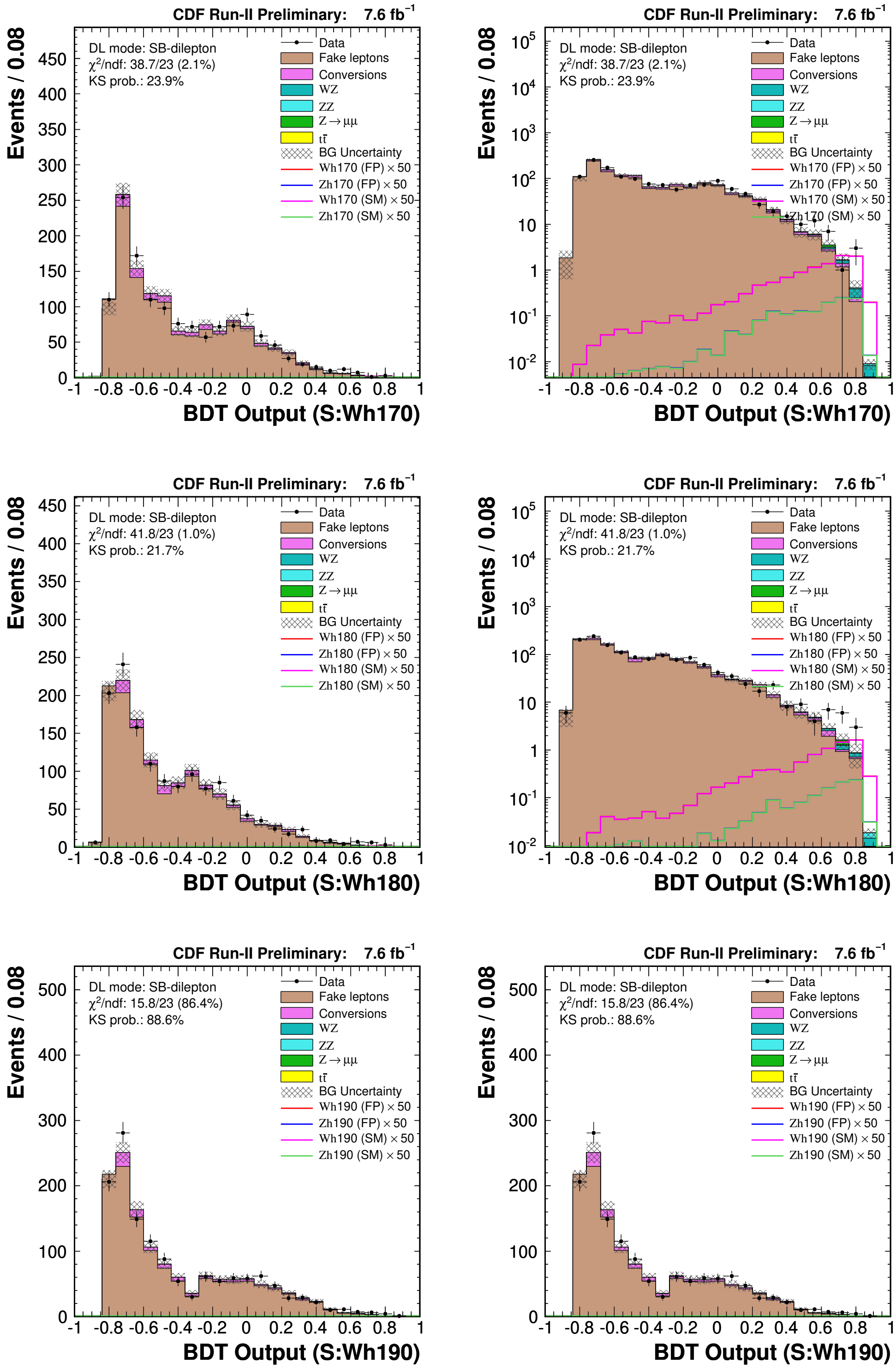

Figure 45: BDT output for in the side-band region (left: linear, right: log).

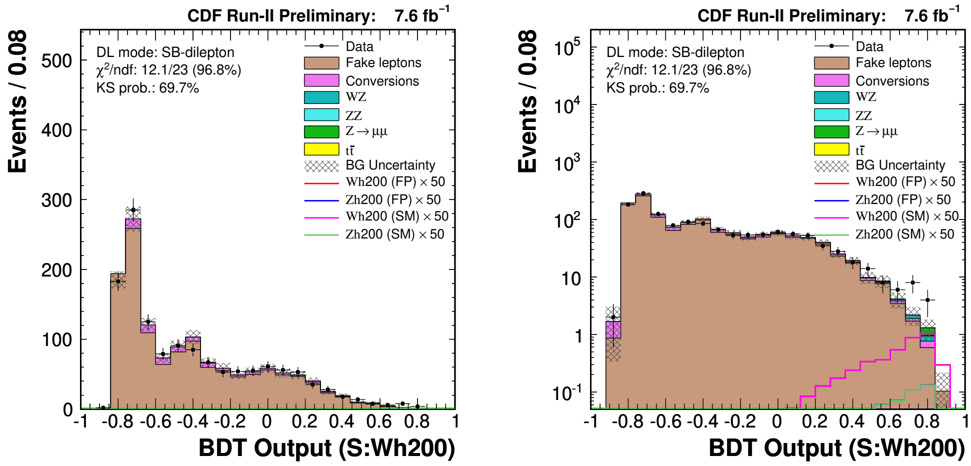

Figure 46: BDT output for in the side-band region (left: linear, right: log).

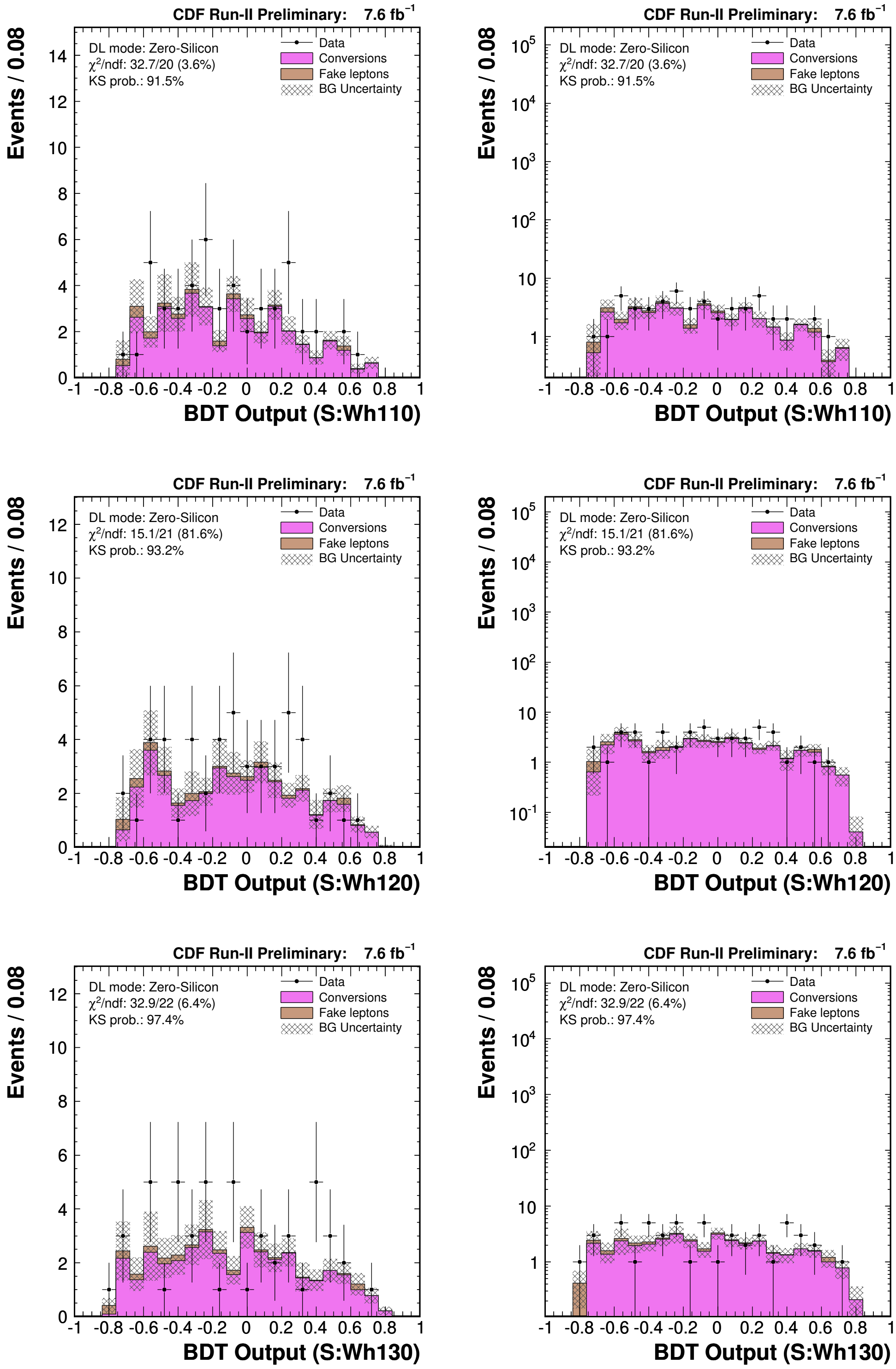

Figure 47: BDT output for in the zero-silicon region (left: linear, right: log).

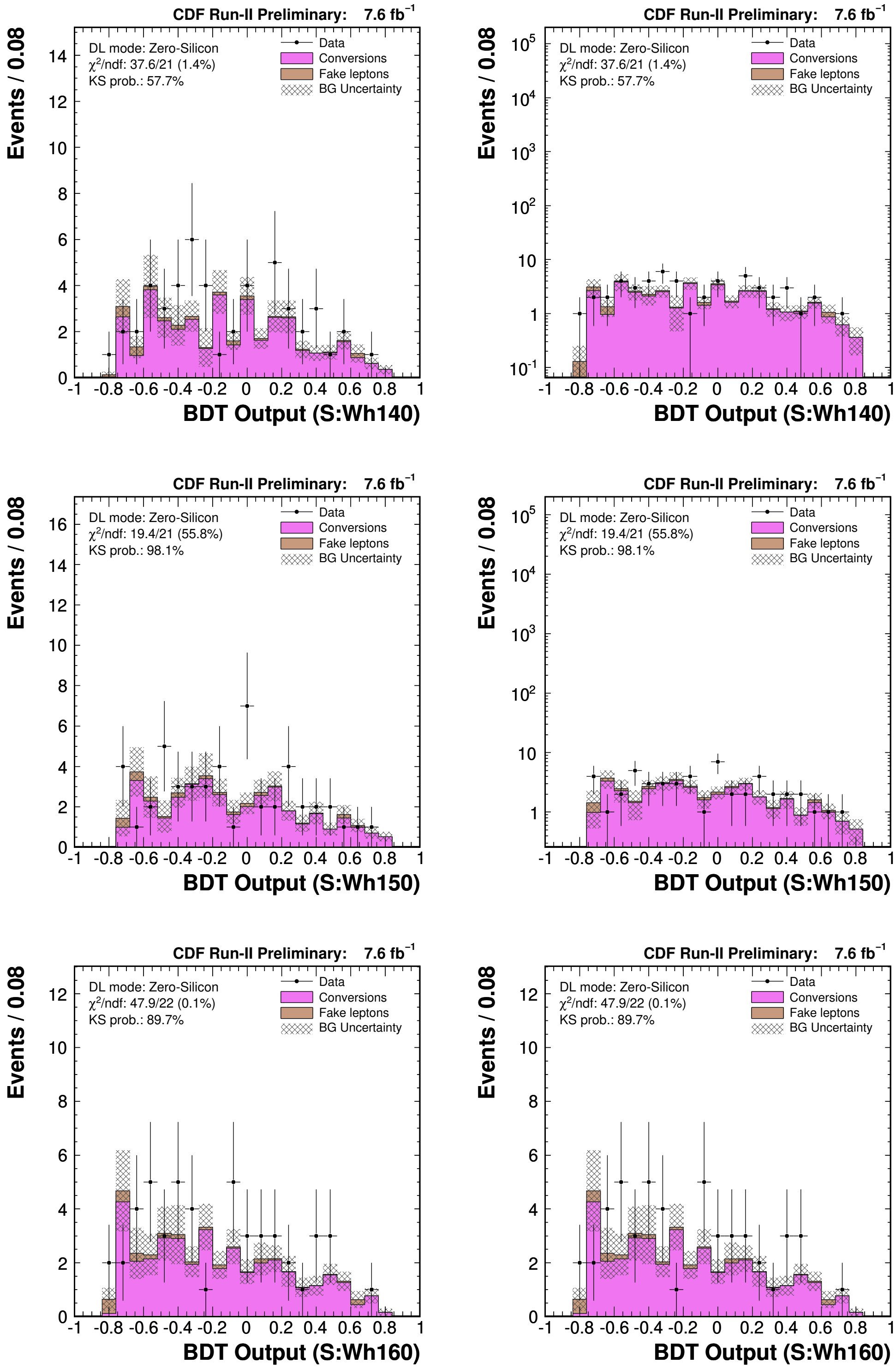

Figure 48: BDT output for in the zero-silicon region (left: linear, right: log).

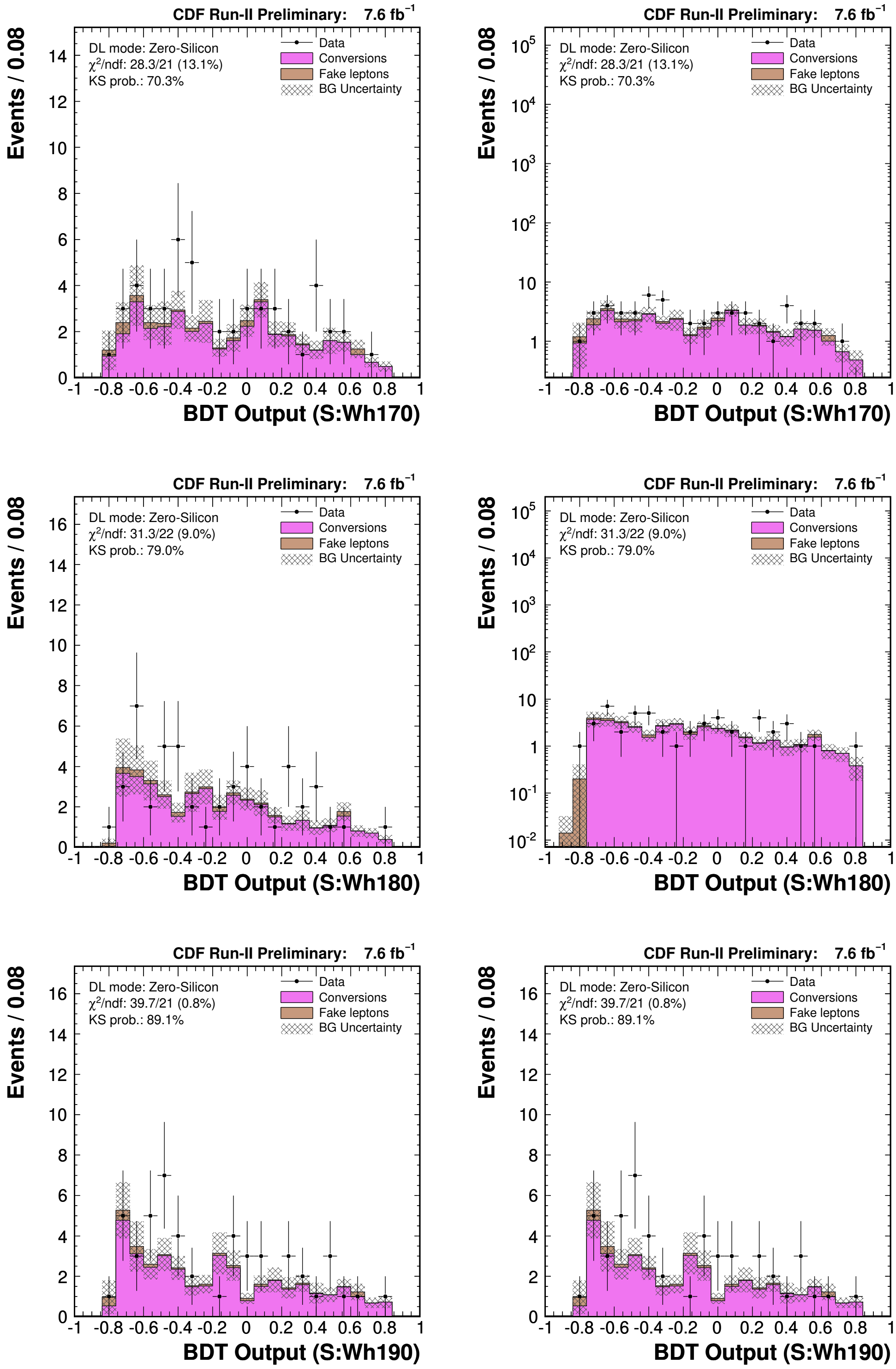

Figure 49: BDT output for in the zero-silicon region (left: linear, right: log).

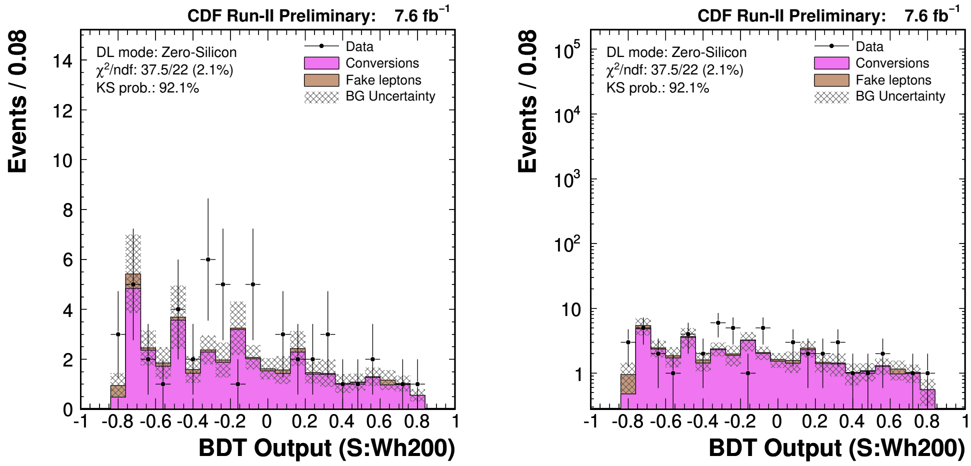

Figure 50: BDT output for in the zero-silicon region (left: linear, right: log).

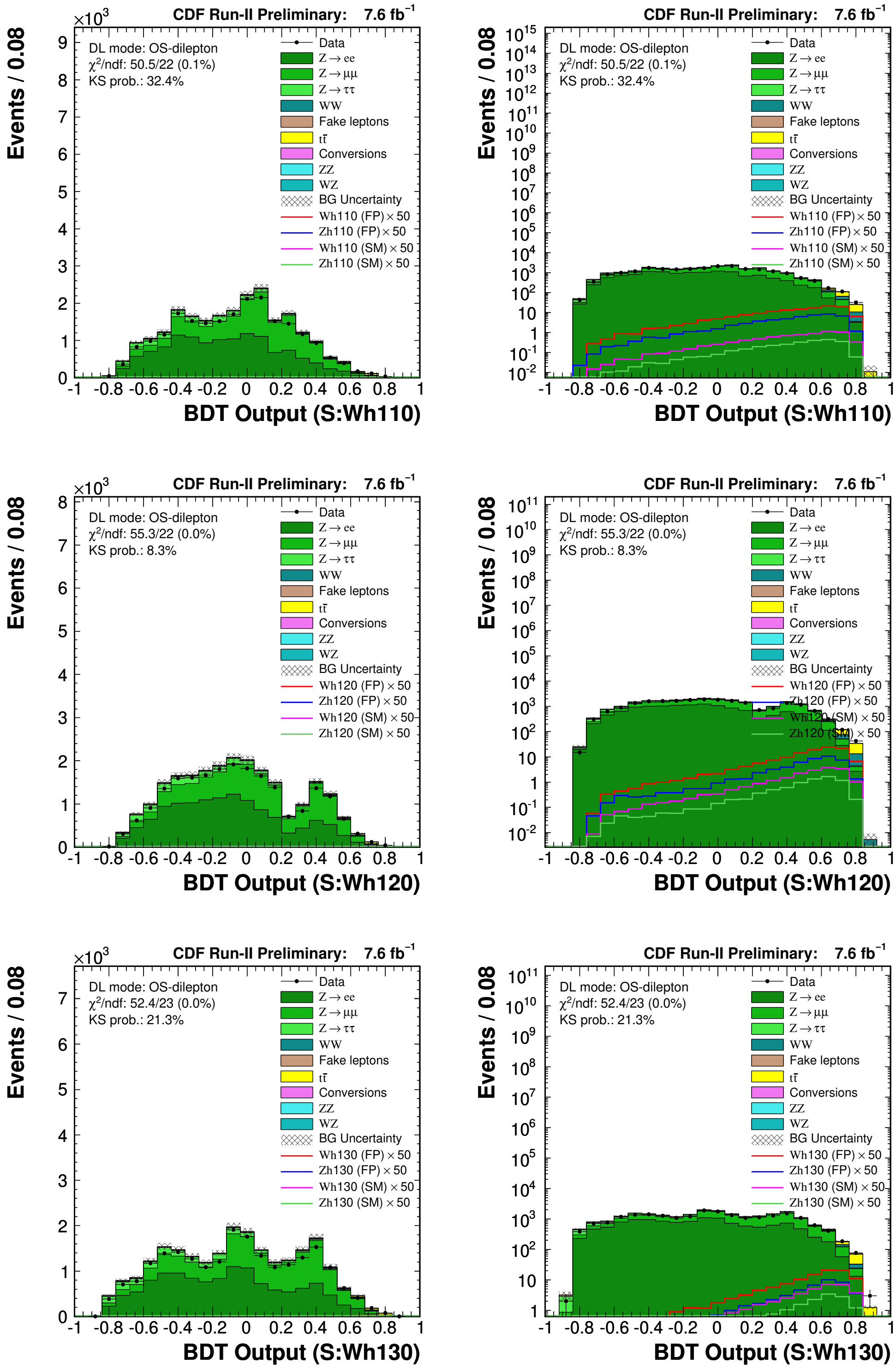

Figure 51: BDT output for in the OS region (left: linear, right: log).

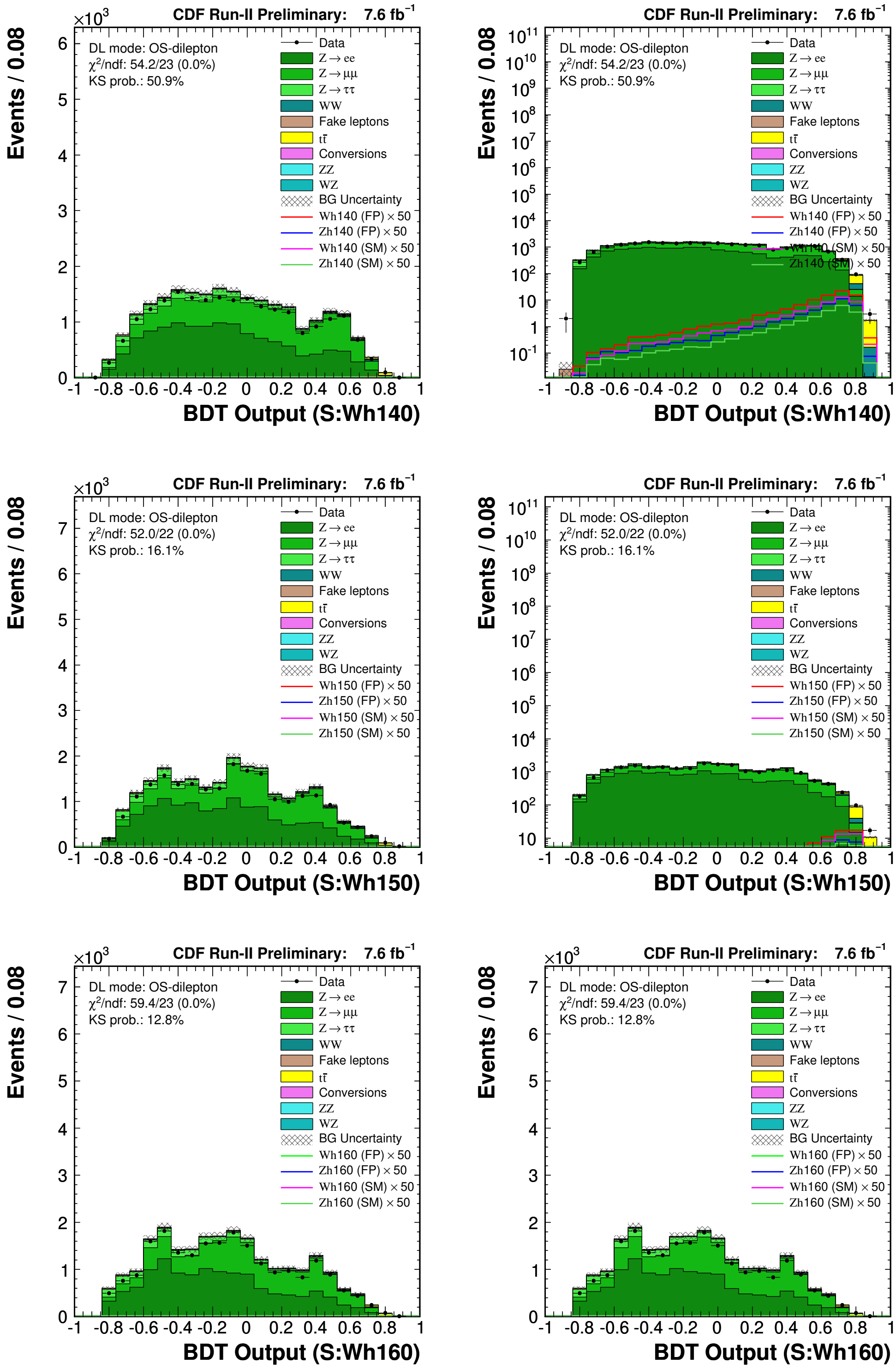

Figure 52: BDT output for in the OS region (left: linear, right: log).

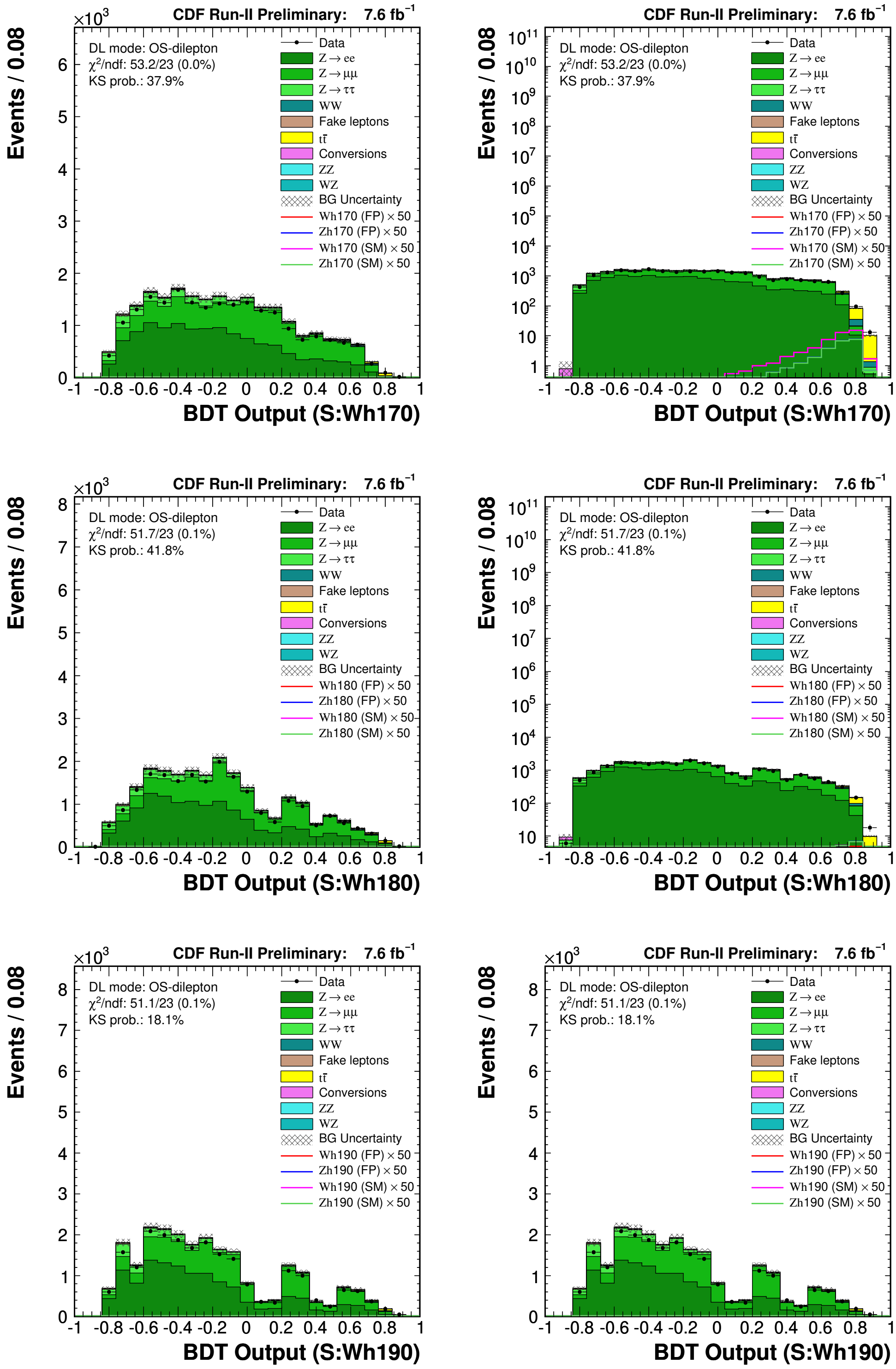

Figure 53: BDT output for in the OS region (left: linear, right: log).

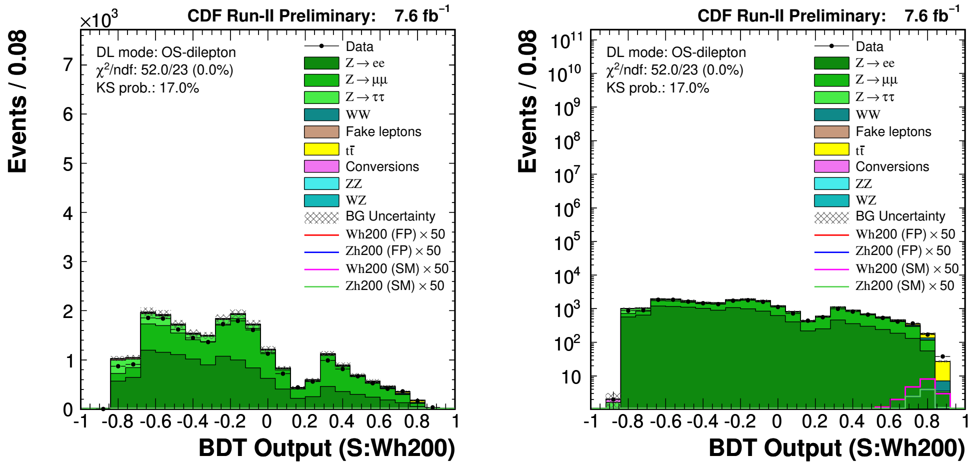

Figure 54: BDT output for in the OS region (left: linear, right: log).

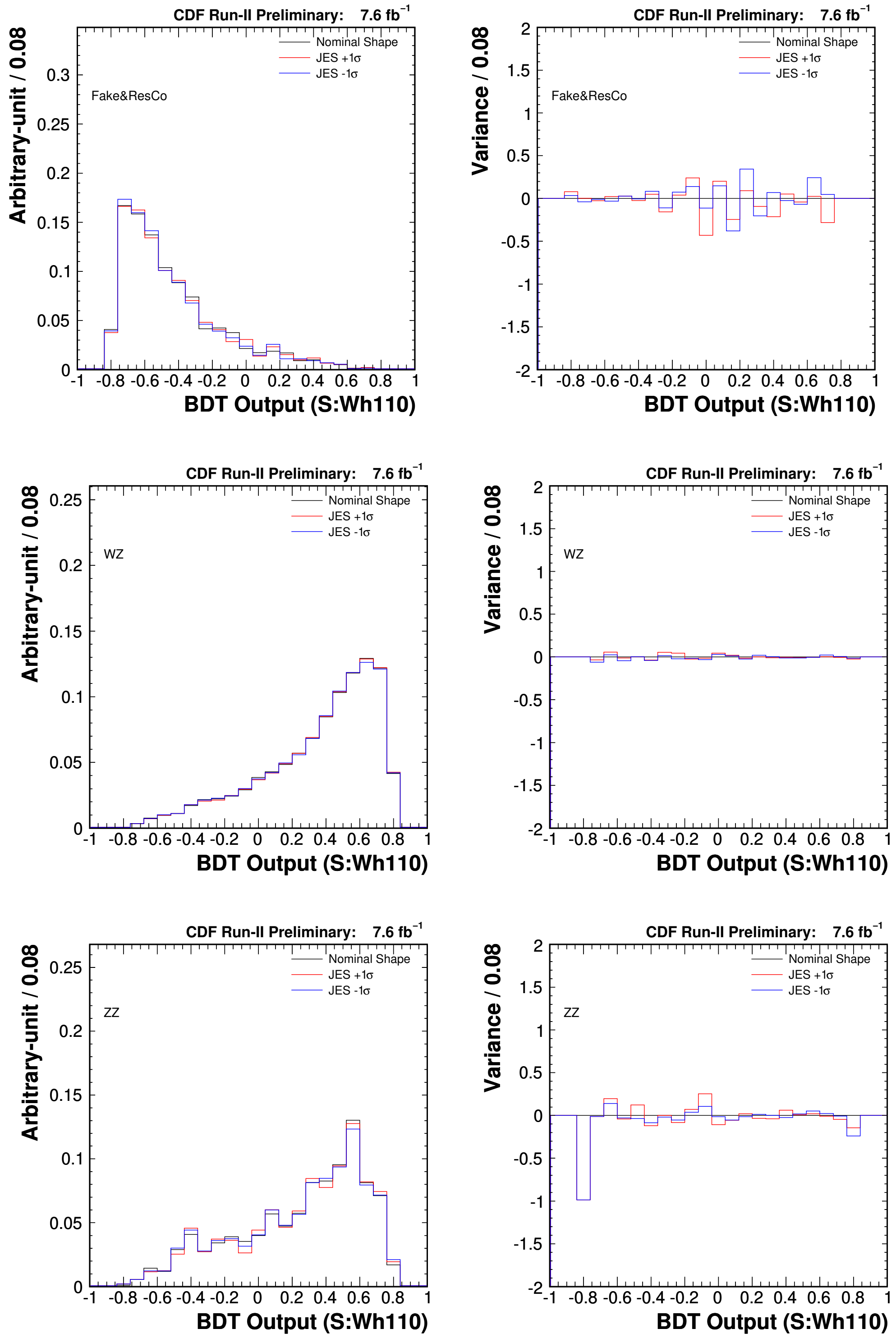

Figure 55: Shape systematic uncertainties due to jet energy scale for Higgs Mass 110 GeV/c^2.

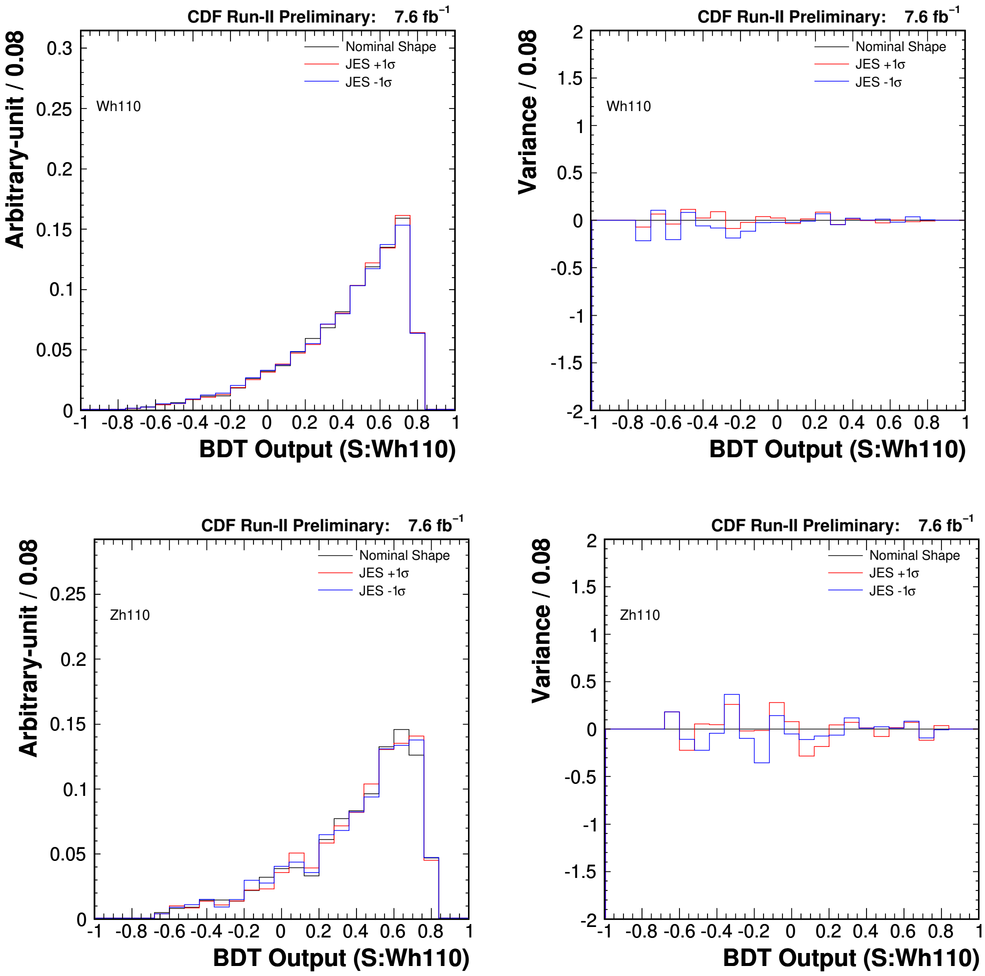

Figure 56: Shape systematic uncertainties due to jet energy scale for Higgs Mass 110 GeV/c^2.

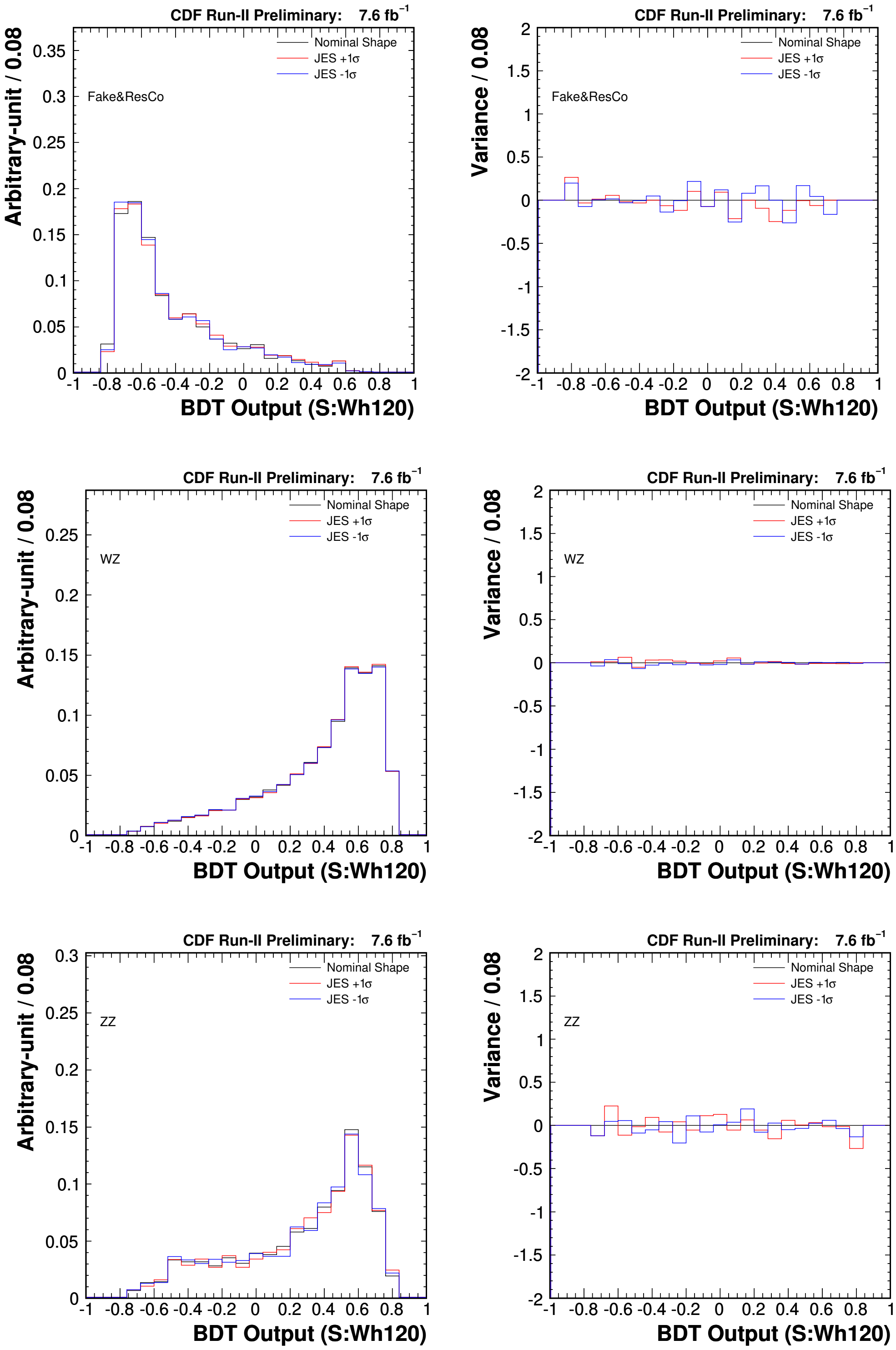

Figure 57: Shape systematic uncertainties due to jet energy scale for Higgs Mass 120 GeV/c^2.

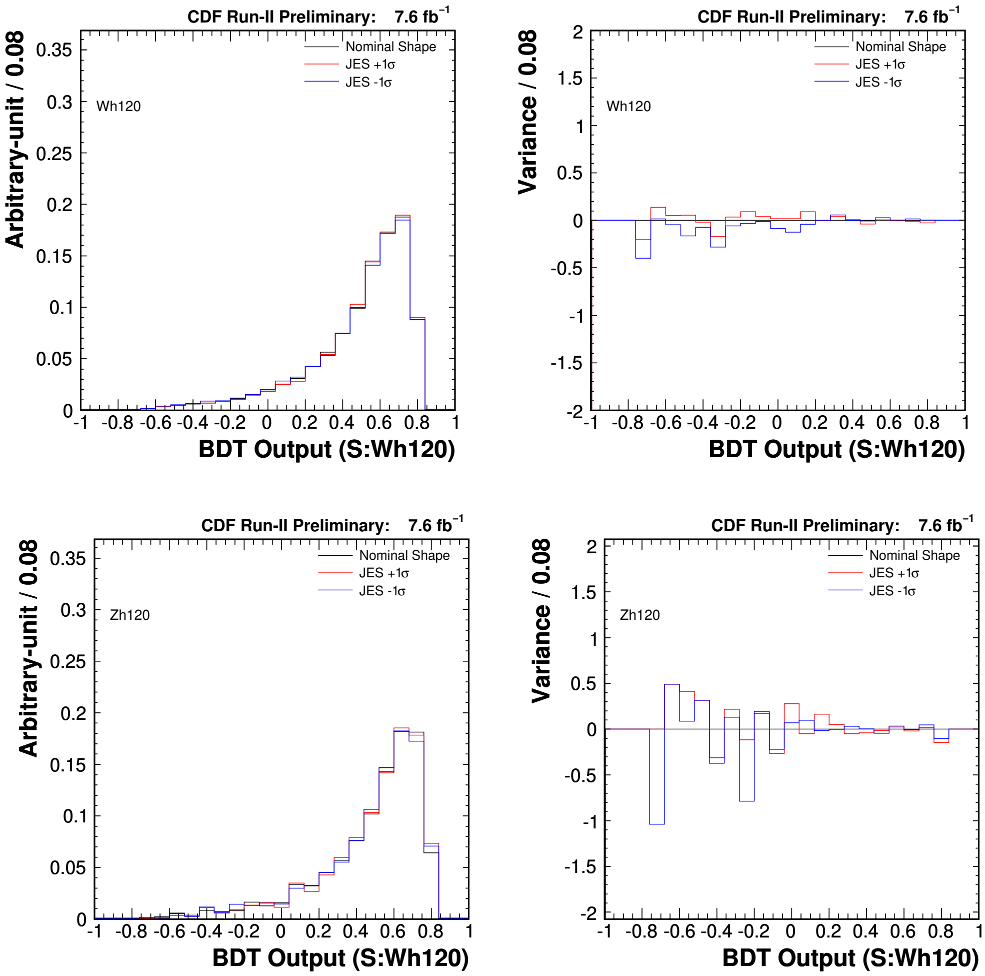

Figure 58: Shape systematic uncertainties due to jet energy scale for Higgs Mass 120 GeV/c^2.

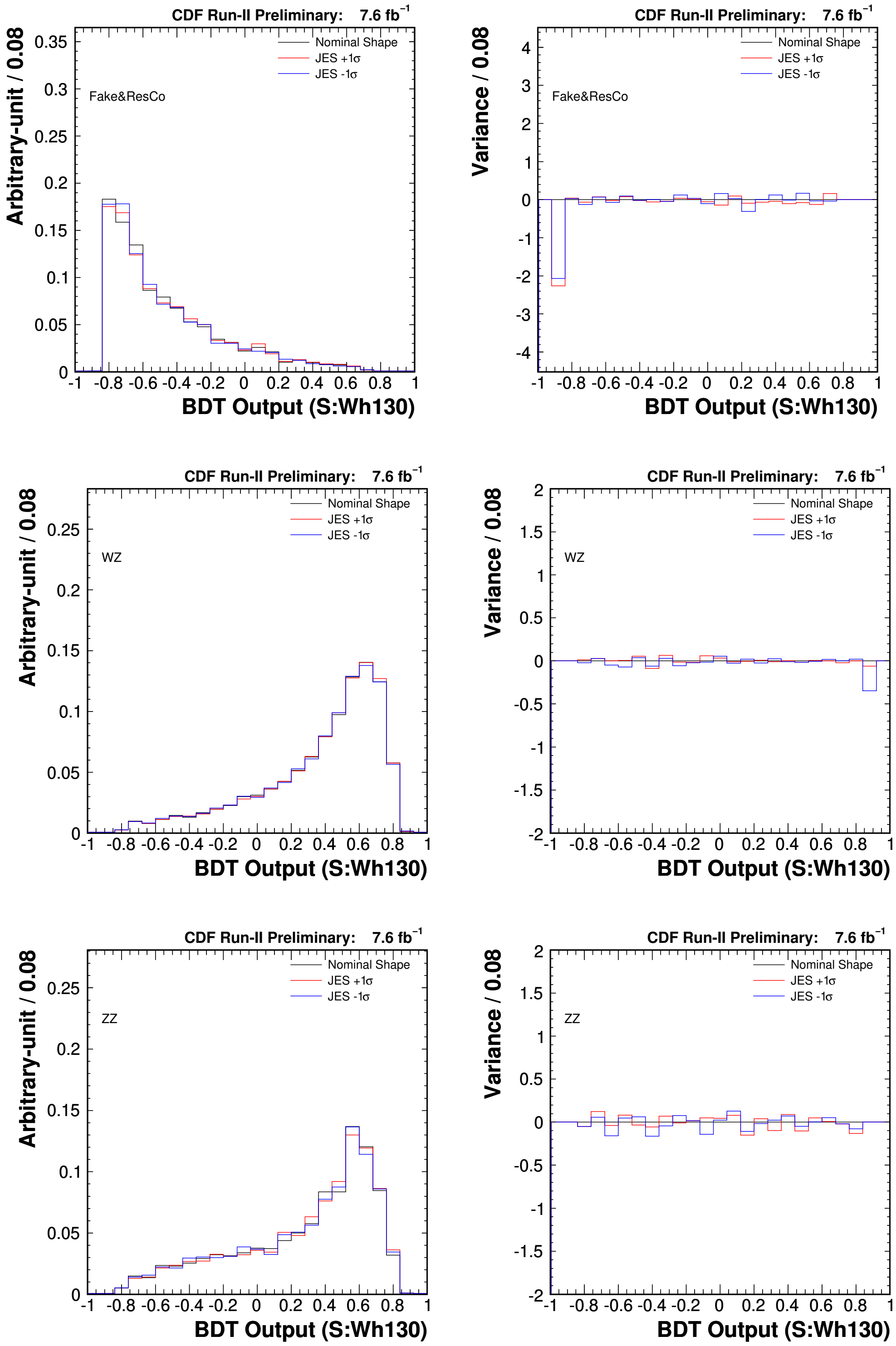

Figure 59: Shape systematic uncertainties due to jet energy scale for Higgs Mass 130 GeV/c^2.

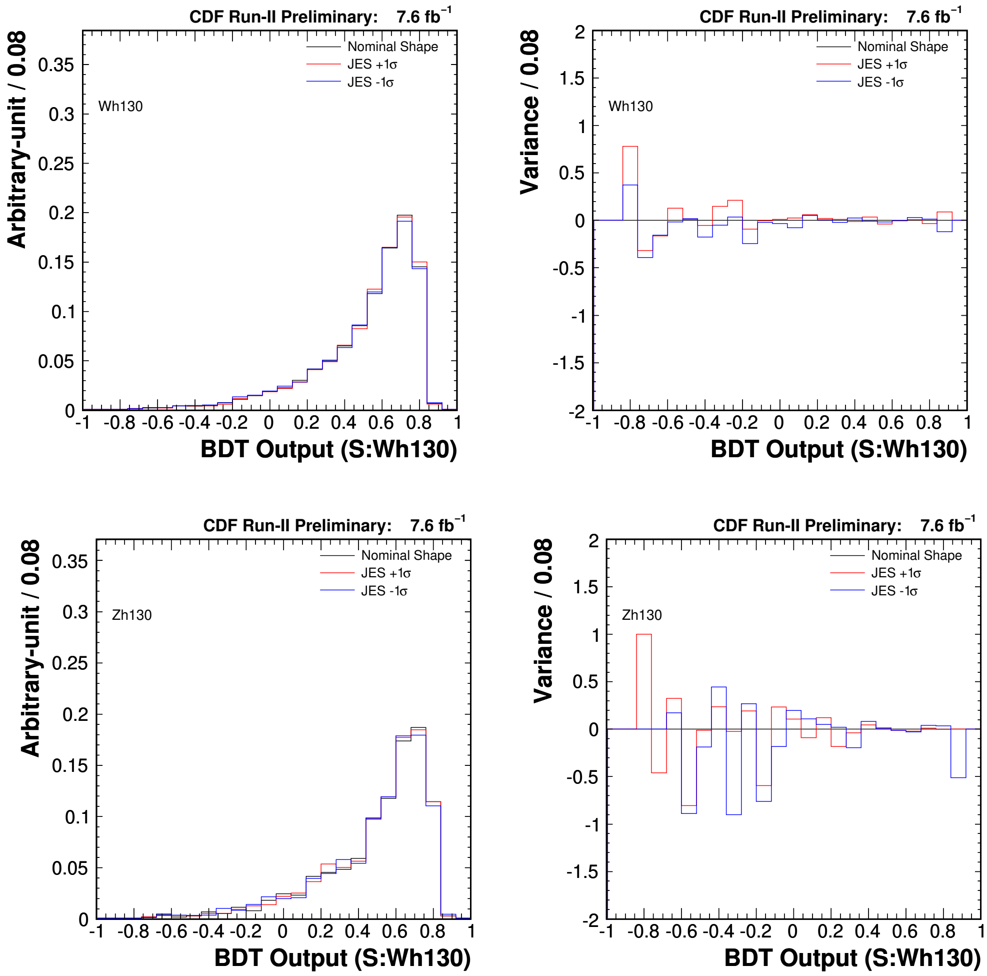

Figure 60: Shape systematic uncertainties due to jet energy scale for Higgs Mass 130 GeV/c^2.

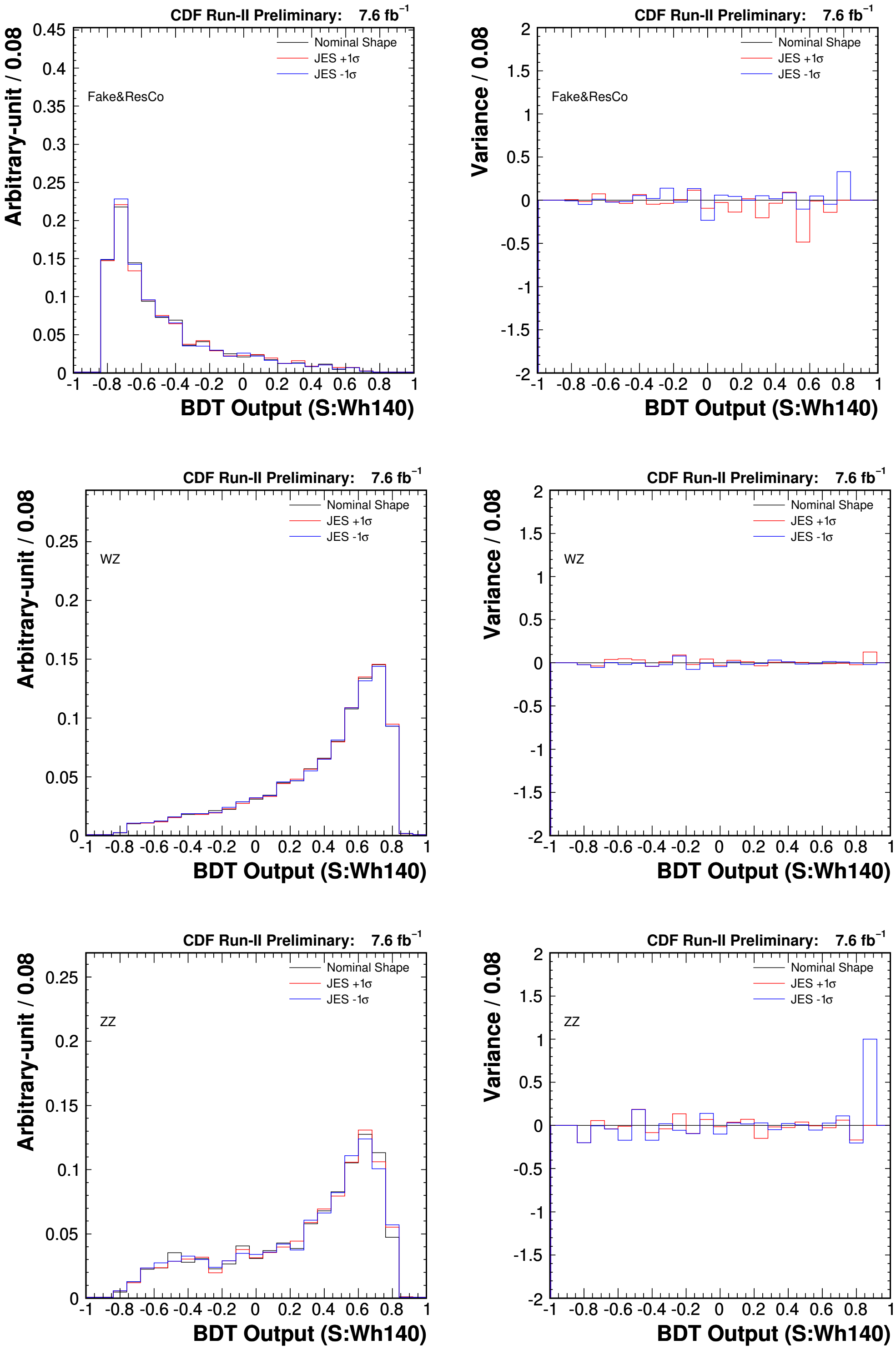

Figure 61: Shape systematic uncertainties due to jet energy scale for Higgs Mass 140 GeV/c^2.

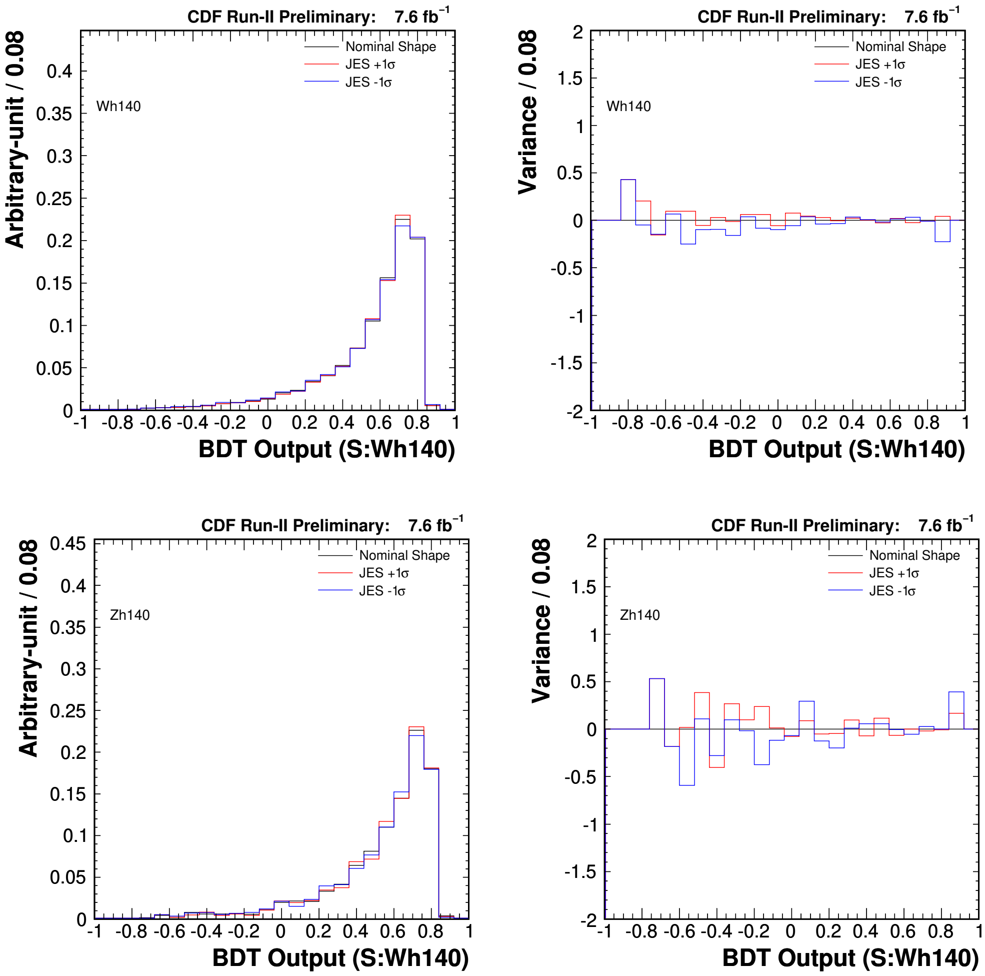

Figure 62: Shape systematic uncertainties due to jet energy scale for Higgs Mass 140 GeV/c^2.

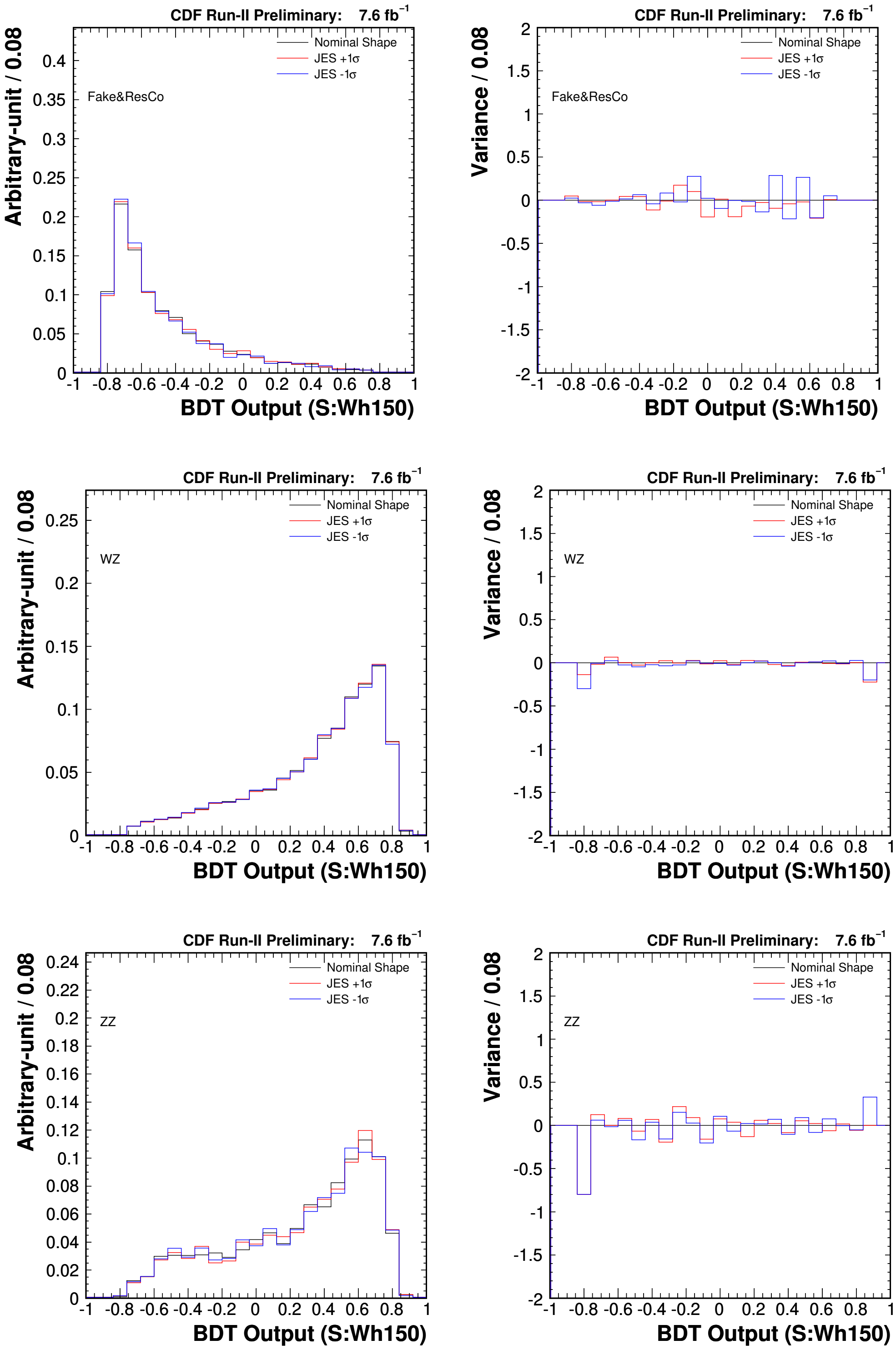

Figure 63: Shape systematic uncertainties due to jet energy scale for Higgs Mass 150 GeV/c^2.

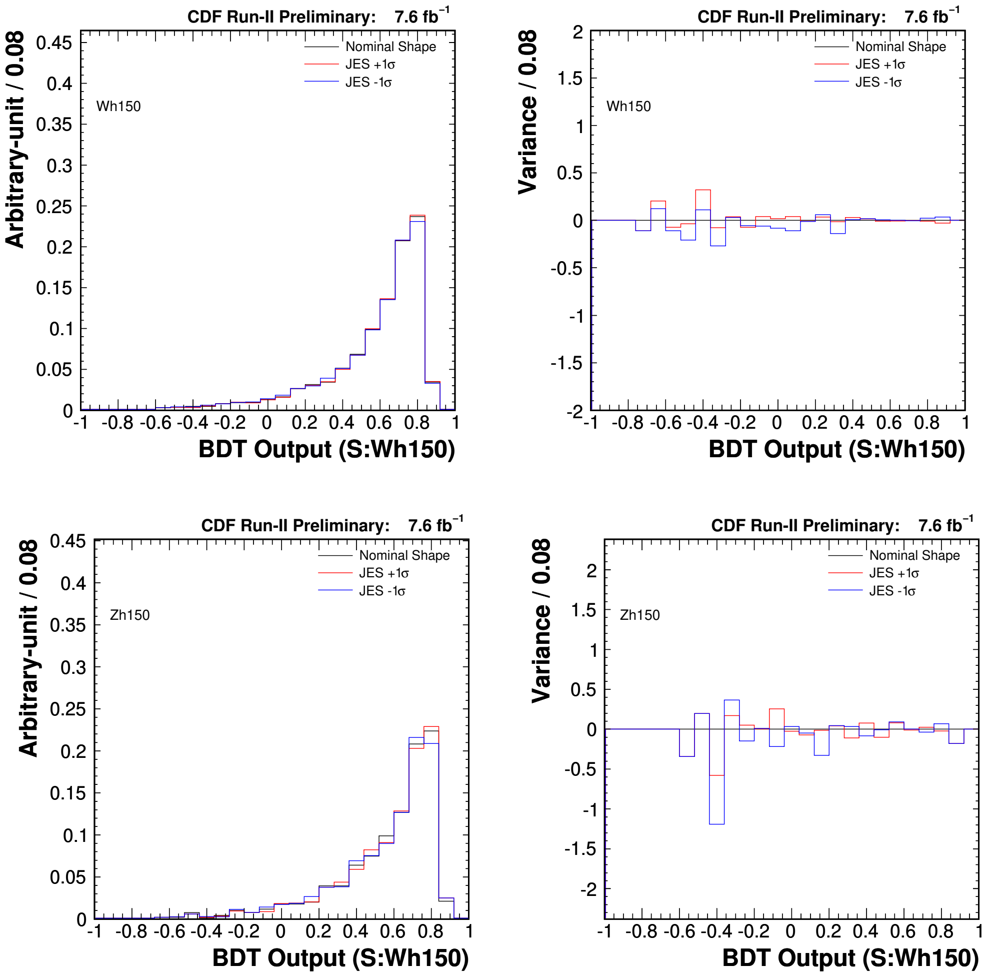

Figure 64: Shape systematic uncertainties due to jet energy scale for Higgs Mass 150 GeV/c^2.

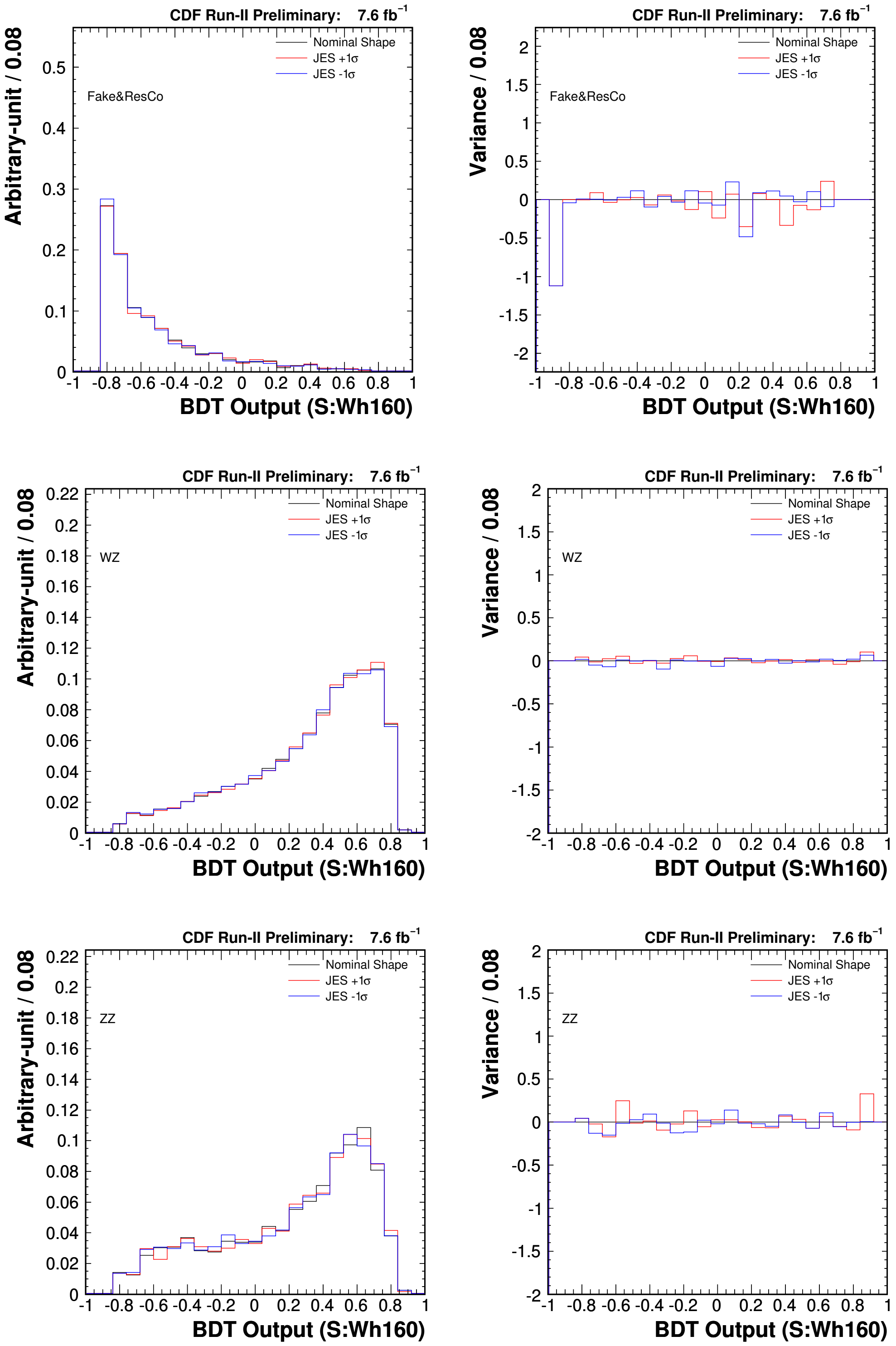

Figure 65: Shape systematic uncertainties due to jet energy scale for Higgs Mass 160 GeV/c^2.

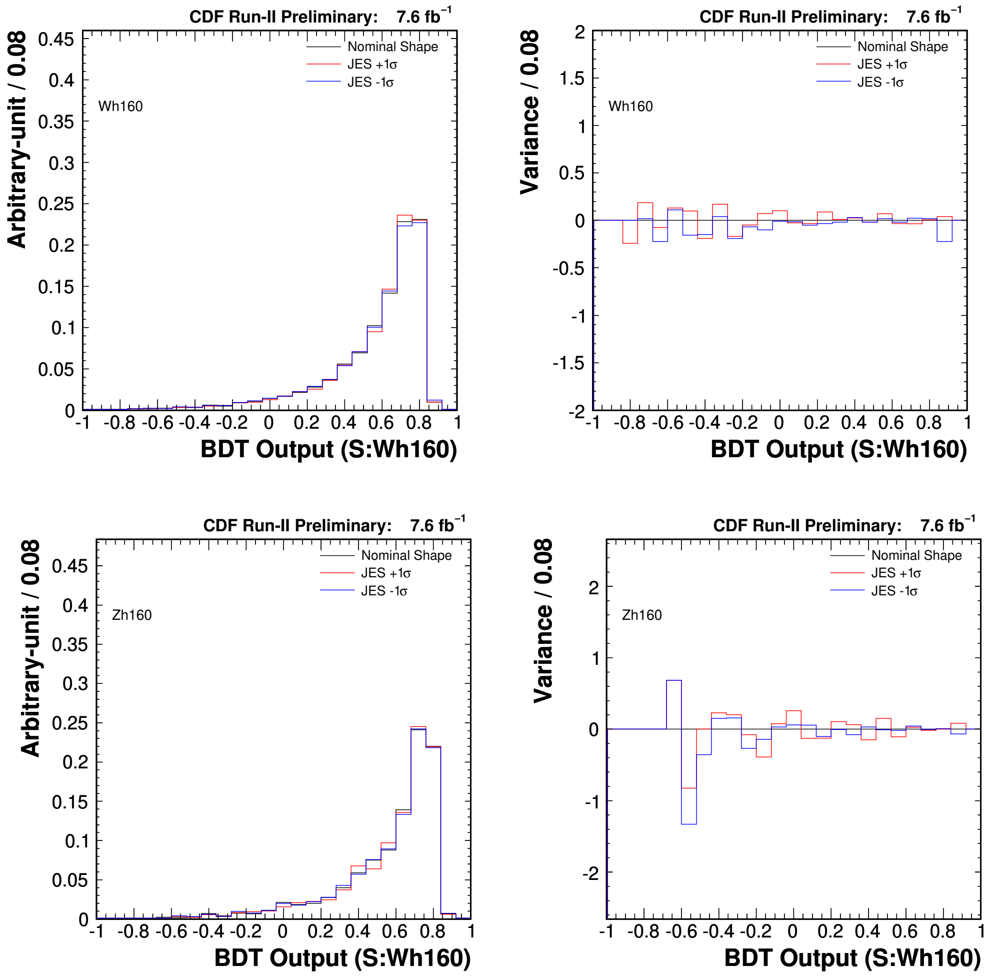

Figure 66: Shape systematic uncertainties due to jet energy scale for Higgs Mass 160 GeV/c^2.

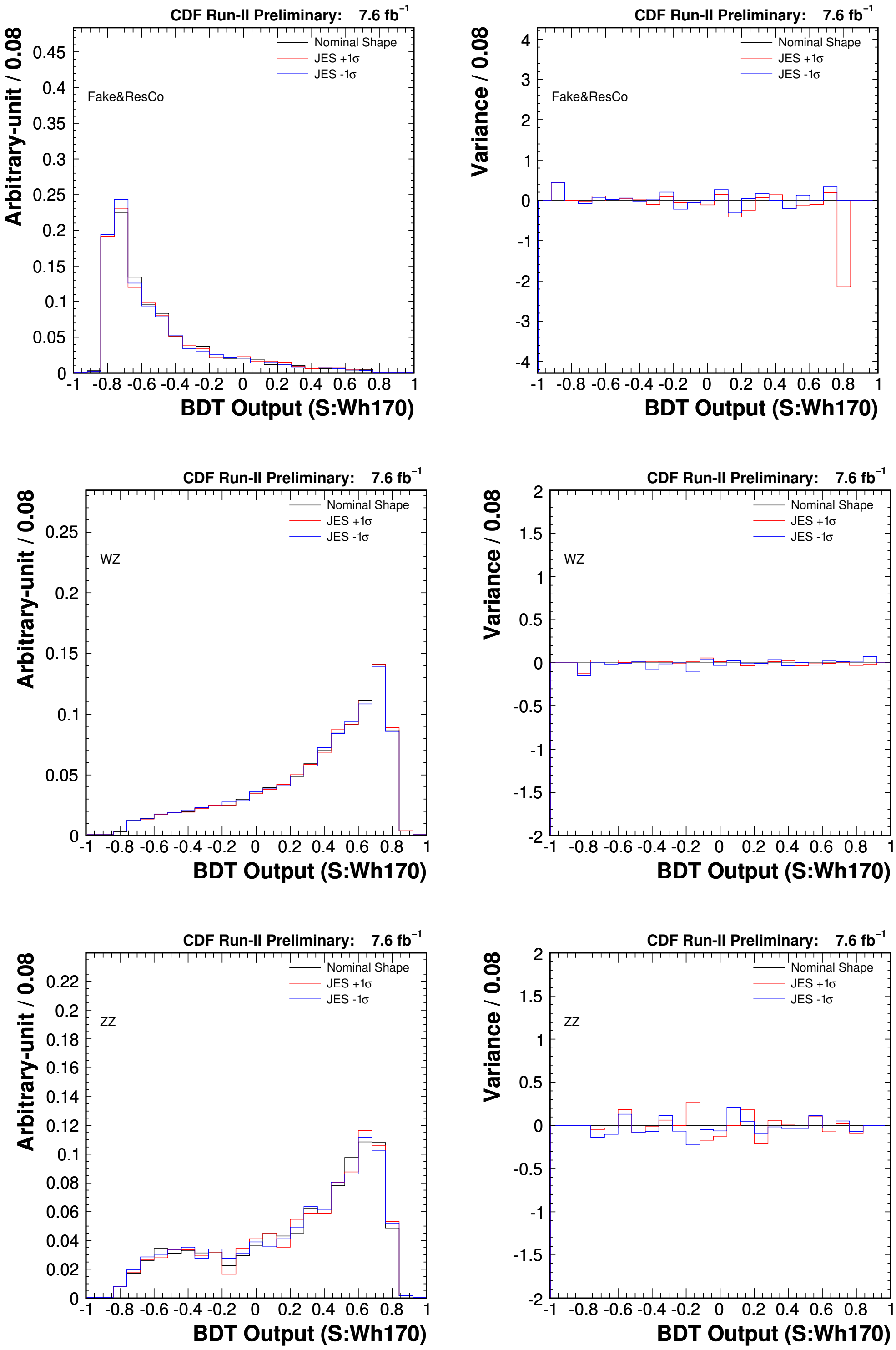

Figure 67: Shape systematic uncertainties due to jet energy scale for Higgs Mass 170 GeV/c^2.

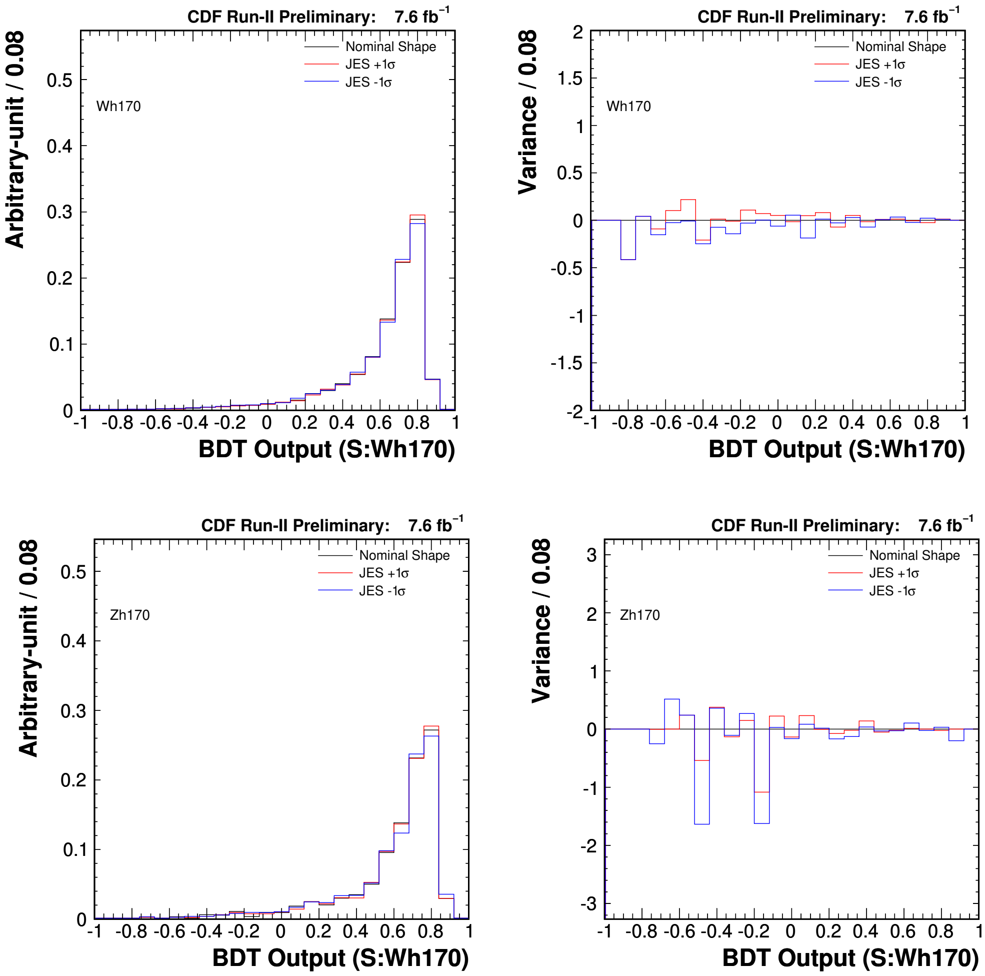

Figure 68: Shape systematic uncertainties due to jet energy scale for Higgs Mass 170 GeV/c^2.

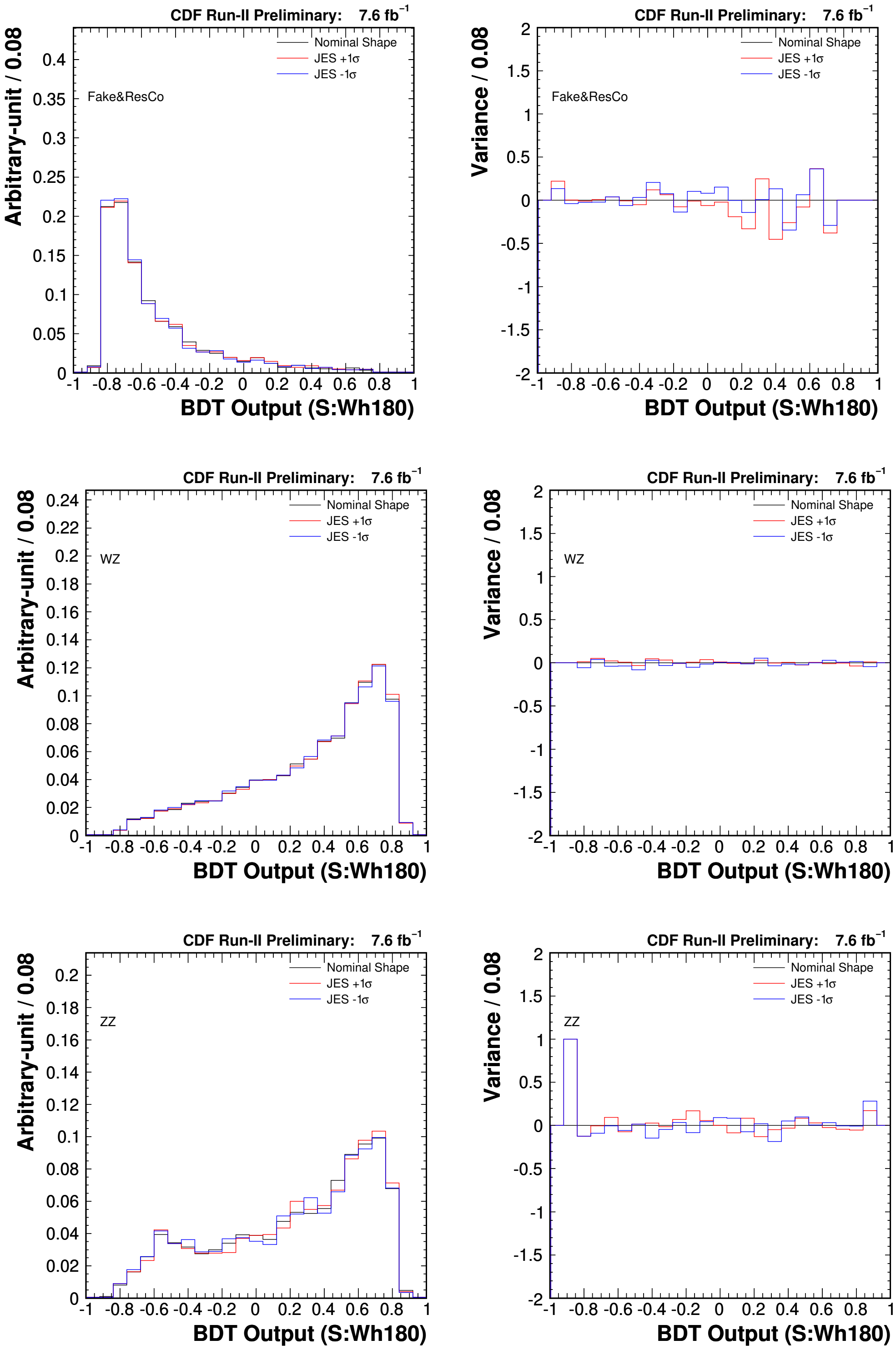

Figure 69: Shape systematic uncertainties due to jet energy scale for Higgs Mass 180 GeV/c^2.

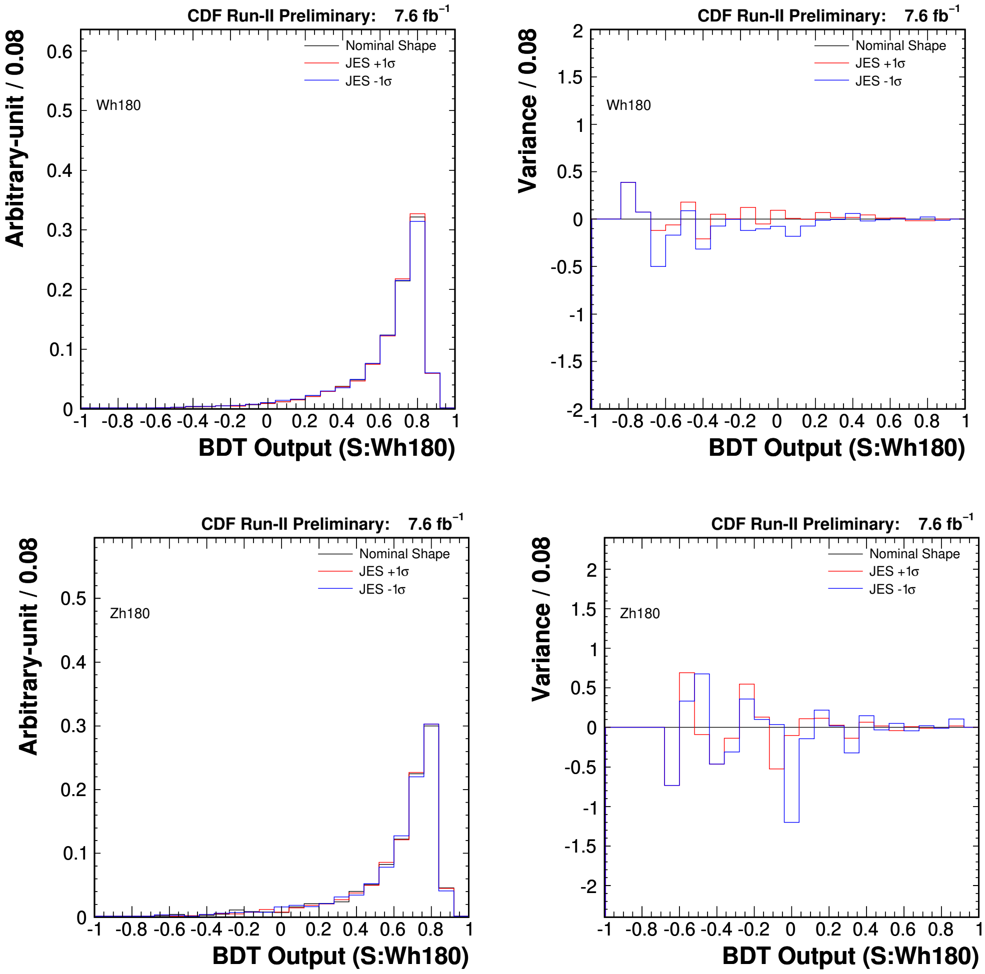

Figure 70: Shape systematic uncertainties due to jet energy scale for Higgs Mass 180 GeV/c^2.

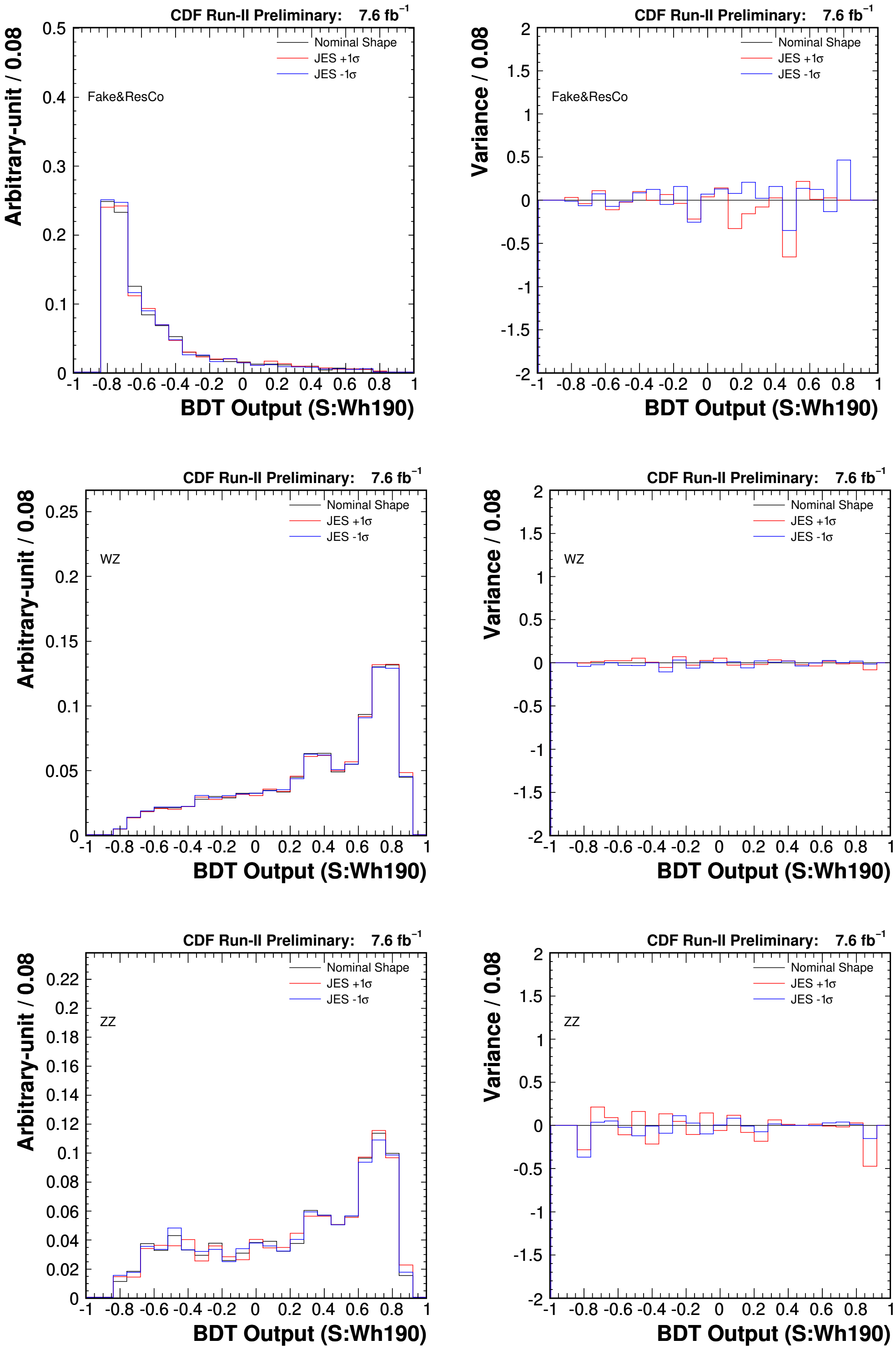

Figure 71: Shape systematic uncertainties due to jet energy scale for Higgs Mass 190 GeV/c^2.

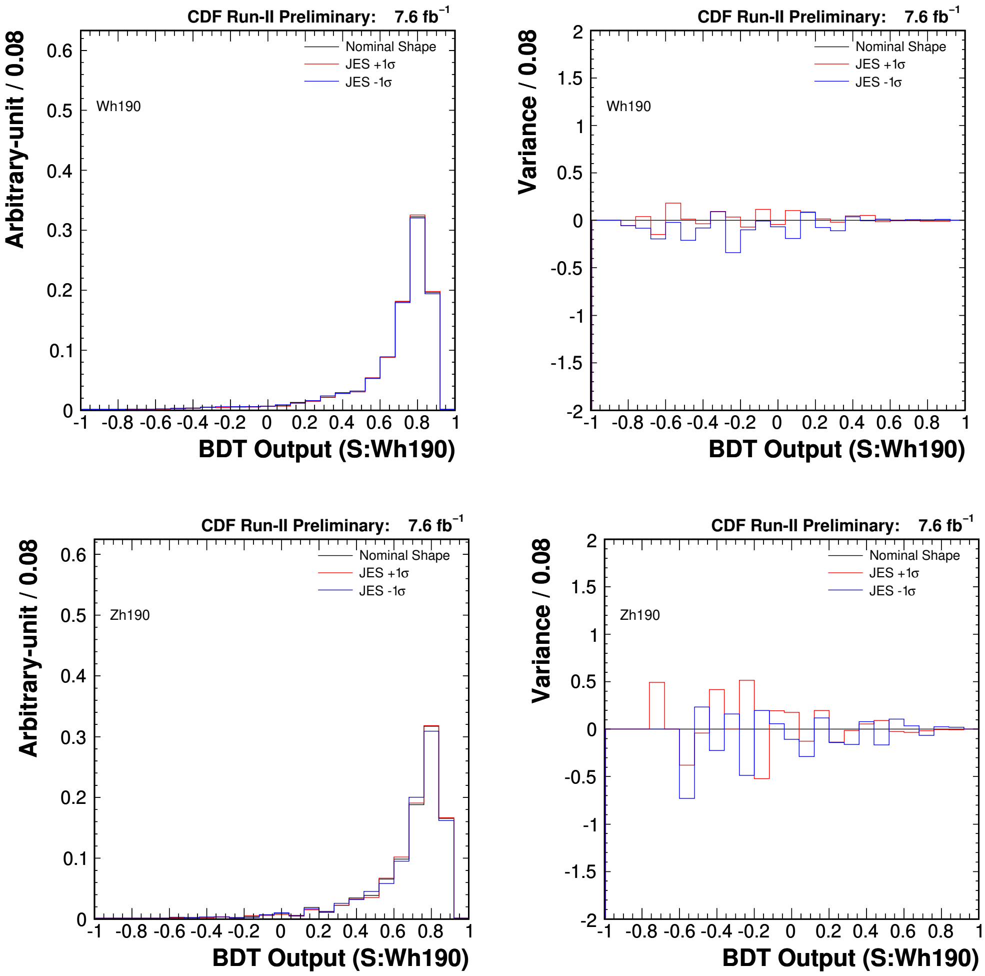

Figure 72: Shape systematic uncertainties due to jet energy scale for Higgs Mass 190 GeV/c^2.

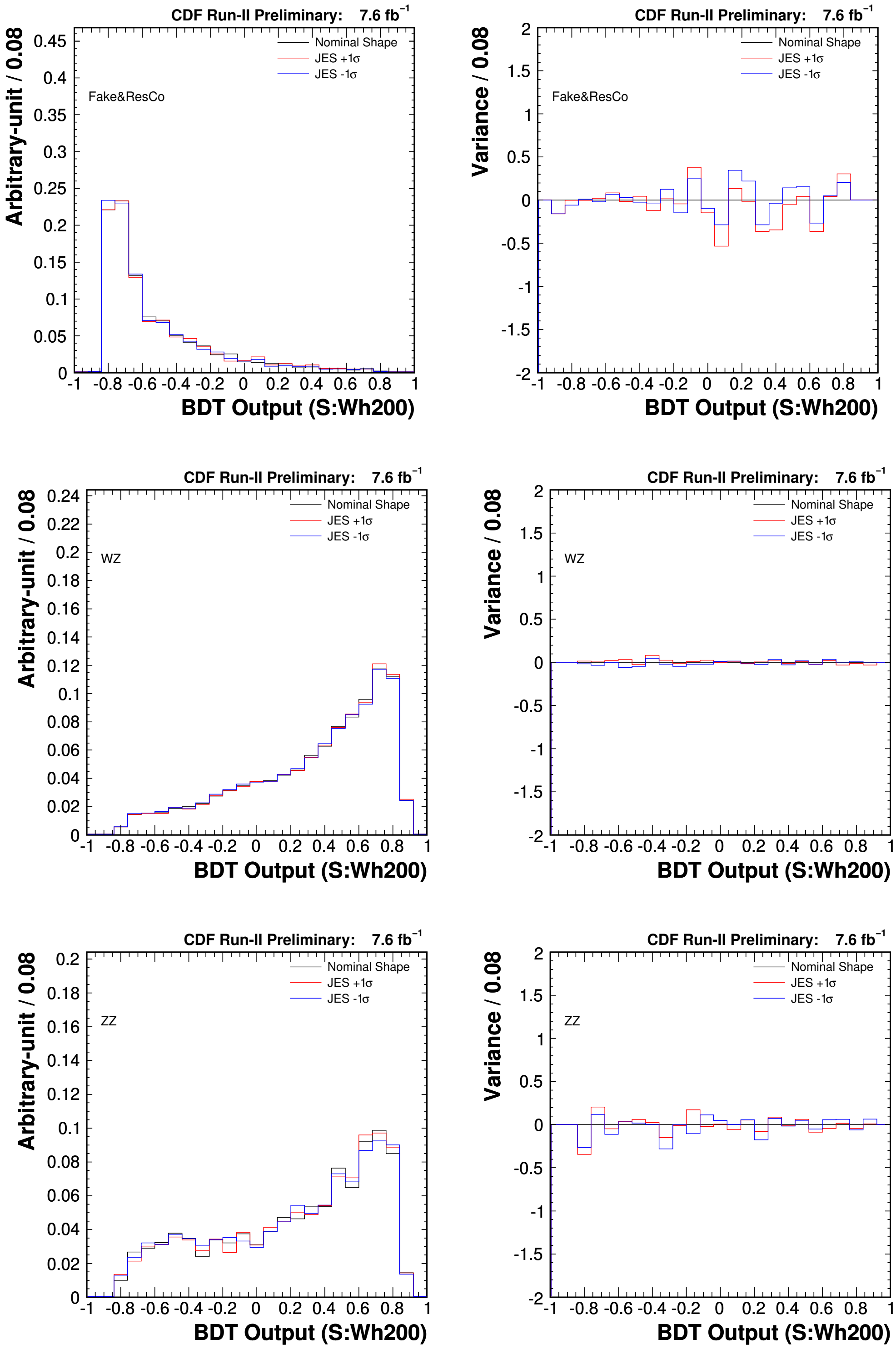

Figure 73: Shape systematic uncertainties due to jet energy scale for Higgs Mass 200 GeV/c^2.

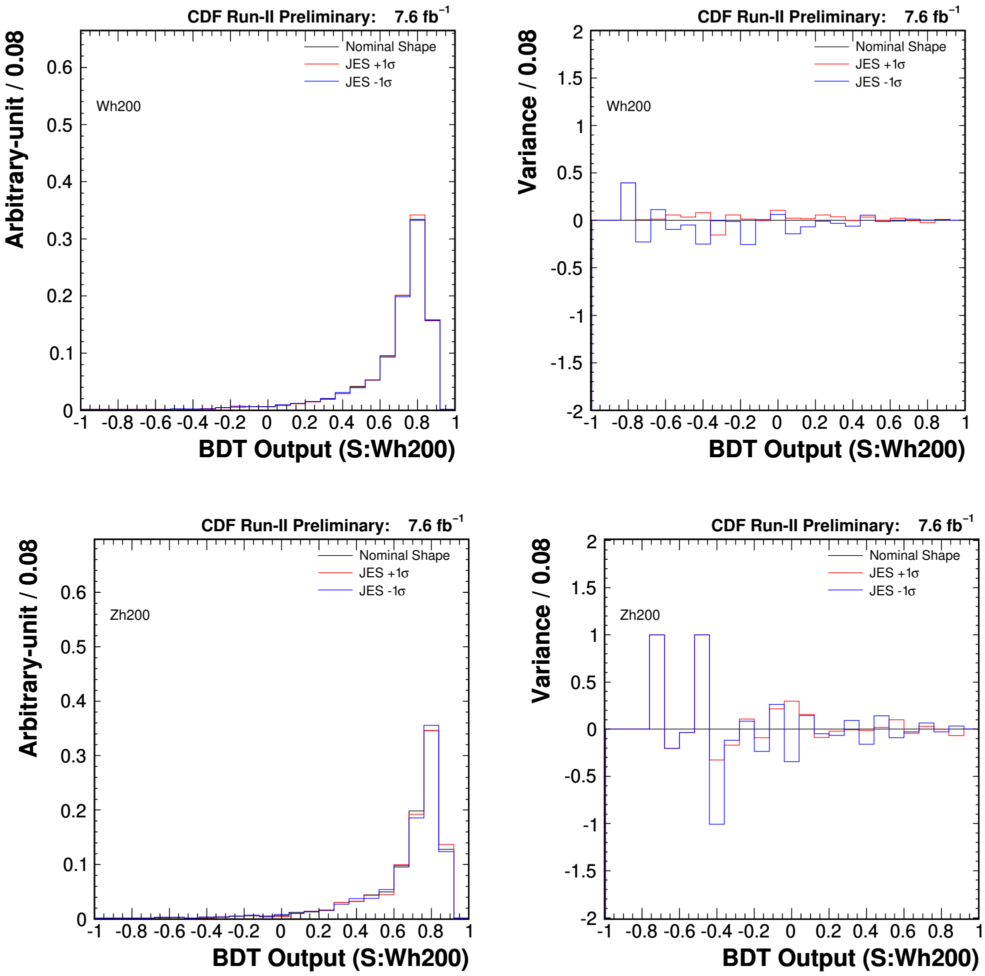

Figure 74: Shape systematic uncertainties due to jet energy scale for Higgs Mass 200 GeV/c^2.

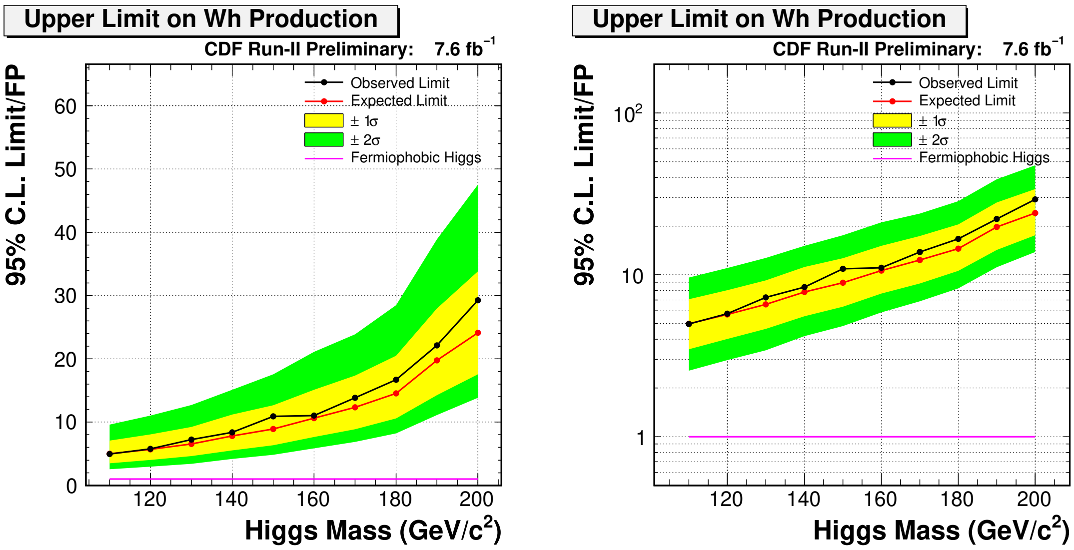

Figure 75: Relative limits on the production cross-section times branching fraction $\sigma(p\bar{p}\to Wh) \times B_F(h\to W^{*+}W^{*-})$ to fermiophobic higgs Prediction at the 95% C.L.

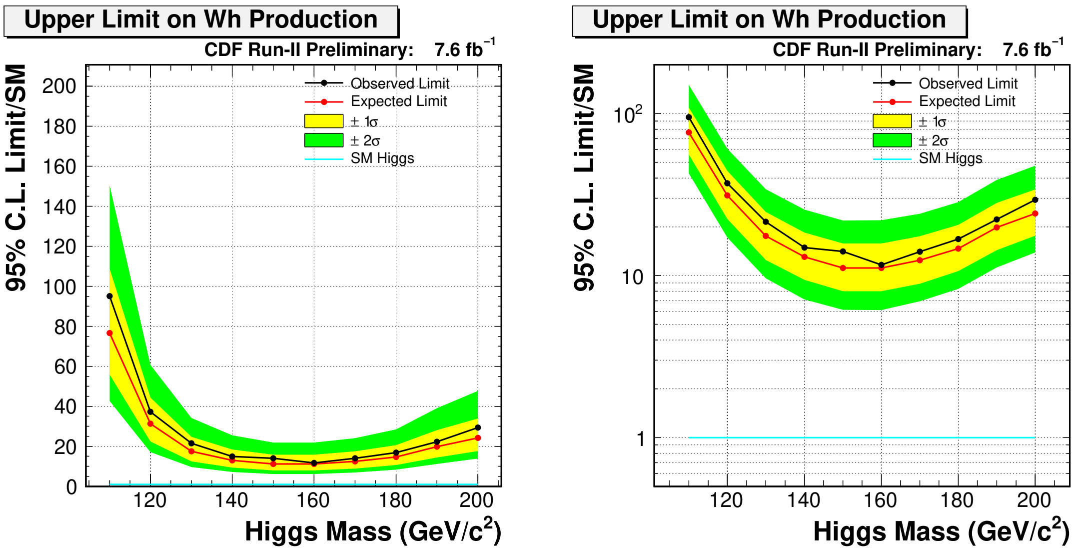

Figure 76: Relative limits on the production cross-section times branching fraction $\sigma(p\bar{p}\to Wh) \times B_F(h\to W^{*+}W^{*-})$ to the Standard Model higgs Prediction at the 95% C.L.

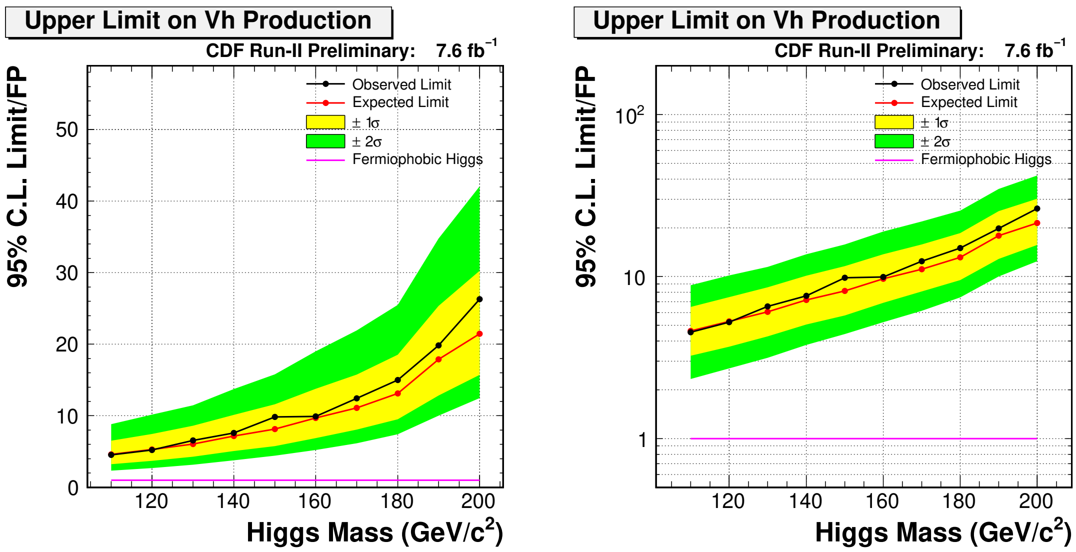

Figure 77: Relative limits on the production cross-section times branching fraction $\sigma(p\bar{p}\to Vh) \times B_F(h\to W^{*+}W^{*-})$ to fermiophobic higgs Prediction at the 95% C.L.

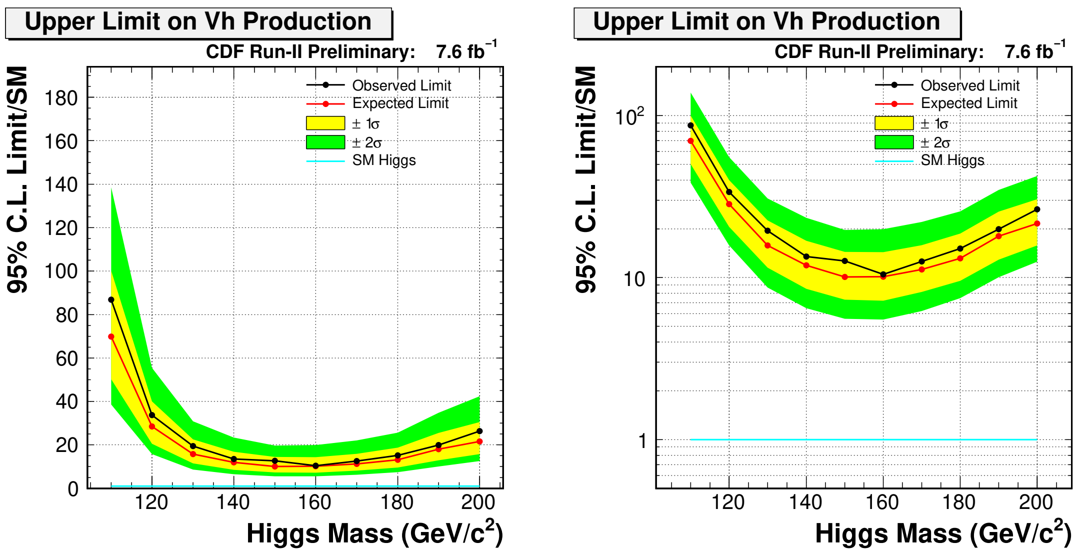

Figure 78: Relative limits on the production cross-section times branching fraction $\sigma(p\bar{p}\to Vh) \times B_F(h\to W^{*+}W^{*-})$ to the Standard Model higgs Prediction at the 95% C.L.

References

[1] Toru Okusawa, Yoshihiro Seiya, Takayuki Wakisaka, and Kazuhiro Yamamoto, "Search for the Wh Production Using High-p_T Like-Sign Dilepton Events in Run II", CDF7262 (Version 3.0).

[2] Toru Okusawa, Yoshihiro Seiya, Takayuki Wakisaka, Kazuhiro Yamamoto, Daisuke Yamato, and Mina Yoshida, "Likelihood-Based Lepton Identification to Search for the Vh Production", CDF10096 (Version 1.0).

[3] Toru Okusawa, Yoshihiro Seiya, Takayuki Wakisaka, and Kazuhiro Yamamoto, "Baseline Selection of High-p_T Dilepton Events to Search for the Wh Production", CDF7260 (Version 3.0).

[4] Toru Okusawa, Yoshihiro Seiya, Takayuki Wakisaka, Kazuhiro Yamamoto, and Daisuke Yamato "Estimation of Monte-Carlo Scale Factors for the High-p_T Like-Sign Dilepton Analysis to Search for the Vh Production", CDF9238 (Version 4.0).

[5] Toru Okusawa, Yoshihiro Seiya, Takayuki Wakisaka, and Kazuhiro Yamamoto, "Study of Conversion Detection Efficiency for the High-p_T Like-Sign Dilepton Analysis to Search for the Wh Production", CDF8078 (Version 2.0).

[6] Toru Okusawa, Yoshihiro Seiya, Takayuki Wakisaka, and Kazuhiro Yamamoto, "Study of Fake-Lepton Rates for the High-p_T Like-Sign Dilepton Analysis to Search for the Wh Production", CDF9239 (Version 2.0).

[7] Toru Okusawa, Yoshihiro Seiya, Takayuki Wakisaka, and Kazuhiro Yamamoto, "Search for the Wh Production Using High-p_T Like-Sign Dilepton Events in Run II", CDF7262 (Version 2.0).

[8] A.Hocker, P.Speckmayer, J.Stelzer, F.Tegenfeldt, H.Voss, K,Voss, "TMVA Toolkit for Multivariate Data Analysis with ROOT Users Guide".

[9] Torbjorn Sjostrand, Stephen Mrenna, and Peter Skands, "PYTHIA 6.4 Physics and Manual". hep-ph/0603175.

[10] K.A.Assamgan *et al*, "THE HIGGS WORKING GROUP: Summary Report" hep-ph/0406152v1.

[11] J. M. Campbell and R. K. Ellis, "Update on vector boson pair production at hadron colliders" Phys. Rev. D **60** 113006.

[12] Tom Junk, "Sensitivity, Exclusion and Discovery with Small Signals, Large Backgrounds, and Large Systematic Uncertainties" CDF8128 (Version 2.4).